NINEVAH UNIVERSITY

College Of Electronics Engineering

Electronic Engineering Department

Resolution Enhancement for Angle of Arrival Estimation of Waves Using Root-Eigenvector Method

A Thesis Submitted by

Aya Saud Abood Alshaker

M.Sc./ Thesis

in

Electronic Engineering

Supervised by

Assist Prof. Dr. Mujahid Fahmy Ibrahem

Al-Azzo

Resolution Enhancement for Angle of Arrival Estimation of Waves Using Root-Eigenvector Method

A Thesis Submitted by

Aya Saud Abood Alshaker

To

The Council of College of Electronic Engineering

Ninevah University

As a partial fulfillment of the Requirements

For the Degree of Master of Science

In

Electronic Engineering

Supervised by

Assist Prof. Dr. Mujahid Fahmy Ibrahem Al-Azzo

بِسْمِ اللَّهِ الرَّحْمَنِ الرَّحِيمِ

"يَرْفَعِ اللَّهُ الَّذِينَ آمَنُوا مِنكُمْ وَالَّذِينَ أُوتُوا الْعِلْمَ دَرَجَاتٍ"

سورة المجادلة

الاية (11)

صَدَقَ اللهُ العَظِيمُ

Supervisor's Certification

I certify that the dissertation entitled (**Resolution Enhancement for Angle of Arrival Estimation of Waves Using Root-Eigenvector Method**) was prepared by (**Aya Saud Abood Alshaker**) under our supervision at the Department of Electronic Engineering, Ninevah University, as a partial requirement for the Master of Science Degree in Electronic Engineering.

Signature:

Name: Assist Prof. Dr. Mujahid Fahmy Ibrahem Al-Azzo

Date: /   /2024

Report of Linguistic Reviewer

I certify that the linguistic reviewing of this dissertation was carried out by me, and it is accepted linguistically and in expression.
Signature:

Name: Saleh Abdullah AbdulRahman

Date: /   /2024

Report of the Head of Department

I certify that this dissertation was carried out in the Department of Electronic Engineering. I nominate it to be forwarded to discussion.
Signature:

Name: Assist. Prof. Dr. Harith Al-Badrani

Date: /   /2024

Report of Head of Postgraduate studies Committee

According to the recommendations presented by the supervisor of this dissertation and the linguistic reviewer, I nominate this dissertation to be forwarded to discussion.
Signature:

Name: Prof. Dr. Qais Thanon Najim

Date: /   /2024

Committee Certification

We the examining committee, certify that we have read this dissertation entitled (**Resolution Enhancement for Angle of Arrival Estimation of Waves Using Root-Eigenvector Method)** and have examined the postgraduate student (**Aya Saud Abood Alshaker)** in its contents and that in our opinion; it meets the standards of a dissertation for the degree of Master of Science in Electronic Engineering.

Signature:
Name: Assist. Prof. Dr. AbdulSattar
Mohammed Khidhir
Head of committee
Date: /   /2024

Signature:
Name: Assist. prof. Aws Zuheer
Yonis Alashqar
Member
Date: /   /2024

Signature:
Name: Dr. Zainab Rami Saleh
Alomari
Member
Date: /   /2024

Signature:
Name: Assist. Prof. Dr. Mujahid
Fahmy Ibrahem Al-Azzo
Member and Supervisor
Date: **/**   /2024

The college council, in its   ………… meeting on   /   /2024, has decided to award the degree of Master of Science in Electronic Engineering to the candidate.

Signature:
Name: Prof. Khaled Khalil Muhammed
Dean of the College
Date: /   /2024

Signature:
Name: Assist. Prof. Dr. Bilal A. jebur
Council registrar
Date: **/**   /2024

ACKNOWLEDGEMENTS

ABSTRACT

An enhancement of resolution for Angle of Arrival (AoA) estimation is useful for incoming radio waves received by uniform linear arrays (ULA). One of the modern techniques for determining the angle of any approaching or receiving target is the Root Eigenvector (R-EV).

The Root Eigenvector (R-EV) algorithm, which in this thesis is compared to the conventional method of Fast Fourier transforms (FFT), is one of the high-resolution methods for locating and finding angles. The angle of any approaching or receiving object's radiating wave with a small error rate compared to other methods of AoA.

The high-resolution algorithms concentrate on the distinct properties of the signal covariance matrix in addition to dividing the observation space into two subspaces, one for the signal and one for the noise.

Before starting to study the R-EV method, a few determinations for Angle of Arrival (AoA) parametric methods are present. These determinations preceded the R-EV in terms of the results achieved and the mathematical representation such as Pisarenko Harmonic Decomposition (PHD) and Multiple Signal Classification (MUSIC).

The R-EV and FFT methods are implemented in MATLAB environment. A range of studies have been simulated with different numbers of antennas, different values of angles. Different values for the distance between elements whether single or multiple sources. Also, these simulated results are analyzed to see the effect of changing these parameters on determining the Angle of Arrival using R-EV and FFT by calculating the percentage of error in each case.

The results proved the super accuracy of R-EV and achieved exceptionally low error rates even with the addition of noise the maximum error that got reached 4 % when M, number of samples (sensors) equal to 8. For the rest of the cases, the error rate did not exceed 2%,. In contrast, FFT did not achieve the same efficiency as R-EV because of having higher error rates and requiring a greater number of elements than R-EV.

TABLE OF CONTENTS

TABLE of FIGURES

LIST of TABLES

LIST of ABBREVIATIONS

Abbreviations	Name
AoA	Angle Of Arrival
AWGN	Additive White Gaussian Noise
DFT	Discreet Fourier Transform
DoA	Direction Of Arrival
DSP	Digital Signal Processing
DTFT	Discreet Time Fourier Transform
EGMs	Eigenvalue Grads Methods
EV	Eigen Vector
FFT	Fast Fourier Transform
IEDs	Improvised Explosive Devices
LP	Linear Prediction
ML	Maximum Likelihood
MUSIC	Multiple Signal Classification
PHD	Pisarenko Harmonic Decomposition
PSD	Power Spectral Density
R-EV	Root Eigen Vector
R-MUSIC	Root Multiple Signal Classification
SE	Spectral Estimation
SNR	Signal To Noise Ratio
SSLs	Single-Station Locators
T	Matrix Transpose

T_X	Transmitter
ULA	Uniform Linear Array
WWS	Wide-sense stationery

LIST of SYMBOLS

Symbol	Name
A	Matrix of Steering Vectors
c	Wave Speed
D	Dimension of Antenna
d	Distant between elements
f_c	Carrier Frequency
H	Complex Conjugate Transpose
I	Identity Matrix
L	Number of Sources
M	Number of Elements
n	Additive Noise
q	Matrix of Eigenvector
R_η	Auto Correlation Noise Matrix
R_x	Auto Correlation Signal Matrix
r_y	Auto Correlation Sequence
SE	Spectral Estimation
t	Propagation Time
u	Eigenvector
x	Source Signals
y	Receiver Signals
α	Geometric Phase Shift
θ	Angle of Arrival

γ	Wavelength
λ$_i$	Eigenvalues
σ	White Noise Variance
$\hat{P}$MU	MUSIC Estimation Frequency Function
$\hat{P}EV$	Eigen Vector Estimation Frequency Function
$\hat{P}PHD$	Pisarenko Estimation Frequency Function

CHAPTER ONE

Introduction and Literature Review

1.1 Introduction

The term "array signal processing" refers to the processing of information signals obtained from a network of sensors running in different environments (e.g., at ground level, above ground level, or underwater). There are various kinds of sensors, such as antennae for radio astronomy, radio communications, and radar, hydrophones for sonar, geophones for seismology, ultrasound, and X-ray detectors for medical imaging [1].

The sensors are developed with the same fundamental goal in each of these incredibly varied array signal processing applications: to act as an interface between the environment in which the array is embedded and the signal processing portion of the system [1], [2].

Since Newton's prism experiments with sunlight, spectrum estimation has involved assessing the power or energy distribution concerning the signal's frequency. Through these studies, Newton was able to prove that sunlight is made up of a band of colors, each of which has a unique wavelength[3]. The fast Fourier transform (FFT), an effective technique for computing the discrete Fourier transform, was rediscovered in 1965, marking a significant turning point for the field's future growth [4].

John Burg soon afterward published his work, which presented a completely novel method of spectrum estimate based on the maximum entropy concept. Many academics have followed up on his work over the following three decades, creating a plethora of novel spectrum estimation techniques and applying them to a wide range of physical processes from different scientific domains[5].

One of the significant and developing study areas in array signal processing is AOA estimation. The term "Angle-of-Arrival (AoA) estimation" describes the

procedure of determining the Angle for several electromagnetic radio frequency waves from the outputs of several receiving antennas that make a sensor array [6]. Radar, sonar, wireless communications, etc. are just a few of the many industries where AoA estimation is a significant issue in array signal processing.

The accuracy of this Angle of Arrival prediction significantly influences the effectiveness of antennas. It utilizes the digital output for each sensor array's output. A single fixed antenna used for AoA estimate has a low resolution, to improve parameter estimation and signal reception a variety of antennas is used. An array of antenna sensors performs better, increases accuracy, and enhances the resolution [7].

1.2 Literature Reviews

There are a lengthy history of research into AoA estimate techniques that reaches more than 40 years. Researchers have been trying to solve the issues related to AoA, that are accurately estimating the angles of arrival, reducing the transmitting power, and locating the beam in the desired direction.

In general, angle finding methods are categorized into Conventional methods and the Subspace methods.

The first method is the Conventional method, also known as the Classical method. For example, spatial filtering or beamforming was the initial method used to handle data gathered from an array of sensors in space-time.

The notion of colored space-time waveform transmission serves as the foundation for space-time coding. It permits the transmission of various waveforms with a broad angular coverage in various directions [8].

The traditional (Bartlett) beamformer, which goes back to the Second World War, merely applied spectrum analysis based on Fourier to spatiotemporally sampled data [9].

However, the spatial filtering strategy has several serious drawbacks, regardless of the available data collecting time and Signal-to-Noise ratio (SNR),

the performance of the device in question is particularly directly influenced by the physical size of the array (the aperture). The classical methods may be thought of statistically as spatial expansions of spectral Wiener filtering [10].

After that, the ability to resolve closely separated signal sources was improved using adaptive beamformers and traditional time delay estimation techniques [11]. With the expansion of time-delay estimating approaches to many signals (initially, these methods only employed two sensors), and the constrained resolution of beamforming, academics' interest in statistical signal processing has grown.

The output energy in the interference direction can be kept constant while the output energy in the desired direction is minimized using the Capon approach in 1969. Although this approach is reliable and does not require many sources in advance, its resolution falls short [12]. At this point, it is worth mentioning that the word "resolution" is employed casually. It refers to the ability to separate between two closely spaced signal sources [9].

The second category of AoA methods is the subspace Method or the High-resolution method. These methods outperform more traditional algorithms in terms of performance. The decomposition of the Covariance Eigen matrix into the Noise Subspace and the Signal Subspace is the foundation of this approach. The spatial spectrum of the antenna is determined using this method, and the direction of arrival is determined using the spatial spectrum peaks [13].

In 1973 Vladilen Fedorovich Pisarenko showed that second-order statistics may be used to retrieve AOAs. Pisarenko made the initial discovery of this technique while doing research on how to determine the frequencies of complex signals that are present in white noise. The Pisarenko Harmonic Decomposition Method try to lower the (MSE) Mean Square Error of the Output Array [14].

The minimal Norm Method, developed by Kumaresan and Tufts in 1982 [15], is an approach that is used to solve the AOA estimation issue in a way like

the MUSIC algorithm and is described as "the vector lying in the noise subspace whose first element is one having minimum norm".

The Min Norm approach attempts to solve the issue of high computational complexity, but it encounters difficulty in that it creates spurious peaks in other sites, which hinders the algorithm's efficiency [16].

The MUSIC algorithm suggested by Schmidt in 1986, the term "multiple signal classification" (MUSIC) referred to theoretical and experimental methods used to analyze signals received at antenna array elements to extract information about the characteristics of numerous wavefronts arriving there [17].

The Covariance Matrix was the most important component of the MUSIC method since it is divided into the noise subspace and the signal subspace using two separate orthogonal matrices. The covariance matrix is diagonal in this approach because it assumes that noise is significantly uncorrelated in every channel [18].

Because of its high-resolution capability, the MUSIC algorithm offers reliable performance and has been utilized extensively up to this point. Even though the MUSIC algorithm has many advantages, it is being constrained by several obstacles and competing with current methods. It is unable to detect the Direction of Arrival (DoA) of signals that are coupled because it is costly and computationally hard since it entails looking for peaks.

In 1990, a novel method for estimating direction from noisy multi-experiment data was presented, based on eigen analysis. This novel technique which is called the Method of Direction Estimation (MoDE) offers the performance of the Maximum Likelihood (ML) method (the MoDE and ML estimators coincide as the number of data samples increases), with a modest computational effort comparable to other eigen analysis-based techniques like the MUSIC algorithm [19].

In 1992 Friedlander and Weiss developed the concepts of spatial smoothing and array interpolation combined to create a computationally efficient estimate approach [20].

In 1995, by Serebryakov a new article was added to the AoA development based on examining the capacity of a minimal energy adaptive beamformer for communication to determine the positions of two narrowband sources with equal energy but near separation [21].

In 1997 Shaker Verlag released Haardt's outstanding PhD dissertation on array signal processing for DOA calculations. It gives a thorough analysis and investigation of the ESPRIT technique to make it easier for a reader to check on this important reference without being too confused [22].

In 2000 by Jingqing Luo and Zhiguo Zhang a set of extremely basic arithmetic known as the Eigenvalue Grads Methods (EGMs) is introduced in this study following some examination of the eigenvalues of the auto-correlation matrix, and the simulation results are compared with those of the AIC and MDL technique [23].

In 2004 new novel methodology by Chong-Ying and Yong-shun which estimates DoAs with high precision and does not need knowledge of the number of signal sources, uses the linear prediction (LP) or Pisarenko method in combination with the adaptive signal parameter estimation and classification technique (ASPECT). ASPECT is used to locate erroneous peaks in DoAs and can simultaneously count the number of signal sources. The approach allows for the reduction of computational complexity and the enhancement of spectral resolution [24].

In 2007, Zhang Xiaofei, and Lv Wen developed a unique approach for DoA estimation that fully utilizes the signal and noise subspaces. It performs better than MUSIC and Improved MUSIC and exhibits superior performance under low SNR, tiny snapshot, and coherent source circumstances. This approach is

resilient and widely used because, in addition to its low complexity, it is simple to implement [25].

In 2011, Aifei Liu, and Guisheng Liao proposed an entirely novel DoA estimation technique based on the eigen decomposition of an array output vector's conjugate and a covariance matrix created by the dot product of the array output vector and the latter. A technique provided to concurrently estimate the DoA and gain-phase errors without joint iteration by fusing the novel DoA estimation with the traditional gain-phase error estimation. Theoretical research demonstrates that the suggested approach behaves well regardless of phase errors and performs without dependence on phase faults [26].

In 2015, Pascal Vallet, Xavier Mestre, and Philippe Loubaton developed the MUSIC method. In the asymptotic regime, when the number of samples and sensors approaches infinity at the same rate, this study addresses the statistical performance of subspace AoA estimation using a sensor array. When the number of sources and their AoA stay constant, improved subspace AoA estimators known as developed MUSIC and demonstrated to be consistent and asymptotically Gaussian-distributed [27].

In 2018, Qingli Yan, Jianfeng Chen, and Geoffrey Ottoy is addressed in this paper the performance degradation issues of the Angle of Arrival (AoA)-based acoustic localization methods in the presence of unreliable bearing measurements (outliers) [28].

In 2020, Chudnikov and Shakhtarin in their paper discussed methods for the direction of arrival estimation (DoA) in MIMO radar sensors with a small antenna array with collocated elements. An algorithm for processing a data array in the "channel-range-speed" coordinates is presented in the context of signal sources localization with the main digital beamforming methods [29].

In 2023, Tobias Margiani, Silvano Cortesi presented a paper related to AoA, this work provided a thorough analysis and evaluation of Angle of Arrival (AoA) UWB measurements utilizing a small, low power integrated

a new commercial module with integrated Phase Difference of Arrival estimate[30].

1.3 Application for AoA

In many aspects of radio communications, direction finding is crucial. Most of them require determining an emitter's direction in relation to a predetermined reference direction (such as true north, magnetic north, or the heading of a ship, car, or airplane).

Fixing the location of emitters is one of the most crucial applications for direction finders. This may involve finding shipwrecked people, tracking down unauthorized signals like those from unlicensed base stations, unwanted emissions from industrial facilities, or even signals used to remotely detonate improvised explosive devices (IEDs). Radio position fixing is crucial in the field of military radio reconnaissance because it allows for the acquisition of tactical structure images, which are then used to evaluate the danger posed by an opponent.

Single-station locators (SSLs) only employ one direction finder, while two methods are applied. When using shortwave signals that travel via the ionosphere for position fixing, direction finders that measure both the azimuth and elevation of the incident wave must be used. The distance to the emitter may be calculated using an estimate of the virtual height of the ionosphere's reflecting layer; the intersection with the line of bearing (LOB) then provides the emitter location.

1.4 Aim of the Work

This research aims to study a new method for AoA estimation to obtain high accuracy in determining the angle and direction of the received signals.

The focus will be on a class of Eigenvector algorithms known as Root-Eigenvector (R-EV), and before starting to study this method, it is necessary to

make a quick study of the principles of AoA methods that led to Root-Eigenvector.

The study will contain an explanation of the receiving antenna system (Uniform linear array), the mathematical description of the previous methods gradually from the classical method: Fast Fourier Transform (FFT) to the modern method of Root-Eigenvector, and detailed MATLAB simulation results for each algorithm will be presented.

The thesis will focus on the following points:

1. researching the classical methods for AoA (FFT) and studying the basics of the high-resolution methods including Root-Eigenvector (R-EV) method and making a complete study.

2. Studying the eigenvector and eigenvalues of the autocorrelation matrix.

3. Performing the problem analysis for the two methods (Root-Eigenvector, FFT) and making a simulation using MATLAB.

4. Comparing the performance during changes in the parameters that affect the response of the methods.

1.5 Thesis Layout

This thesis is made up of several investigations that were conducted with these objectives. Five chapters provide a comprehensive study of the proposed method and a comparison to the classical method.

Beyond this introduction chapter, chapter two offers the background theory of frequency estimation that is separated into two parts: Traditional techniques DFT or FFT and Subspace approaches like PHD, MUSIC, and R-EV methods. Those methods of DoA estimate are contrasted with simulation results, as well as the mathematical description for the DoA estimation approach system developed in this thesis.

Chapter three and chapter four are demonstrated using the MATLAB program, Chapter three includes an investigation and comparison between the two methods of AoA estimations (FFT and Root-Eigenvector) without noise, Chapter four studies the effect of adding white noise to the signals, finally chapter five focuses on the conclusions and future works.

CHAPTER TWO

Theoretical Background

2.1 Overview

This chapter explains the basis of the working principles and theoretical background of the topics considered in this thesis. As a start, frequency estimation for AoA algorithms was studied, which was classified into two main parts:

(1) non-parametric like Fourier Transform,

(2) parametric like Pisarenko Harmonic Decomposition (PHD), MUSIC, and eigenvector.

Finally, the main method for the subject of this research is explained, Root-Eigenvector (R-EV). After that, Angle of Arrival (AoA) detailed study for the signal model and data model is illustrated, furthermore, a linear antenna array is used to describe this model. Finally, the Root-Eigenvector is employed to find the Angle of Arrival estimation.

2.2 Frequency Estimation

The process of estimating a signal's spectral density (sometimes referred to as its power spectral density) from a series of time samples is called spectral estimation.

Spectral estimation (SE) is one of the most important parts of the processing and interpretation of signals. It is considered a fundamental analysis tool with numerous uses. The following statement captures the core of the spectrum estimation issue: "Determine the distribution of total power over frequency from a finite record of a stationary data stream".

Most of the signals encountered in applications are such that their variation in the future cannot be known exactly; instead, it is only possible to make

probabilistic statements about that variation. The mathematical tool is used to describe such a signal of random sequence, which consists of an ensemble of realizations, each one having some associated probability of occurrence. Since the experimenter often only sees one realization of the signal out of the whole ensemble of realizations. Unfortunately, this is not feasible as, when seen as discrete-time sequences, the realizations of a random signal lack Discreate Time Fourier Transform (DTFT) since they lack finite energy. A random signal's average power spectral density used to describe it as random signals typically have finite average powers [31].

To distinguish between stationary and non-stationary signal for a random process $y(m)$, a process is said to be stationary if every single time the random variable at this time has the same density function; this signal is said to be strict sense stationary (SSS) if it is stationary for all orders $L > 0$ and has the same L^{th}-order joint density functions for processes $y(m)$ and $y(m + k)$.

Also, Wide-Sense Stationary (WSS) is another type of stationarity; and a random process; $y(m)$ is said to be wide-sense stationary if all three of the following requirements are met [32]:

1. The mean of the procedure is constant, $m_y(m) = m_y$.

2. The autocorrelation, $r_y(k, l)$ for the random variables $y(k)$ and $y(l)$ depends only on the difference, $(k - l)$, this difference is called the *lag,* $r_y(k, l) = Q_y(k - l)$

3. The process variance is finite, $c_y(0) < \infty$.

Additionally, it is supposed that a random process $y(m)$ is ergodic if, with probability one, all the statistical averages can be calculated from a single sample according to the function of the procedure. If temporal averages generated by a single realization are identical to statistical (ensemble) averages, the random process is effectively ergodic. It is possible to try and estimate group averages under these circumstances using temporal averages from one realization [32].The Discrete Fourier Transform (DFT) is a representation for

finite-length sequences that is an easy function of an integer variable, k, and can be computed using a digital computer. The M-point DFT for a finite-length sequence $y(m)$ of length M that equals zero outside of the interval $[0, M-1]$ is [32]:

$$Y_k = \sum_{m=0}^{M-1} y_m e^{\frac{-2\pi jkm}{M}} \quad , k = 0, 1, 2, \dots, M-1 , \qquad 2.1$$

where Y_k is the kth coefficient of the DFT that should be complex and y_m refers to the mth sample of the time series which consists of M samples and complex exponential.

For ease of notation 2.1, is frequently written as [32]:

$$Y_k = \sum_{m=0}^{M-1} y_m W^{mk} \quad , k = 0, 1, \dots, M-1 , \qquad 2.2$$

Where $W = e^{\frac{-2\pi j}{M}}$.

Since that y_m are sometimes values of a function at points for discrete time, the index k is often called the "frequency" of the DFT. The DFT is also known as the "discrete time, finite range Fourier transform".

The common inverse of the DFT exists, and as its form is extremely close to that of the DFT, the inverse of equation (2.1) [32] is:

$$Y_m = \frac{1}{M} \sum_{k=0}^{M-1} Y_k e^{\frac{2\pi jkm}{M}} . \qquad 2.3$$

This equation is called the inverse discrete Fourier transform (IDFT), since the FFT is an algorithm for efficiently computing the discrete Fourier transform (DFT) for the estimation of the frequency content of a discrete and finite time series, it makes use of the possibility of doing an iterative computation of the DFT's coefficient, which saves a significant amount of computing time [33].

The power spectrum density PSD defined as the DTFT of the covariance sequence [32]:

$$P(w) = \sum_{k=-\infty}^{\infty} R(k) e^{-jwk} . \qquad 2.4$$

Given the power spectrum, the autocorrelation sequence R(k) may be determined by taking the inverse discrete-time Fourier transform of $P(w)$ [32]:

$$R(k) = \frac{1}{2\pi} \int_{-\pi}^{\pi} P(w)e^{jwk}\, dw. \qquad\qquad 2.5$$

Therefore, the autocorrelation sequence of the Fourier transform is the power spectrum, estimating the power spectrum of FFT is like estimating the autocorrelation.

For an autocorrelation ergodic process also detriment using the time average[32]:

$$R_y(k) = \lim_{M\to\infty} \left\{ \frac{1}{2M+1} \sum_{m=-M}^{M} y(m+k)y^*(m) \right\}. \qquad\qquad 2.6$$

As a result, in principle, calculating the power spectrum is simple if *y(m)* is known for every *m*, as all that is required in computing the Fourier transform of the autocorrelation sequence $R_y(k)$ using equation (2.6) to estimate the autocorrelation sequence. However, there are two drawbacks to this strategy that make spectrum estimation a difficult issue. First, there is never an infinite quantity of data to deal with, and it is frequently very little. As is the case, such a restriction could be a defining feature of the data-collecting process. The second issue is that the data is frequently tainted by interference signals or noise, as a result, the challenge of spectrum estimation entails predicting $\widehat{P}_y(e^{j\omega})$ given a limited set of noisy y(m) data.

For example, if $y(m)$ is known and has p^{th} order autoregressive process, then the values measured from y(m) may be used for estimation of the parameters of the all-root model, $a_P(k)$, and these estimations of the parameters, $\widehat{a_p}(k)$, may then, in turn, be used to estimate of the power spectrum as follows[32]:

$$\widehat{P}_y(e^{j\omega}) = \frac{1}{\left| \sum_{k=0}^{p} \widehat{a_p}(k)e^{-jk\omega} \right|^2}. \qquad\qquad 2.7$$

Figure 2.1 shows the classification of AoA methods.
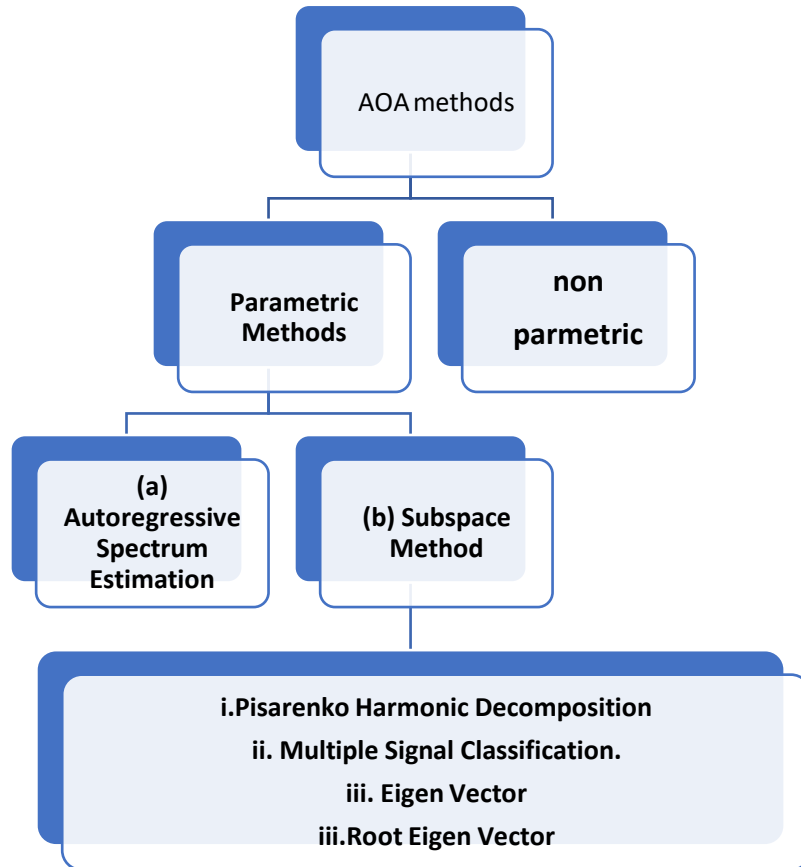
Figure 2.1 classification of AoA methods.

2.2.1 Non-Parametric Methods

The foundation of classical Angle of Arrival (AoA) techniques is beamforming. The beamforming approach's basic concept is to "steer" the array in a single direction at a time while measuring the output power. The maximum output power will be seen when the "steered" direction and a signal's AoA line up. The creation of a suitable output power that will be closely connected to the AoA is essentially what goes into developing AoA estimate systems[34].

The term "nonparametric" refers to an estimation that makes no assumptions about the way the data produced. Starting with the provided data, it estimates the autocorrelation sequence of the random process. Next, a Fourier transform of an approximated autocorrelation sequence used to determine the power spectrum. Following are several methods for estimating the

autocorrelation sequence for the process of an ergodic autocorrelation *y(m)* that is only recorded over a finite range, such as $m = 0, 1, ..., M - 1$.

Then, using the following, the estimation of autocorrelation sequence is calculated:

$$\hat{r}_y(k) = \frac{1}{M} \sum_{m=0}^{M-1} y(m + k)y^*(m) .$$ 2.8

The periodogram was the first type of nonparametric estimate proposed by Chuster in 1898.

The Fourier transform of the autocorrelation sequence is the wide-sense stationary random process's power spectrum, as given by the following equation:

$$P_y(e^{jw}) = \sum_{k=-\infty}^{\infty} r_y(k) e^{-jk\omega}$$ 2.9

Consequently, the estimate of the spectrum may be thought of as an autocorrelation estimation issue. Equation (2.9) uses the time average to calculate the autocorrelation for an ergodic autocorrelation and an infinite quantity of data.

However, the autocorrelation sequence may be obtained if $y(m)$ is measured over a limited range, where $m = 0, 1, ..., M - 1$ derived for equation (2.10).

It expresses as follows to ensure that the values of $y(m)$ that are outside of the range $[0, M - 1]$ are eliminated from 2.8:

$$\hat{r}_y(k) = \frac{1}{M} \sum_{m=0}^{M-1-k} y(m + k)y^*(m) , \text{k=0,1,...,M-1,}$$ 2.10

The discrete-time Fourier transform of $\hat{r}_y(k)$ yields a periodogram, which is an estimation of the power spectrum known as periodogram.

$$\hat{P}_{per}(e^{jw}) = \sum_{k=-M+1}^{M-1} \hat{r}_y(k)e^{-j\omega k} .$$ 2.10

Thus, $y_M(m)$ is the product of *y(m)* with a rectangular window w_R

$$y_M = w_R y(m)$$ 2.11

In terms of $y_M(m)$ the autocorrelation sequence estimation may be written as follows:

$$\hat{r}_y(k) = \frac{1}{M}\sum_{m=-\infty}^{\infty} y_M(m+k)y_M{}^*(m) = \frac{1}{M}y_M(k)y_M{}^*(-k) .\qquad 2.12$$

Taking the Fourier transform FT and using the convolution theorem, the periodogram becomes:

$$P_{per}(e^{jw}) = \frac{1}{M}\,Y(e^{jw})Y^*(e^{jw})^* = \frac{1}{M}\left|Y(e^{jw})\right|^2.\qquad 2.13$$

$Y^*(e^{jw})$ is a complex conjecture of $Y(e^{jw})$.

So, $Y_M(e^{jw})$ is the discrete-time Fourier transform of the M-point data sequence $y_M(m)$ as follows:

$$Y_M(e^{jw}) = \sum_{n=\infty}^{\infty} y_M(m)e^{-j\omega m} = \sum_{m=0}^{M-1} y(m)e^{-j\omega m} .\qquad 2.14$$

A crucial idea in the investigation of the performance of spectral estimators is resolution, which is the capacity to recognize spectral features, although the periodogram is straightforward to generate the power spectrum but resolution is constrained for short data records [35] .

When dealing with sufficiently long data lengths, the periodogram approach offers a considerable resolution; nevertheless, because of their large variance, which does not decrease with data length, they are poor spectrum estimators.

To enhance its statistical features, the periodogram has undergone a few documented revisions. These include the modified periodogram, the periodogram averaging Bartlett's approach, the modified averaging periodogram Welch's method, and the periodogram smoothing Blackman Turkey method [36]. One of the disadvantages of non-parametric methods for AoA estimation, the estimating technique is not intended to consider any potential process information that may be accessible. This feature may have importance in applications especially when information on how the data samples produced is

accessible therefore there was a need to a parametric method that estimates a collection of parameters for the received signal [34].

2.2.2 Parametric Methods

The estimation of frequencies contains two or more close frequencies signal problem and estimation of θ angle in AoA.

The following represent a study for some of Parametric Methods:

(a) Autoregressive Spectrum Estimation

This section gives a mathematical description of the Autoregressive (AR) process corrupted by additive (white) noise. In this section, the special case is considered in which the signal is sinusoidal corrupted by additive white noise [2].

In a communication system, the signal transferred to an array antenna is typically distorted by noise. These disturbances are often uncorrelated, but the pure signals that various elements receive are associated since they come from the same sources [37].

The following matrix can be utilized to represent the autocorrelation sequence. By considering that y is the sampled data vector [32]:

$$y = [y(0), y(1), y(2), \ldots, y(p)]^T, \qquad 2.15$$

Where the T is the transpose operator. Then, the autocorrelation matrix R_y of y is the correlation matrix becomes[32]:

$$R_y = E\{y\, y^H\}, \qquad 2.16$$

Where E { } is the statistical expression.

Equation (2.17) defines the degree of correlation of the data signals received by array elements * denotes complex conjugate transpose[32]:

$$R_y = E\{yy^H\}$$

$$= E \begin{bmatrix} y(0)y^*(0) & y(0)y^*(1) & \ldots & y(0)y^*(p-1) \\ y(1)y^*(0) & y(1)y^*(1) & \ldots & y(1)y^*(p-1) \\ \ldots & \ldots & \ldots & \ldots \\ y(p-1)y^*(0) & y(p-1)y^*(1) & \cdots & y(p-1)y^*(p-1) \end{bmatrix}, 2.17$$

$$= \begin{bmatrix} r_y(0) & r_y^*(1) & r_y^*(2) & \cdots & r_y^*(p) \\ r_y(1) & r_y(0) & r_y^*(1) & \cdots & r_y^*(p-1) \\ r_y(2) & r_y(1) & r_y(0) & \cdots & r_y^*(p-2) \\ \vdots & \vdots & \vdots & \cdots & \vdots \\ r_y(p) & r_y(p-1) & r_y(p-2) & \cdots & r_y(0) \end{bmatrix} \qquad 2.18$$

Taking the expected value and using the property of Hermitian, the autocorrelation sequence leads to producing the $p * p$ autocorrelation matrix.

The power spectrum related to a pth order autoregressive process[32]:

$$\mathbf{P_y}\left(e^{j\omega}\right) = \frac{|b(0)|^2}{\left|1+\sum_{k=1}^{p} a_p(k)e^{-jk\omega}\right|^2} \qquad 2.19$$

Thus, an estimate of the power spectrum may be obtained using the data provided by $b(0)$ that represent the Autoregressive coefficient, and $a_p(k)$ can be determined.

$$\widehat{\mathbf{P_{AR}}}\left(e^{j\omega}\right) = \frac{|\widehat{b}(0)|^2}{\left|1+\sum_{k=1}^{p} \widehat{a_p}(k)e^{-jk\omega}\right|^2} \qquad 2.20$$

Several methods are available for estimating the all-pole parameters, as autoregressive spectrum estimation necessitates the identification of an all-pole model for the process.

But each approach produces an estimate of the power spectrum in precisely the same manner, i.e., by using equation (2.20), once the all-pole parameters have been obtained. This discussion includes an overview of some of the characteristics of Autocorrelation modeling approaches and how they relate to spectrum estimation.

In the autocorrelation method of all-pole modeling, the autoregressive (AR) coefficients $\widehat{a_p}(k)$ in the all-pole modeling autocorrelation approach are found by solving the autocorrelation normal equations[32]:

$$\begin{bmatrix} r_y(0) & r_y^*(1) & r_y^*(2) & \cdots & r_y^*(p) \\ r_y(1) & r_y(0) & r_y^*(1) & \cdots & r_y^*(p-1) \\ r_y(2) & r_y(1) & r_y(0) & \cdots & r_y^*(p-2) \\ \vdots & \vdots & \vdots & \cdots & \vdots \\ r_y(p) & r_y(p-1) & r_y(p-2) & \cdots & r_y(0) \end{bmatrix} \begin{bmatrix} 1 \\ a_p(1) \\ a_p(2) \\ \vdots \\ a_p(p) \end{bmatrix} = \varepsilon_p \begin{bmatrix} 1 \\ 0 \\ 0 \\ \vdots \\ 0 \end{bmatrix} \qquad 2.21$$

The autocorrelation sequence of *y(m)* is known as

$$r_y(k) = \frac{1}{M} \sum_{m=0}^{p-1-k} y(m+k) y^*(m) \text{ , k=0,1, 2,...., p.} \qquad 2.22$$

Solving Eq. (2.21) for the coefficients $a_p(k)$, results in:

$$||b(0)|^2 = \varepsilon_p = \left| r_y(0) + \sum_{k=1}^{p} a_p(k) \hat{r}_y(k) \right|^2 \qquad 2.23$$

(b) Subspace Method

The data for a single signal is constrained to a one-dimensional subspace that is defined by the steering vector A (θ), if y(t)=A(θ)x(t) for the L signals, the observed data vectors y(t)=A(θ)x(t) are restricted to L-dimensional signal subspace is named the **signal subspace.** An array that receives signals that are distorted by noise is named the **noise subspace**. Normally, these disturbances are uncorrelated, however, the pure signals received by various components are correlated since they came from the same source. It may be possible to properly extract the AoA information by utilizing that property, and the spatial covariance matrix presented and used to identify AoA [38].

The parametric (subspace) approach, which predicated on the idea that the process may be characterized by a parametric model, is a conceptually distinct method of estimating the spectrum of a random process. The process spectrum then represents in terms of the model's parameters based on the model. The method therefore has three steps:

(1) choosing a suitable parametric model (typically predicated on prior information about the process).

(2) estimating the model parameters.

(3) computing the spectrum using the parameters so determined.

Because they may attain higher resolution than nonparametric approaches, parametric spectrum estimating techniques referred to as high-resolution techniques in the literature [5].

The high-resolution property is often possessed by approaches that rely on the decomposition of the observation space into signal and noise subspaces. When two signals, subject to how close they may be in frequency terms, can be separated (referred to as resolved or detected) despite the signal-to-noise ratio (SNR), it is say that the method has a high resolution. This is the case when the model is verified, and the number of samples used for the estimation of the correlation matrix and the observations tends to the infinite[39], [40].

In summary, these techniques depend on a set of the basic proven properties of the space matrix defined by R_{yy}, firstly, the space is classified into two sections subspace for noise and subspace for signal, the steering *A(θ)* vectors approach the signal subspace, finally, the noise subspace is spanned by the eigenvectors attached with eigenvalues that have a smaller value of the correlation matrix, unlike the signal subspace that attached with larger eigenvalues [41]. This section's focus is on these models, concentrating on the parameter estimation issue and implementation format.

i.   Pisarenko Harmonic Decomposition (PHD) Method

For estimating the frequency and magnitude, Pisarenko Harmonic Decomposition (PHD) algorithm is proposed [17]. Since it has several uses in high-resolution spectrum estimation and array signal processing issues, the Pisarenko harmonic decomposition (PHD) approach has lately drawn a lot of interest [42]. PHD analysis is mainly used to estimate the frequency and magnitude parameters of sinusoidal signals exposed to white noise [43]. Pisarenko proved that the frequencies may be obtained from the eigenvector corresponding to the least eigenvalue of the autocorrelation matrix based on

carathedory theory [32]. Before solving the matrix's eigenvalues and accompanying eigenvectors, a correlation matrix made up of the values of all sample points' autocorrelation functions must first be produced. Following these steps, the frequency value of each component may be calculated using the orthogonality between the signal space and noise space as identified by the eigenvectors. Finally, the equation for the autocorrelation function may be used to solve the magnitude value [43], [44].

In PHD method, it is assumed that q complex exponentials in white noise make up *x(m),* and that q is a known quantity. The eigenvector corresponding to the lowest eigenvalue spans the noise subspace, which has a size of one, $\lambda_{min} = \sigma_\eta^2$, Assuming that this noise eigenvector is denoted by the symbol u_{min}, it follows that each of the signal vectors $\boldsymbol{q_i}$, and they are orthogonal to each other[32]:

$$\boldsymbol{q_i^H u_{min}} = \sum_{k=0}^{L} u_{min}(k)e^{-jk\omega_i} = 0; \, for \, i = 1,2,3, \dots, L \qquad 2.24$$

let U_{min} be the kth component of $\mathbf{u_{min}}$,

$$U_{min}(e^{j\omega}) = \sum_{k=0}^{L} u_{min}(\alpha)e^{-jk\omega} = 0 \qquad 2.25$$

for each of the complex exponential frequencies w_i where $i = 1, 2, \dots, L$ is equal to zero. The noise eigenvector's z-transform, also known as an eigenfilter U_{min}, has L zeros on the unit circle[32]

$$U_{min}(z) = \sum_{k=0}^{L} u_{min}(k)z^{-k} = \prod_{k=1}^{L}(1 - e^{j\omega k}z^{-1}) \qquad 2.26$$

The roots of the eigen filter may be used to obtain the frequencies of the complex exponentials. Additionally, a frequency estimate function is explained as [32]:

$$\hat{P}_{PHD}(e^{j\omega}) = \frac{1}{|\boldsymbol{q^H u_{min}}|^2} \qquad 2.27$$

The powers P_{PHD} can be obtained from the eigenvalues of R_y by following the steps below once the frequencies of the complex exponentials have been identified. Let us assume that the signal subspace Eigenvectors $u_1, u_2, u_3, \dots, u_L$ so will become[32]:

$$u_i^H u_i = 1 \ , i \ = \ 1,2,\dots,L \qquad\qquad 2.28$$

$$R_y \, u_i = \lambda_i u_i \ , i \ = \ 1,2,\dots,L \qquad\qquad 2.29$$

$$R_y = R_x + R_\eta = \sum_{i=1}^{L} P_i q_i q_i^H + \sigma_\eta^2 I \qquad\qquad 2.30$$

The left side of Equation (2.29) is multiplied by the u_i^H, it will result:

$$u_i^H R_y \, u_i = \lambda_i u_i u_i^H = \lambda_i \ , i \ = \ 1,2,\dots,L \qquad\qquad 2.31$$

When the formula for R_y is include from Equation (2.30) into Equation (2.31), the equation get[32]:

$$u_i^H R_y u_i = u_i^H \left\{ \sum_{k=1}^{L} P_k q_k q_k^H + \sigma_\eta^2 I \right\} u_i = \lambda_i \ , \qquad\qquad 2.32$$

Equation (2.32) can summarize as:

$$\sum_{k=1}^{L} P_k \left| q_i u_k^H \right|^2 = \lambda_i - \sigma_\eta^2 \ , \qquad\qquad 2.33$$

$$\left| u_i q_i^H \right|^2 = \left| U_i \left(e^{j\omega k} \right) \right|^2 \ , \qquad\qquad 2.34$$

Where:

$$U_i \left(e^{j\omega k} \right) = \sum_{r=0}^{L} u_i(r) e^{-jlr\omega} \qquad\qquad 2.35$$

Equation (*2.36*) may be simplified to:

$$\sum_{k=1}^{L} P_k \left| U_i \left(e^{j\omega_k} \right) \right|^2 = \lambda_i - \sigma_{\eta}^2 \qquad 2.36$$

A collection of L linear equations with L unknowns:

$$\begin{bmatrix} \left| U_1\left(e^{j\omega_1}\right) \right|^2 & \left| U_1\left(e^{j\omega_2}\right) \right|^2 & \cdots & \left| U_1\left(e^{j\omega_L}\right) \right|^2 \\ \left| U_2\left(e^{j\omega_1}\right) \right|^2 & \left| U_2\left(e^{j\omega_2}\right) \right|^2 & \cdots & \left| U_2\left(e^{j\omega_L}\right) \right|^2 \\ \cdots & \cdots & \cdots & \cdots \\ \left| U_L\left(e^{j\omega_1}\right) \right|^2 & \left| U_L\left(e^{j\omega_2}\right) \right|^2 & \cdots & U_L\left(e^{j\omega_L}\right)|^2 \end{bmatrix} \begin{bmatrix} P_1 \\ P_2 \\ \cdots \\ P_L \end{bmatrix} = \begin{bmatrix} \lambda_1 - \sigma_{\eta}^2 \\ \lambda_2 - \sigma_{\eta}^2 \\ \cdots \\ \lambda_L - \sigma_{\eta}^2 \end{bmatrix} \qquad 2.37$$

The Pisarenko harmonic decomposition computationally requires determining the least eigenvalue and eigenvector of the signal autocorrelation matrix This might take a long time to compute for high-order issues, also It needs to know how many complex exponentials exist in the signal.

ii. Multiple Signal Classification Method (MUSIC)

In 1979, Schmidt introduced the Multiple Signal Classification technique (MUSIC), an advancement to the Pisarenko Harmonic Decomposition. Based on the characteristics of the signal and noise subspaces, it employs the eigenvectors decomposition and eigenvalues of the covariance matrix of the antenna array to estimate Angles-of-arrival of sources[45], [46]. Let R_y be the $M * M$ autocorrelation matrix of $y(m)$ with $M > L + 1$. If R_y eigenvalues are listed in descending order $\lambda_1 \geq \lambda_2 \geq \cdots \geq \lambda_L$ and if the related eigenvectors are $u_1, u_2, \ldots, u_L$, these eigenvectors are split into two groups: the $M - L$ noise eigenvectors that, in ideal situations, have eigenvalues equal to σ_{η}^2 and the L signal eigenvectors corresponding to the L biggest eigenvalues. It may be possible to calculate the white noise variance by averaging the $M - L$ lowest eigenvalues[47], [48]:

$$\sigma_{\eta}^2 = \frac{1}{M-L} = \sum_{k=L+1}^{M} \lambda_k \qquad 2.38$$

To calculate the complex exponentials' frequency:

$$U_i(z) = \sum_{k=0}^{M-1} u_i(k)z^{-k} \; ; i = L + 1, \dots, M \qquad\qquad 2.39$$

The frequency estimation function is used in the MUSIC method to average down the impacts of these false peaks [32]:

$$\widehat{P}_{MU}\left(e^{jw}\right) = \frac{1}{\sum_{i=L+1}^{M} |q^H u_i|^2} \qquad\qquad 2.40$$

$$\widehat{P}_{MU}(\theta) = \frac{1}{u_i{}^H(\theta)\, q\, q^H\, u_i(\theta)} \qquad\qquad 2.41$$

The AoA of wave fronts cannot be obtained directly using the MUSIC method. It must compute an average over all vectors of an orthonormal basis of the noise space to determine the precise angles of arrival of the signals. To put it another way, this function's speed and processing capacity are limited since it is necessary to compute the pseudo-spectral on the whole parameters space and look for its minima [28].

iii. Eigen Vector Method (EV)

For determining the frequencies of complex exponentials in noise, Johnson [49] presented the Eigen Vector (EV) approach in 1982 in addition to the Pisarenko and MUSIC methods.

The MUSIC algorithm and the EV have a close relationship. The EV technique specifically calculates the exponential frequencies from the eigen spectrum peaks [32]:

$$\widehat{P}_{EV}\left(e^{jw}\right) = \frac{1}{\sum_{i=L+1}^{M} \frac{1}{\lambda_i}|q^H u_i|^2} \qquad\qquad 2.42$$

The u_i is the eigen-vector related to the eigen-value λ_i ,if the autocorrelation and the White Gaussian Noise are known perfectly for then the eigen-values in the equation above are like the white noise variance σ_η^2 [32]:

$$\lambda_i = \sigma_\eta^2 \qquad\qquad 2.43$$

To a precise degree, the MUSIC pseudospectrum and the EV eigen spectrum will be identical, but with estimated autocorrelations the eigenvector

method differs from the MUSIC algorithm and appears to produce fewer spurious peaks.

iv. Root-Eigenvector Method (R-EV)

The EV and MUSIC technique have passed through several modifications to simplify, improve performance, and improve resolution. This is the situation with the linear and equidistant antenna array[50].

The benefit of R-EV is that it directly calculates the AoA by searching for polynomial zeros, eliminating the need to look for maxima in the case of MUSIC and Eigen Vector. This technique is only applicable to networks of regularly spaced linear antennas. Additionally, it makes use of certain characteristics of the received signals to shorten computation time and enhance angular resolution[40].

The input data covariance matrix R_{yy} is written as[50]:

$$R_{yy} = AR_{xx}A^H + \sigma_\eta^2 I_M \, , \qquad 2.44$$

Where R_{xx} is the signal correlation matrix, σ_η^2 is the noise common variance, and I_M is the identity matrix of rank M, A is a matrix formed by M steering vectors of sources, Suppose that the eigenvalues of R_{yy} are $\{\lambda_1, \dots, \lambda_M\}$ so that.

$$\left| R_{yy} - \lambda_i \, I_M \right| = 0 \qquad 2.45$$

Then, the substitution of 2.44 into 2.45 results:

$$\left| AR_{xx}A^H + \sigma_\eta^2 I_M - \lambda_i \, I_M \right| = 0 \qquad 2.46$$

Assume that $AR_{xx}A^H$ has eigenvalues e_i then:

$$e_i = \sigma_\eta^2 - \lambda_i \qquad 2.47$$

A has full column rank since it consists of an array's linearly independent steering vectors, and if the incident signals are not significantly correlated, the signal correlation matrix R_{xx} is nonsingular.

It can be demonstrated that the matrix $AR_{xx}A^H$ is positive semidefinite with rank L when the number of incident signals (L) is smaller than the number of elements (M) due to a complete column rank A and a nonsingular R_{xx}.

This suggests that e_i of $AR_{xx}A^H$, or $M - L$ of eigenvalues, are zero. According to Equation (2.47), $M - L$ of the R_{yy} eigenvalues are the least and equal to the noise variance σ_η^2.

$$\lambda_{L+1} = \cdots \lambda_{min} = \lambda_M = \sigma_\eta^2 \qquad 2.48$$

However, not every eigenvector corresponding to the noise space will be precisely the same when the autocorrelation matrix R_{yy} is computed from a limited data sample set of the received signals. Instead, as the number of samples used to get an estimate of R_{yy} increases, they will appear as a closely spaced cluster with a decreasing variation in their spread.

Each eigenvector q_i is linked to a certain eigenvalue λ_i as follows:

$$(\boldsymbol{R_{yy}} - \lambda_i \boldsymbol{I_M})\mathbf{q}_i = 0 \quad i = L + 1, L + 2, \dots, M \qquad 2.49$$

Regarding of these eigenvectors linked to the $M - L$ lowest eigenvalues, can obtain:

$$(\boldsymbol{R_{yy}} - \sigma_\eta^2 \boldsymbol{I_M})\mathbf{q}_i = AR_{xx}A^H\mathbf{q}_i + \sigma_\eta^2 \boldsymbol{I_M}\mathbf{q}_i - \sigma_\eta^2 \boldsymbol{I_M}\mathbf{q}_i \qquad 2.50$$

$$= AR_{xx}A^H\mathbf{q}_i = 0 \qquad 2.51$$

Since $\boldsymbol{R_{xx}}$ is nonsingular and $\mathbf{A}$ has full rank, this implies that:

$$\boldsymbol{A^H}\mathbf{q}_i = 0 \qquad 2.52$$

This indicates that the L steering vectors that comprise $\mathbf{A}$ are orthogonal to the eigenvectors linked to the M – L lowest eigenvalues.

So, the Root-Eigenvector is based on the idea of an orthogonal vector method that considers there is a vector, orthogonal to a matrix $\mathbf{A}$ ($\boldsymbol{i.e.,A^H q_i} = \boldsymbol{0}$), $\boldsymbol{q} = q_0, q_1, \dots, q_{M-1}$ which means that $\boldsymbol{q}$ **is** located in the noise subspace , given that the structure of the columns of A for the uniform linear array is

known and that the dot product of q with any of the i columns of A is zero, the dot product expansion that follows may be expressed as:

$$q\, a(\beta_i) = q_0 + q_1 e^{-j\beta_i} + q_2 e^{-2j\beta_i} + \cdots + q_{M-1} e^{-j(M-1)\beta_i} = 0 \quad 2.53$$

The polynomial of $u(z)$ is defined as:

$$q(z) = q_0 + q_1 z + q_2 z^2 + \cdots + q_{M-1} z^{M-1} = 0 \qquad 2.54$$

This analysis indicates that the covariance matrix R_{yy} eigenvectors correspond to two orthogonal subspaces: the non-principal eigen subspace (noise subspace) and the principal eigen subspace (signal subspace).

The steering vectors corresponding to the AoA are in the signal subspace and orthogonal to the noise subspace.

The AoAs may be found by looking through all potential array steering vectors to identify those that are perpendicular to the space that the non-principal eigenvectors span.

The noise eigenvectors must be arranged in a matrix to create the noise subspace $\mathbf{Q}_\eta = [\mathbf{q}_{L+1,\dots}, \mathbf{q}_M]$,the projection of the steering vector on the noise subspace for a linear antenna array with uniform spacing may be described by taking the inverse of $\alpha^H(\beta)\, \mathbf{Q}_\eta\, \mathbf{Q}_\eta^H \alpha(\beta) = 0$, [32]:

$$\widehat{P}_{EV}(\beta) = \frac{1}{\frac{1}{\lambda_i} \{\alpha_i^{\,H}(\beta)\, \mathbf{Q}_\eta\, \mathbf{Q}_\eta^{\,H} \alpha_i(\beta)\}} \qquad 2.55$$

The Root-Eigenvector algorithm's basic idea is to create a polynomial of degree $2(M-1)$ and retrieve its roots[51].

The Root-Eigenvector technique calculates all the roots, and it then uses the largest-magnitude roots inside the unit circle to estimate the signal AoAs [52].

As mentioned previously, $\mathbf{Q}_\eta$ is the noise eigen vector.

$$\Gamma_\eta = \mathbf{Q}_\eta\, \mathbf{Q}_\eta^{\,H} \qquad 2.56$$

$$P_{R-EV}^{-1}(\beta) = \frac{1}{\lambda_i} \{\alpha_i^{\,H}(\beta)\, \mathbf{Q}_\eta\, \mathbf{Q}_\eta^{\,H} \alpha_i(\beta)\} \qquad 2.57$$

$$P_{R-EV}^{-1}(\beta) = \frac{1}{\lambda_i} \{\boldsymbol{\alpha_i}^{\mathbf{H}}(\boldsymbol{\beta})\boldsymbol{\Gamma_\eta}\,\boldsymbol{\alpha_i}(\boldsymbol{\beta})\} \qquad\qquad 2.58$$

Using the representation of analytical expression for the steering vector $\alpha_k(\boldsymbol{\beta}) = e^{-j\beta(k-1)d}$ of the kth elements of the linear network (k=1,2 ,…, M), equation 2.58 can rewrite to be:

$$P_{R-EV}^{-1}(\beta) = \sum_{k=1}^{M}\frac{1}{\lambda_k}\sum_{h=1}^{M} e^{-j\beta(k-1)d}\Gamma_{kh}e^{j\beta(h-1)d} \qquad\qquad 2.59$$

Γ_{kh} is the element of the kth line and the hth column of Γ. By merging the two sums in 2.59, the following representation are obtain:

$$P_{R-EV}^{-1}(\beta) = \sum_{C=-M+1}^{M-1}\frac{1}{\lambda_C} \{\Gamma_C e^{-jC\beta d}\} \qquad\qquad 2.60$$

And $\Gamma_c = \sum_{k-h=C}\Gamma_{kh}$,Equation 2.94 can be written into R-EV polynomial which is a function of z represents by:

$$R(z)=\sum_{C=-M+1}^{M-1} D_C z^C \qquad\qquad 2.61$$

and

$$z = e^{-jd\beta} \qquad\qquad 2.62$$

2.3 Angle of Arrival (AoA)Estimation

The main goal of Angle-of-arrival estimation, also known as Angle finding, is to determine the angle at which electromagnetic (radio or acoustic) or auditory signals will impinge on a sensor or antenna array [53], [54]

In both military and civilian applications, such as search and rescue, seismology, and other fields, it is necessary to locate and monitor signal sources, this necessitates the use of AoA estimation.

Regarding AoA estimates, several theories and methods have been established for array signal processing that will be discussed until explain the main method in this thesis, known as the Root-Eigenvector method.

2.3.1 Data model for AoA

Most modern techniques for signal processing are model- based, meaning they make assumptions about the data that is seen in the actual world [34].

The following assumptions are:

- **Far-field assumption**

The far-field approximation assumes that the L signal sources are spaced apart from the array. So that, the signals formed by each source propagate to each element in an equal direction. Thus, the propagating fields of the L signals arriving at the array are parallel to each other.

This assumption can, in general, be realized by making the distance between the signal sources and the array much larger than the dimension of the antenna array. As a rule of thumb, the distance should be more than $d \gg \frac{2\mathrm{D}^2}{\gamma}$ where D is the array's size and γ is the wavelength of the signals.

- **AWGN channel**

A complex Additive White Gaussian Noise (AWGN) has been suggested to be the source of the noise in the AWGN channel. Additive, because it is

combined with any possible inherent information system noise, a zero means that a spatially uncorrelated random process that is uncorrelated with the signals is used to generate the additive noise. White refers to the notion that the information system's power spectral density is constant over the whole frequency range [55].

The noises are uncorrelated between all elements and have a common variance σ_N^2 Throughout the whole array.

- **Transmission Medium**

The signals are produced by L sources, pass through a medium, and then meet an M-element antenna or sensor array. It is assumed that the transmission medium between the sources and the array is linear and isotropic, meaning that the medium's physical characteristics are the same in all directions; signals or waves at any given place may be superimposed linearly; the position of the target in relation to the antenna system and the direction of signal transmission have no effect on the medium's characteristics[29].

A signal traveling through the medium and then impinging on or being received by any element of the M-element array can be computed as a linear superposition of signals wavefronts produced by the L source element because the medium's isotropic and linear characteristics, which guarantees two things,

First, the propagation property of the waves does not change with the DOAs of signals, and second, the DOAs of the signals do not affect the wave propagation properties of the waves. Additionally, it is assumed that each receiver elements piece has a gain of one.

- **Narrowband Approximation**

The signals come from various sources, but since they share a carrier frequency f_c, their frequency contents are concentrated close to that frequency. Any one of the instantaneous signals with respect to *r* that refer to narrowband coming from the sources can be described mathematically as[40]:

$$x_i^r(t) = a_i(t)cos[2\pi f_c t + \beta_i(t)], \ 1 \leq i \leq L \qquad 2.63$$

The signals are narrowband as long as their amplitudes a_i (t), and information-bearing phases β_i (t) vary slowly with respect to τ, where is the propagation time of the wave signals between elements[40]. Otherwise:

$$a_i(t - \tau) \approx a_i(t) \text{ and } \beta_i(t - \tau) \approx \beta_i(t), \qquad 2.64$$

The Fourier transform in equation 2.63 has most of its frequency components close to the carrier frequency fc ensured by the slow varying of $a_i(t)$ and phases $\beta_i(t)$. A phrase that works well can get a mathematical analysis by defining the complicated signal's or phasor's envelope[40]:

$$x_i^{env}(t) = a_i(t)e^{j\beta_i(t)} \qquad 2.\,65$$

Such that

$$x_i^r(t) = Real\{x_i^{env}(t)e^{j2\pi f_c t}\}, \qquad 2.66$$

Most receivers, which divide the received signals into in-phase (the real portion) and quadrature (the imaginary part) components, enable this type of complex (or analytical) signal.

Figure 2.2 represents the configuration of the system and explains the four assumptions, d acts the distance between the source and the first (antenna) element.
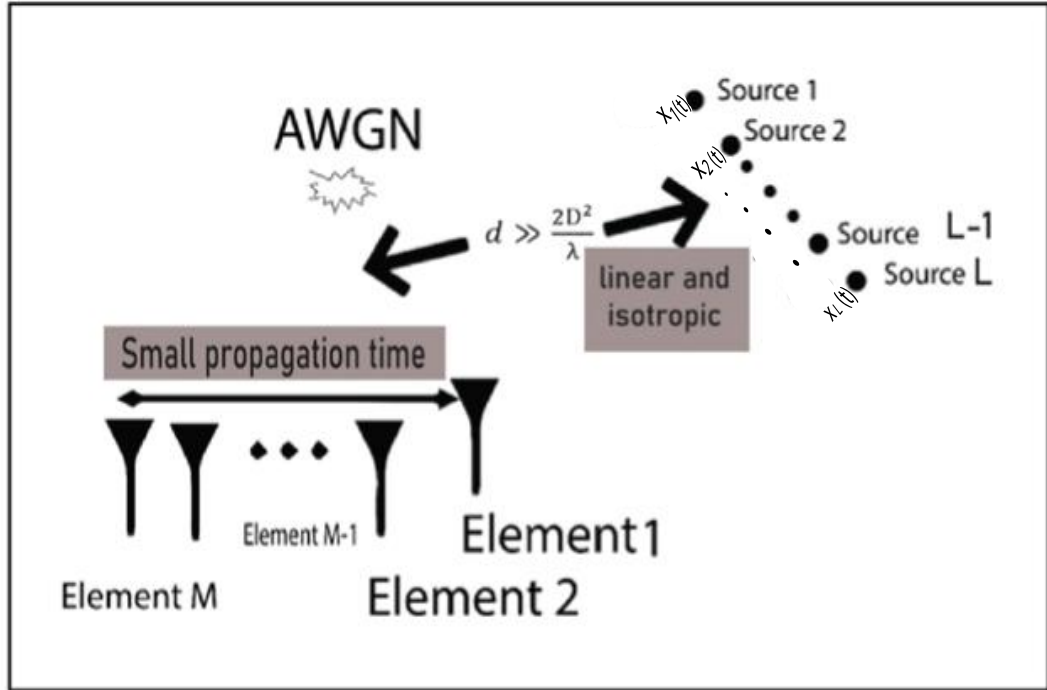
Figure 2.2 Data model for AoA with some assumption [56]

2.3.2 Linear Antenna Array

A collection of antennas located in a certain arrangement used for sending or receiving the same signals is known as an antenna array. When the distance between elements is equal, it is also known as a Uniform Linear Antenna array (ULA). A common term for each antenna in an array is an element transducer or sensor [57], [58].

Each transducer changes the received electromagnetic wave or mechanical vibration into a voltage. The signals that all the array members in ULA have received will be processed for several purposes, including the AoA estimates.

The reason for using this type of antenna is to offer several advantageous characteristics, such as the ability to apply fast subspace algorithms, like Root-Eigenvector (R-EV), to improve computing efficiency. Typically, increasing the array aperture is preferred to increase resolution. When the ULA's inter-element spacing is fixed, this can be accomplished by adding more sensors.

The uniform linear array geometry consists of M elements numbered 0, 1, …, M-1. The numbers and spacing of a ULA's components have a significant impact on the array performance. More electromagnetic fields can be collected by a big array than by a small array. So, the array performance of a ULA is strongly influenced by the numbers of sensors and spacing of its elements [59].

The Nyquist sampling theorem states that two samples are needed for each period of the signal's highest-frequency Fourier component. In this instance, every wavelength requires two spatial samples, resulting in an element spacing of d=0.5 γ.

For numbering items, the right antenna is known as element-1 and represents the reference item; the second and third antennas are known as element-2 and element-3, respectively, from right to left until reach the last antenna, element-M.

The distance between any two antennas is represented by d, and the waves received by the array at the angle are represented by θ.

The receiving path from the source to the second and third element is longer than the path of the source to the first element (reference) and equal to:

$$c_m = (m-1)d.\sin\theta \quad , \text{m=1,2 ,3} \qquad 2.\,67$$

$$c_2 = d.\sin\theta \qquad 2.\,68$$

$$c_3 = 2d.\sin\theta \qquad 2.\,69$$

In this case, let's suppose that the reference element received a wave signal:

$$y_{1=}x(t) \qquad \textit{2. 70}$$

The signals obtained by antenna 2 and 3 may therefore be expressed as follows:

$$y_2 = xe^{-j\varphi c_2} = xe^{-j\frac{2\pi d}{\gamma}\sin\theta} \qquad 2.\,71$$

$$y_3 = xe^{-j\varphi c_3} = xe^{-j2\frac{2\pi d}{\gamma}\sin\theta} \qquad 2.72$$

Here $\varphi = \frac{2\pi}{\gamma}$ is the phase shift constant for propagating waves in air with the wavelength of propagating γ .
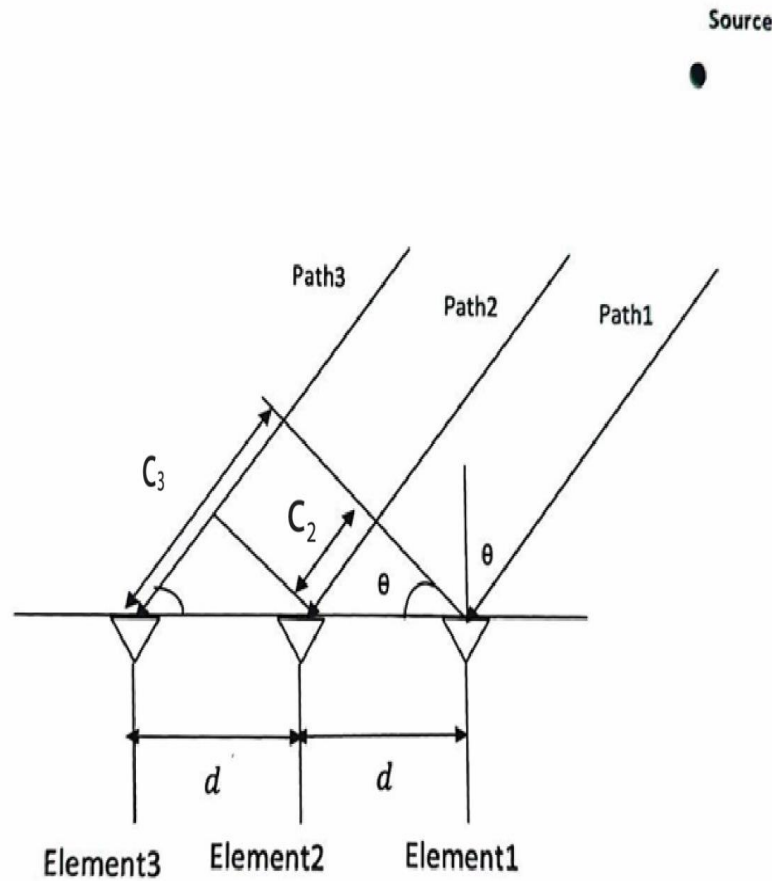
Figure 2.3 three antennas array configuration

The signals received by the three components may be expressed in a more generic form as:

$$y=\begin{bmatrix} y_1 \\ y_2 \\ y_3 \end{bmatrix} = \begin{bmatrix} 1 \\ e^{-j\frac{2\pi d}{\gamma}sin\theta} \\ e^{-j2\frac{2\pi d}{\gamma}sin\theta} \end{bmatrix} x = \begin{bmatrix} 1 \\ e^{-j\mu} \\ e^{-j2\mu} \end{bmatrix} x = \alpha(\mu)x \qquad 2.73$$

Let $\mu=\frac{2\pi d}{\gamma} sin\theta$ and *as* mentioned previously $\alpha(\mu)$ is the steering vector.

An M-element array can be included in equation 2.73 it may be written as follows:

$$y = \begin{bmatrix} y_1 \\ y_2 \\ ... \\ y_M \end{bmatrix} = \begin{bmatrix} 1 \\ e^{-j\frac{2\pi d}{\gamma}\sin\theta} \\ ... \\ e^{-j(M-1)\frac{2\pi d}{\gamma}\sin\theta} \end{bmatrix} x = \begin{bmatrix} 1 \\ e^{-j\mu} \\ ... \\ e^{-j(M-1)\mu} \end{bmatrix} x = \alpha(\mu)x \qquad 2.74$$

and the steering vector for M-elements:

$$\alpha(\mu) = \begin{bmatrix} 1 & e^{-j\mu} & ... & e^{-j(M-1)\mu} \end{bmatrix}^T \qquad 2.75$$

2.3.3 Signal Model of AoA

A signal model suppose a radar system with an array of M sensors $y_1, y_2, ..., y_M$ (antenna components) that receives signals in all directions from L sources $x_1, x_2, ..., x_L$ (targets),M > L The signals detected can be represented as[40] :

$$\mathbf{y(t)}=\mathbf{A}(\theta)\mathbf{x(t)}+ \text{ŋ (t)} \qquad 2.76$$

where y(t) is the M×1 received elements data vector[38]:

$$\mathbf{y(t)} = [y_1, y_2, ..., y_M]^T \qquad 2.77$$

x(t) is the L×1 source signal vector[38]:

$$\mathbf{x(t)}= [\, x_1, x_2, ..., x_L]^T \qquad 2.78$$

noise vector ŋ (t) is an M×1 uncorrelated zero-mean white noises with spatial a covariance matrix that equals to

$$\text{ŋ (t)}= [\text{ŋ}_1, \text{ŋ}_2, ..., \text{ŋ}_M]^T \qquad 2.79$$

A (μ) is an M*L matrix that of steering vectors:

$$\mathbf{A}(\boldsymbol{\mu_i}) = [\, \alpha(\mu_1), \alpha(\mu_2), ..., \alpha(\mu_L)], 1 \le_i \le L \qquad 2.80$$

$\alpha(\mu_i)$ is the geometric phase shift defined at the element of the network and signal depending on the angles of arrival (θ_i).

So,

$$\alpha(\mu_i) = \begin{bmatrix} 1, e^{\frac{-j2\pi d \sin(\theta_i)}{\gamma}}, ..., e^{\frac{-j2\pi d(M-1)\sin(\theta_i)}{\gamma}} \end{bmatrix}^T , \qquad 2.81$$

Where d is the Array Element Spacing, γ is the wavelength of propagating signals, θ_i is the angle of arrival of the target signal from the Lth source.

2.3.4 AoA Problem Formulation

To simplify the problem, suppose the system have a plane wave result from source L falls on array at an angle θ_0 as shown in fig.2.3. The received signals are propagated on all the elements (antennas) of the array and archive an extra distance comparing with the reference element [38].

To find the distance, the following equation can be used:

$$C_{mi} = (m - 1)dsin\theta_i \, , 1 \leq_i \leq L \qquad\qquad 2.\,82$$

Notice that the signal received by the M elements is the same as the transmitted signal by L elements, but there is a phase shift with amount of $e^{-j(m-1)\mu_i}$.
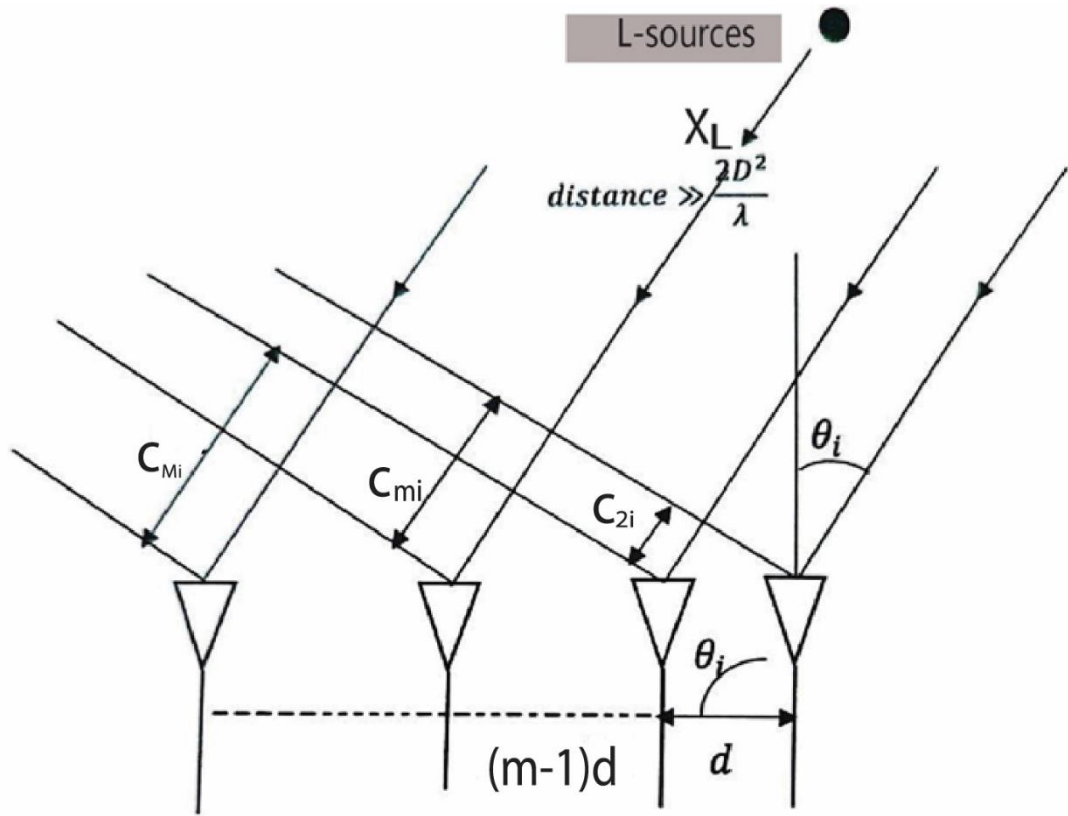
Figure 2. 4 M- antennas array configuration

These factors affected by two functions:

1. spatial frequency μ_i that is limited by $-\pi \leq \mu_i \leq \pi$

2. element's position with respect to the first element.

For each incoming signal there is an angle θ_i that limited by $-90 \leq \theta_i \leq 90$ and this angle have a special frequency μ_i .

Also, the element spacing should be less than $\frac{\gamma}{2}$, if this condition does not achieve, solutions put for the angle that is determined special frequency μ_i.

The received M signal and their noises η_n are deliver from L source x_i, $1 \leq i \leq L$ can be represent as:

$$Y_m = \sum_{i=1}^{L} x_i e^{-j(m-1)\mu_i} + \eta_m , \text{ m=1, 2,..., M} \qquad 2.83$$

The symbol **Y** used to distinguish between the pure signals created by the sources and the noise-added or corrupted signals received or identified. The matrix representation of Equation (*2. 83)* is as follows[38]:

$$Y = [\,\alpha(\mu_1), \alpha(\mu_2), \alpha(\mu_3), \ldots, \alpha(\mu_L)]\begin{bmatrix} x \\ x_2 \\ \ldots \\ x_L \end{bmatrix} + \eta = Ax + \eta \qquad 2.84$$

Where $Y = [y_1, y_2, \ldots, y_M]^T$ is the data vector received by the arrays, the array steering vector that is dependent on spatial frequency μ_i is define as:

$$\alpha(\mu_L) = \begin{bmatrix} 1 & e^{-j\mu_i} & e^{-j2\mu_i} & \ldots & e^{-j(M-1)\mu_L} \end{bmatrix}^T, \qquad 2.85$$

They contain the steering matrix M*L:

$$A = [\,\alpha(\mu_1), \ldots, \alpha(\mu_L)], \qquad 2.86$$

$$= \begin{bmatrix} 1 & 1 & \ldots & 1 \\ e^{j\mu_1} & e^{j\mu_2} & \ldots & e^{j\mu_L} \\ \ldots & \ldots & \ldots & \ldots \\ e^{j(M-1)\mu_1} & e^{j(M-1)\mu_2} & \ldots & e^{j(M-1)\mu_L} \end{bmatrix}, \qquad 2.87$$

Figure 2.5 represents angle of arrival flow chart that act the procedure for the process followed in this work starting from receiving the signals by uniform linear array until getting the required estimated angle by using Root eigen vector.
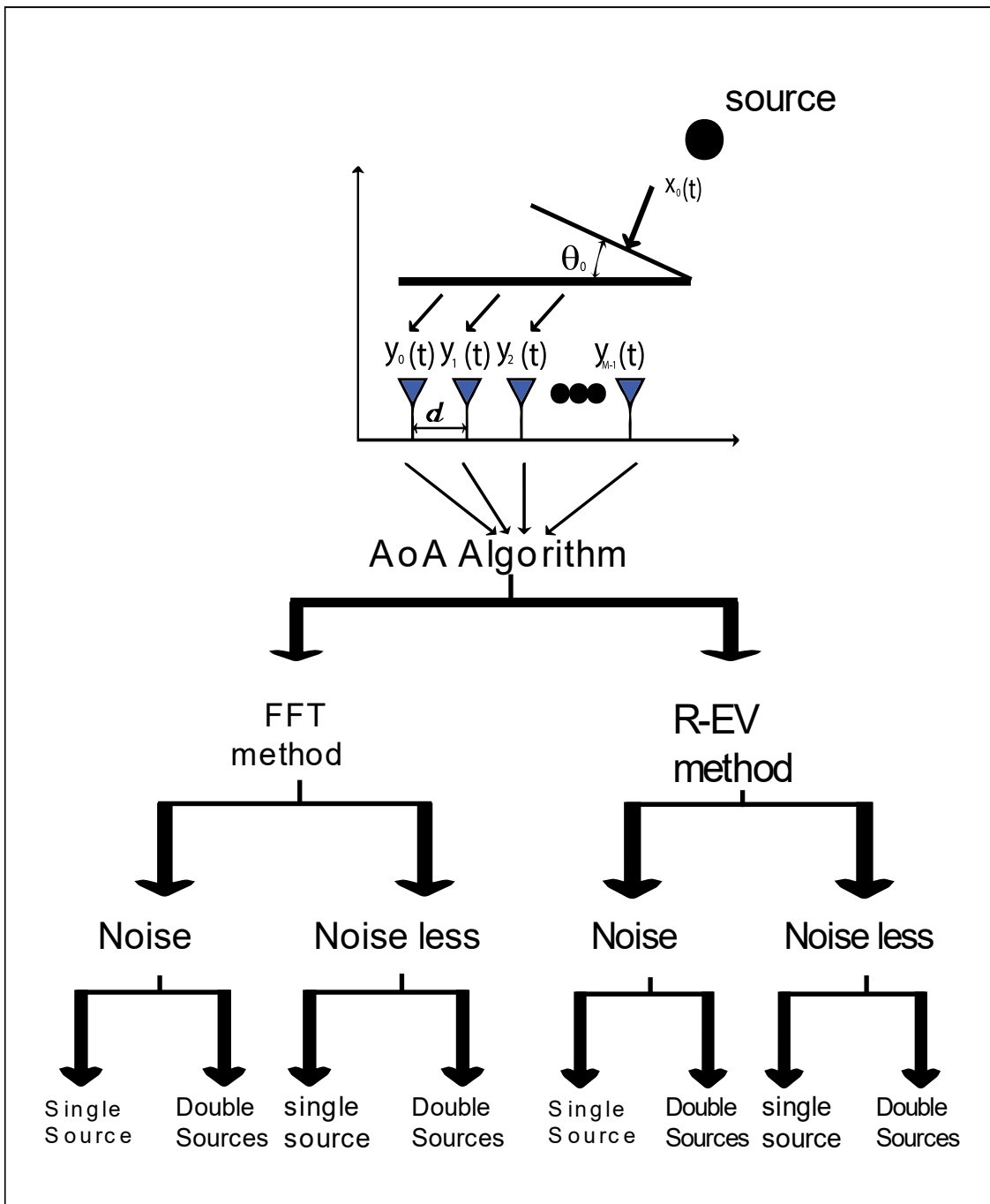
Figure 2.5 The flow chart for AoA

2.3.5 Root-Eigenvector Method for AoA Estimation

In this section of the thesis, the method of root eigenvector to find the angle of arrival estimation is employed.

For $i = 0, 1, \ldots, r - 1$, the polynomial u(z) evaluated at $e^{-j\omega_i}$ is zero, according to equations (2.53) and (2.54). The roots of $q(z)$ may be used to drive θ_i since the angles, ω_i, of these roots are functions of the AoAs (given $that$ $\omega_i = 2\pi d sin(\theta_i)$).

The orthogonal vector methods are summarized as:

1. The first thing to do is to compute any vector that is in the noise subspace.

2. The components of that vector then become the coefficients of a polynomial that is created.

3. The AoAs are calculated using the roots of the polynomial that lie on the unit circle.

Using the representation of analytical expression for the steering vector $\alpha_k(\boldsymbol{\beta}) = e^{-j\beta(k-1)d}$ where $\beta = \frac{2\pi sin\theta}{\gamma}$, substituting β into the equation$\alpha_k(\beta)$ results $\alpha_k(\theta_i) = e^{\frac{-j2\pi(k-1)dsin\theta_i}{\gamma}}$ of the kth elements of the linear network ($k = 1, 2, \ldots, M$), γ is the wavelength for the signals received by ULA and d is the spacing of elements.

Equation 2.58 can rewrite to be:

$$P_{R-EV}(\theta) = \sum_{k=1}^{M} \frac{1}{\lambda_k} \sum_{h=1}^{M} e^{\frac{-j2\pi(k-1)dsin\theta}{\gamma}} \Gamma_{kh} e^{\frac{j2\pi(h-1)dsin\theta}{\gamma}} \qquad 2.88$$

W_{kh} is the element of the kth line and the hth column of Γ. By mix the two sums in Equation 2.88, we obtain the following representation:

$$P_{R-EV}(\theta) = \sum_{N=-M+1}^{M-1} \frac{1}{\lambda_N} \{\Gamma_N e^{\frac{-j2\pi Ndsin\theta}{\gamma}}\} \qquad 2.89$$

and $\Gamma_N = \sum_{k-h=N} \Gamma_{kh}$,Equation 2.89 can be written into Root-EV polynomial which is a function of z represent by:

$$R(z)=\sum_{N=-M+1}^{M-1} \frac{1}{\lambda_N} \{\Gamma_N z^N\}$$

2.90

and $z = e^{\frac{-j2\pi d\sin\theta}{\gamma}}$

Angle-of-arrival of received signals being functions of *z,* calculating the polynomial's (M-1) double roots, whose usable zeros are so on the unit circle, is the issue. These intricate roots' phases line up with the anticipated variations in electric phase. The following equation may then be used to calculate the angles of arrival of signals:

$$\Theta_k = -\sin^{-1}\left[\frac{\gamma}{2\pi d}\arg(z_k)\right]$$

2.91

where is the m closest roots to the unit circle.

CHAPTER THREE

Simulation Results without Noise

3.1 Overview

In this chapter, the simulation results for Angle of Arrival (AoA) estimation methods using MATLAB program are presented, which focus on non-parametric method (FFT) and parametric methods Root_Eigenvector (R-EV) and Eigen Vector (EV).

Various cases are studied using single source and double sources without noise with a different number of antennas that form the uniform linear arrays. For every case the results, discussion, and a comparison will be presented.

Also, a comparison between Root_Eigenvector (R-EV) and the classical method Fourier Transform (FFT) in terms of resolution, accuracy, and complexity. Also, EV is used to implement the spectrum of the signals.

3.2 Simulation Results for Single Source AoA Estimation without Noise

As a start, the simulation is presented for a single source without noise using the two methods of FFT and R-EV, the following variables' values are used in MATLAB program: the spatial sampling interval d is equal to 0.8 cm, the wavelength is equal to 2, the numbers of elements are variable, and the values of angles are variable in different cases.

Firstly, when (FFT) method is used, the angle theta (Θ) is set to 20° as shown in Fig. 3.1 and another angle theta (Θ) is set to 50° in Fig. 3.2.

The angles in these figures are clear but there is a group of sidelobes that affect the accuracy of the required angles. In Fig. 3.1-the number of elements M is limited to 8 in the ULA receiving system, and in Fig. 3.1-b M is equal to 16, the beam is wide because of the uncertainty in estimating AoA. The uncertainty causes problem in estimating AoA for the application that requires precise angles values like military. As the number of elements increases the width of the

required peak becomes less but at the expense of complexity and the same illustration applies to the case in Fig. 3.2.
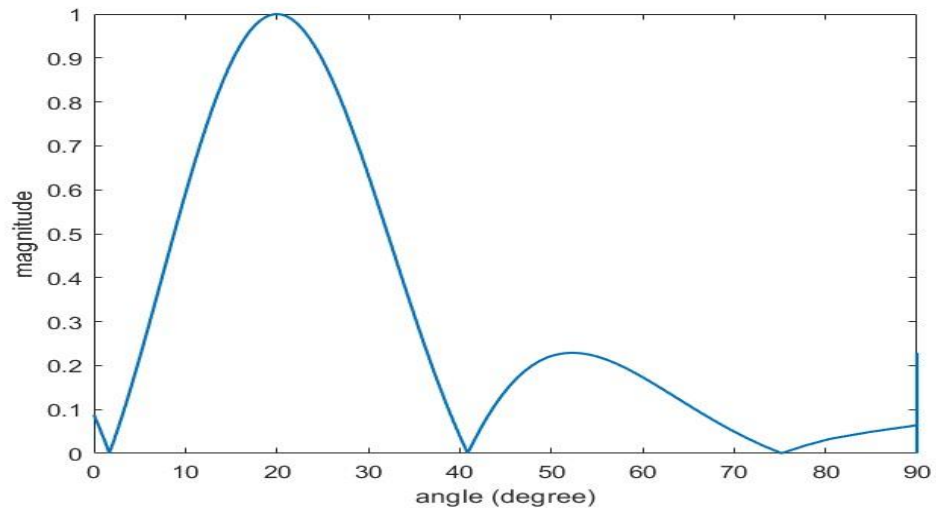
(a)
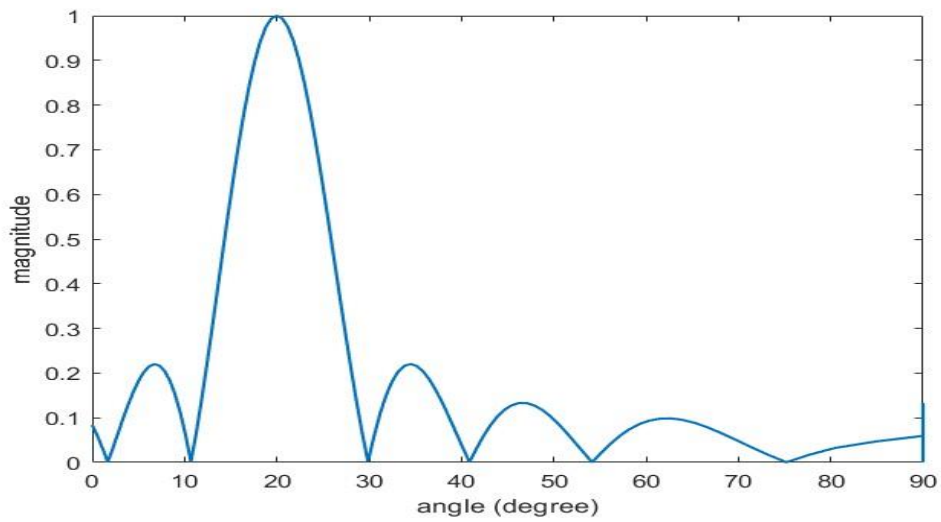
(b)

Figure 3. 1 Single-source simulation using FFT using a Ө =20° without noise at (a) M = 8 and (b) M = 16.
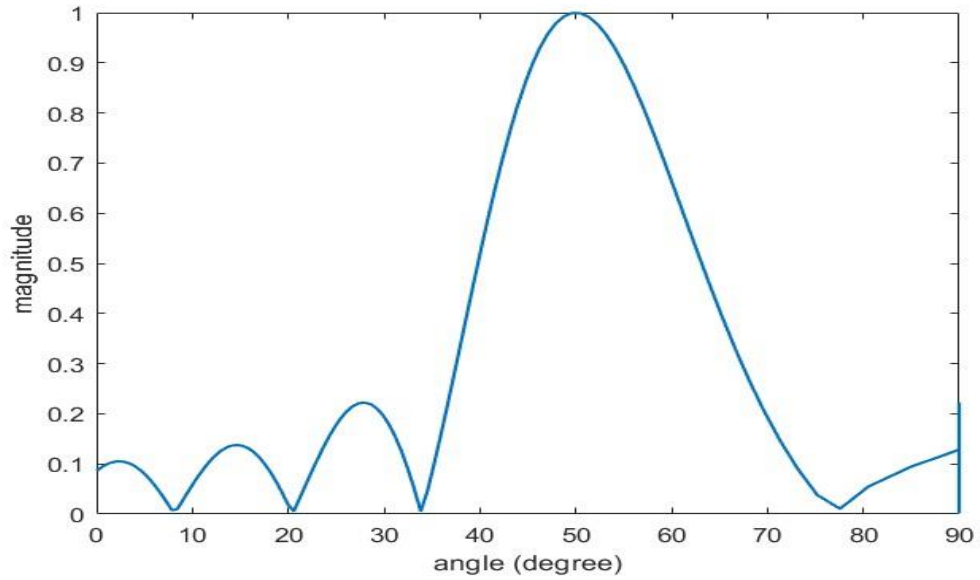
(a)
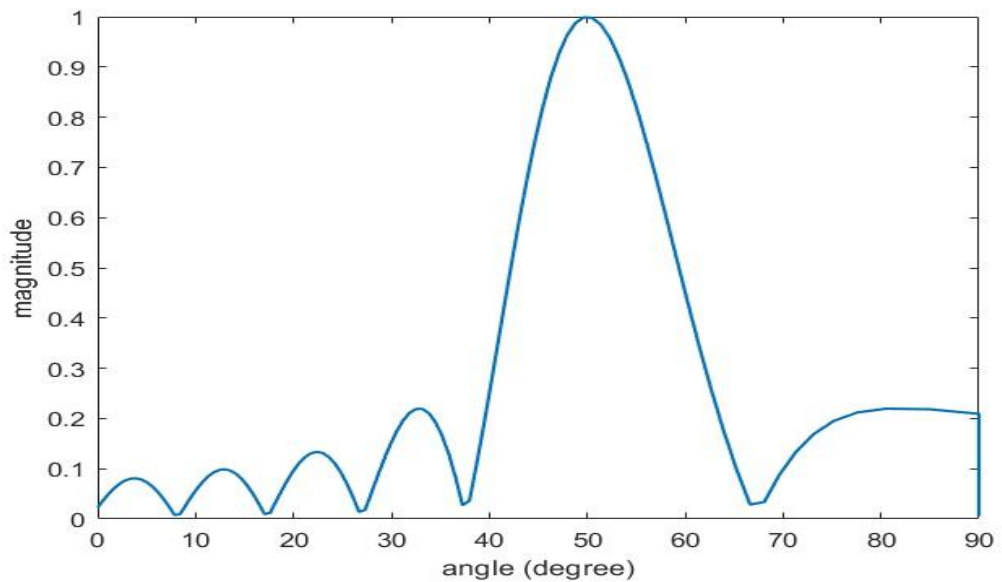
(b)

Figure 3.2 Single-source simulation using FFT using Θ =50° without noise at (a) M = 8 and (b) M = 16.

After that, the efficiency of FFT method using a negative angle (-20) in Fig. 3.3 -a and Fig. 3.3 -b is examined. Moreover, it is possible to find the angles values, but with the presence of a group of small peaks in addition to the required peak that may cause some confusion in the resulted information of the signal.
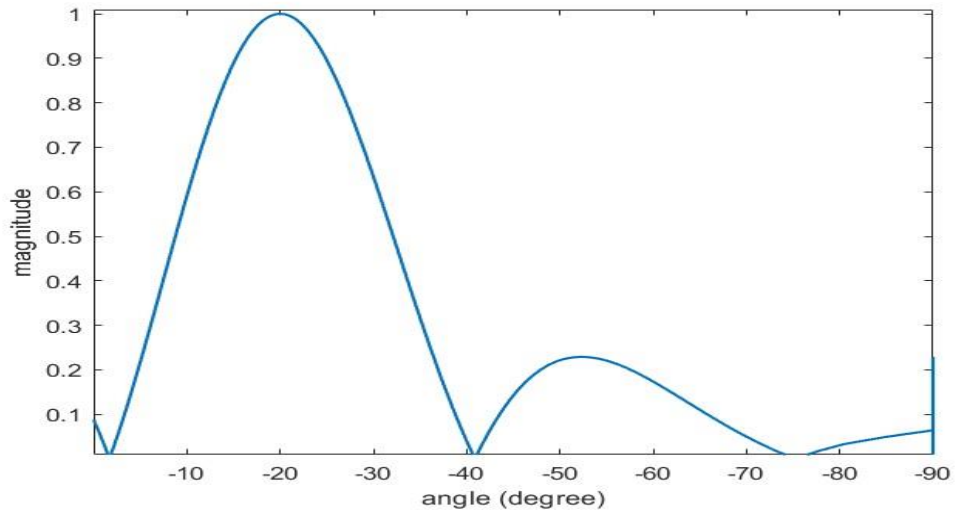
(a)
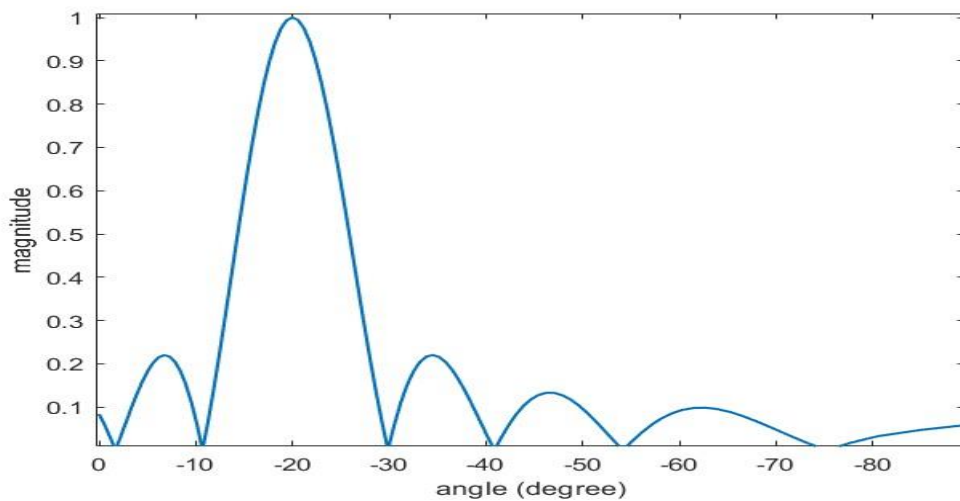
(b)

Figure 3.3 Single-source simulation using FFT using Ɵ =-20° without noise at (a) M = 8 and (b) M = 16.

Then, the high-resolution method Root-Eigenvector (R-EV) is used, the required angle is equal to 20° and maintained an accurate value for the estimated angle that equal to 20°, that is mean it achieved error percentage equal to zero with several elements of less than 10.

In Figure 3.4, using Eigen Vector (EV) method the spectrum is plotted, A comparison between the two forms in Figs. 3.4-a and 3.4-b are presented; there is no noticeable difference, and a number of antennas of less than 9 is enough to get the true value. Also, there are no sidelobes beside the highest peak, and there

is no need to increase the number of elements more than ten, because 8 elements give an acceptable result.
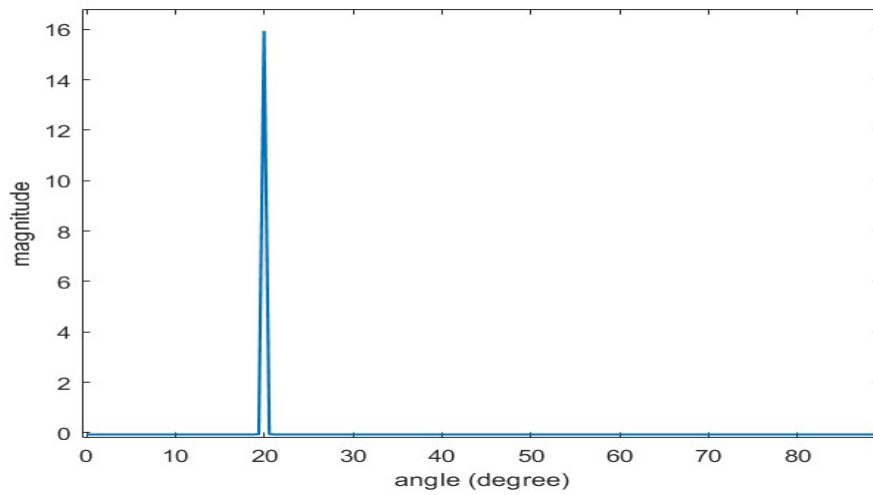
(a)
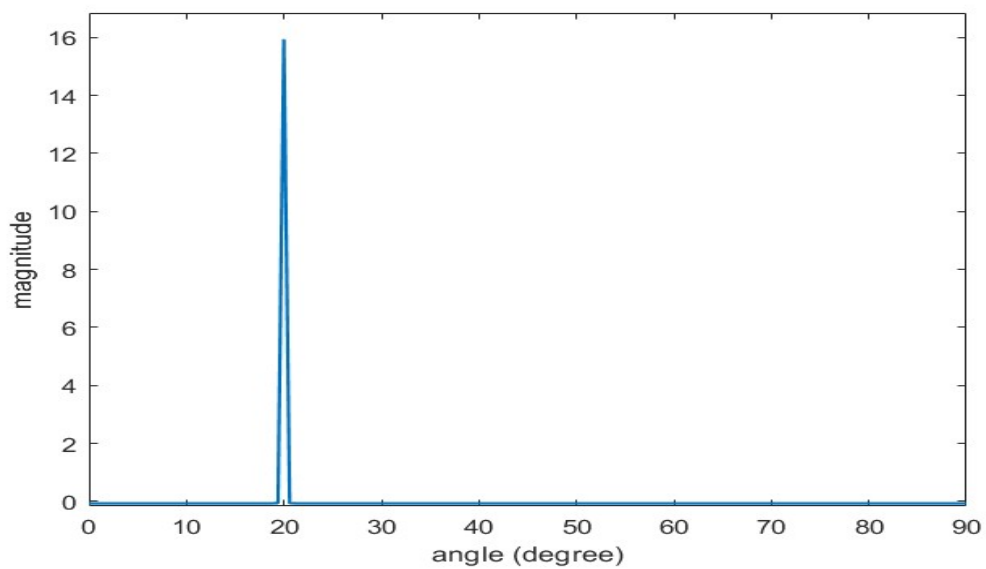
(b)

Figure 3.4 Single-source simulation using EV using Θ =20° without noise at (a) M=8 (b) M=16

The performance of Root Eigenvector method (R-EV) is examined but on the negative angle by specified the angle to -20° and also we maintained an accurate value for the estimated angle that equal to -20°, with error equal to zero %.

Therefore, the eigenvector (EV) spectral estimation method is implemented for the negative angles in Figs. 3.5-a and 3.5-b are obtained, and the negative angle value -20 directly and with a small number of antennas that is equal to 8 elements.
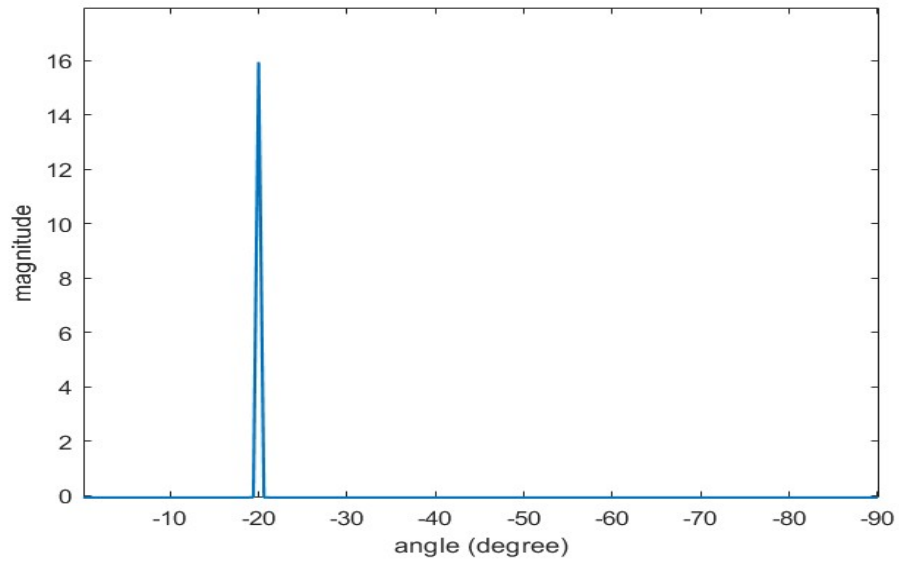
(a)
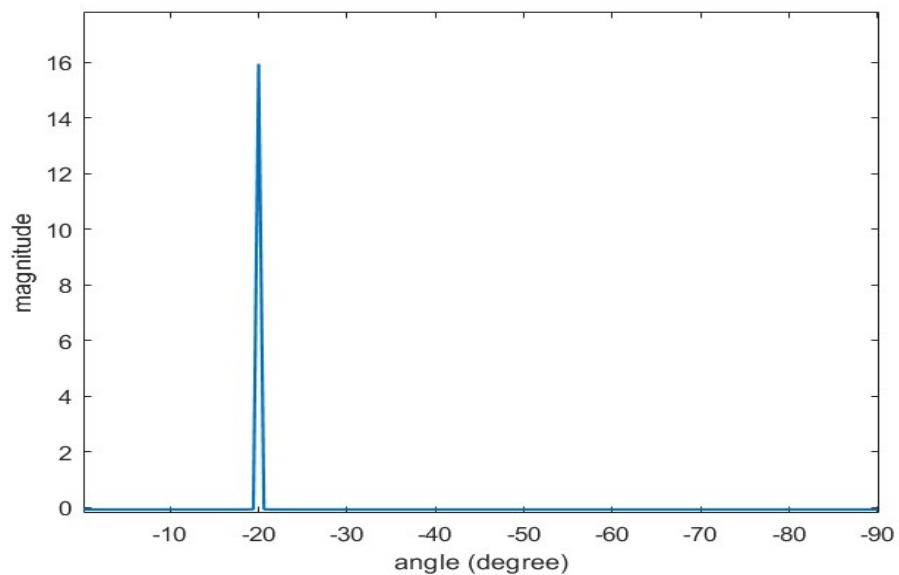
(b)

Figure 3.5 Single-source simulation using EV using Θ =-20° without noise at (a) M=8 (b) M=16

Figure 3.6 shows the implementing performance of the FFT and R-EV methods to estimate an accurate value for the required angles. It represents a relation between a number of elements (receiving antenna) that are changeable and the percentage error.

By changing the number of antennas of ULA (M) from 8 to 26 and computing the percentage error, when using FFT method, the value of error is constant for all value of M being 6.3% at angle is equal to 15°. This value is considered large by considering the absence of noise too Furthermore, the same relation between error and number of elements is applied for Root-Eigenvector R-EV in the same figure , the error are compute and as its clear the percentage error is zero for all values of M, that is prove R-EV method estimate the exact angle for all the impacting singles to ULA without any difference with the real value.
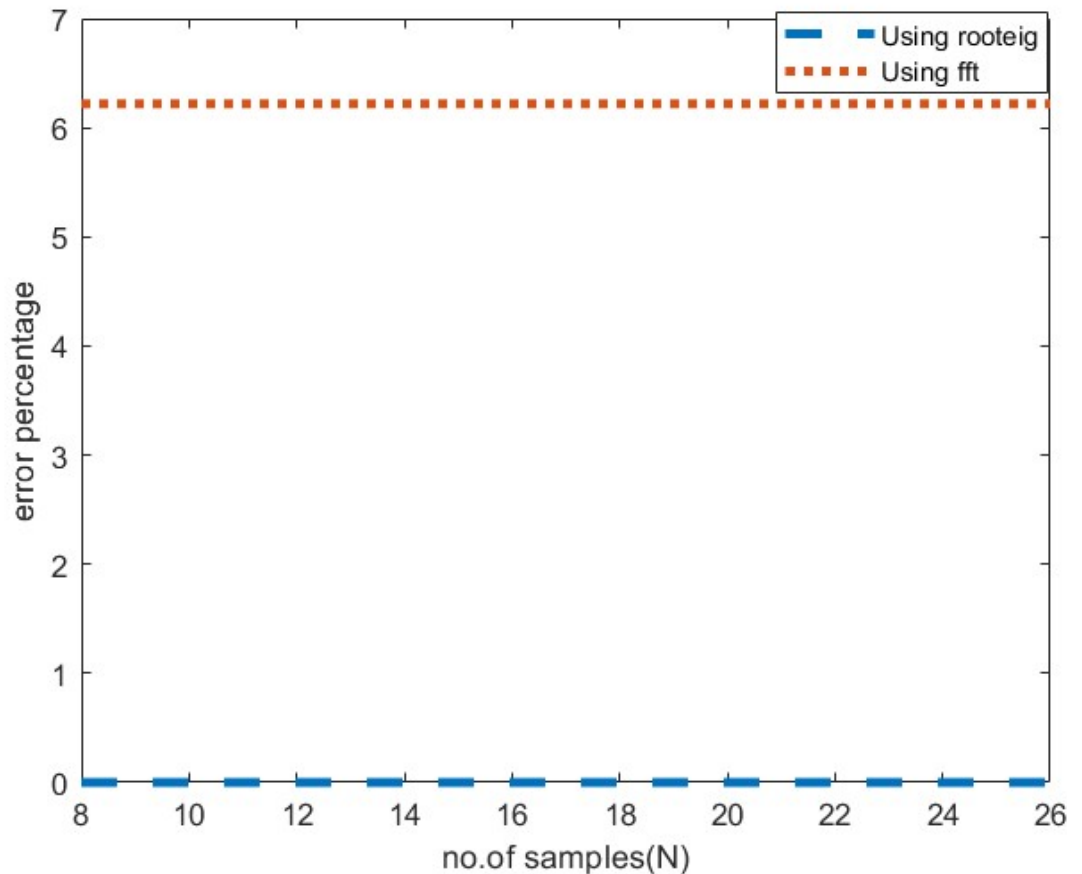
Figure 3.6 Relation between error and number of elements using FFT and R-EV using Θ =15 for single source without noise

3.3 Simulation Results for Double Sources AoA Estimation without Noise

Previously, a study for the receiving signals using a single source was studied for the two methods R-EV and FFT. In this section, the same steps were repeated but using multiple sources.

First, the two angles and the difference between them are set to 10°, these values are applied to the FFT method. As shown in Fig 3.7-a when the number of elements is 8 it looks like there is only one source contrary to the fact that there are two sources and two angles (the signals overlap with each other).

Again, in Figures. 3.7-b, as the number of elements increased to 16, the two angles appeared. This is represented by the two maximum peaks in the figure. Although the two angles appeared. This required many elements, and there is a group of side lobs on the side of the two real angles that made some uncertainty in the results achieved. The percentage error equal to 8.7% and 5.6% respectively for the two used angles.
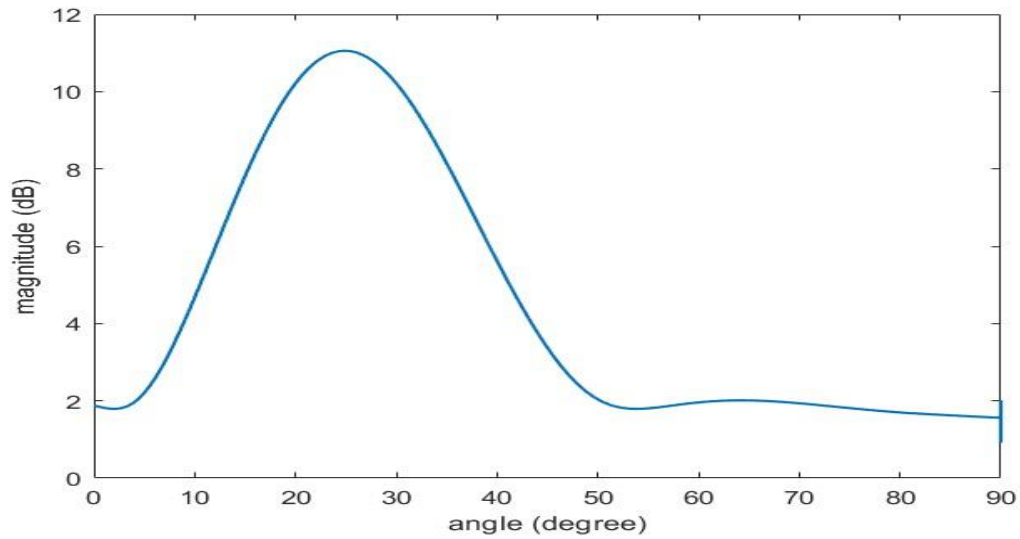
(a)
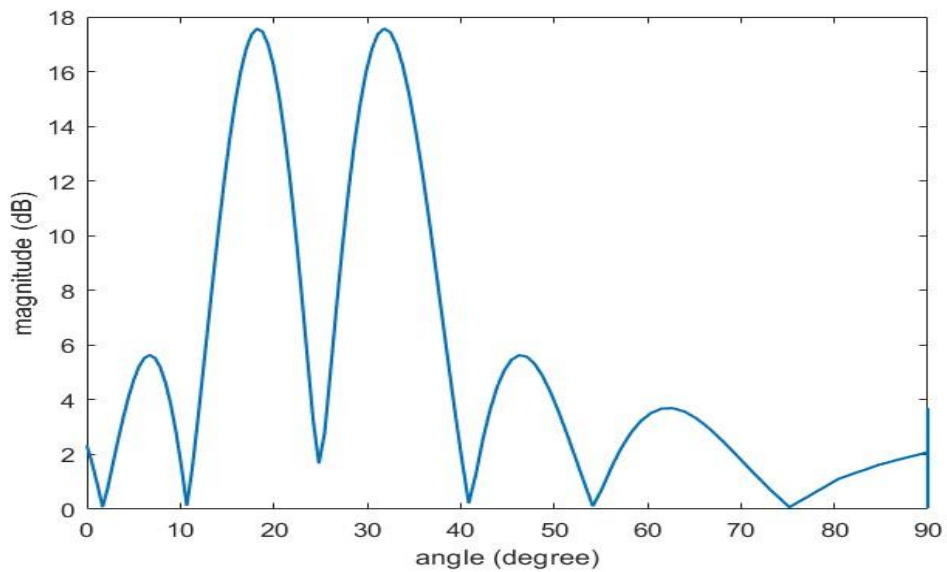
(b)

Figure 3.7 Double- sources simulation using FFT at Θ_1=20 ° and Θ_2=30 °
without noise (a) M=8 (b) M=16

The same case is implemented but using negative angles. When the number of elements was small (8 element), it is not able to distinguish between the two angles, as it is clear in Fig. 3.8-a.

In Fig. 3.8-b the numbers of elements are increased to 16 elements, the angles values reached -17.1° and -30.6° for -20°and -30° respectively. The

percentage error is equal to 15 % for theta1 (th1) equal to -20° and minor error rate for the second angle when (theta2) th2 equals to -30°.
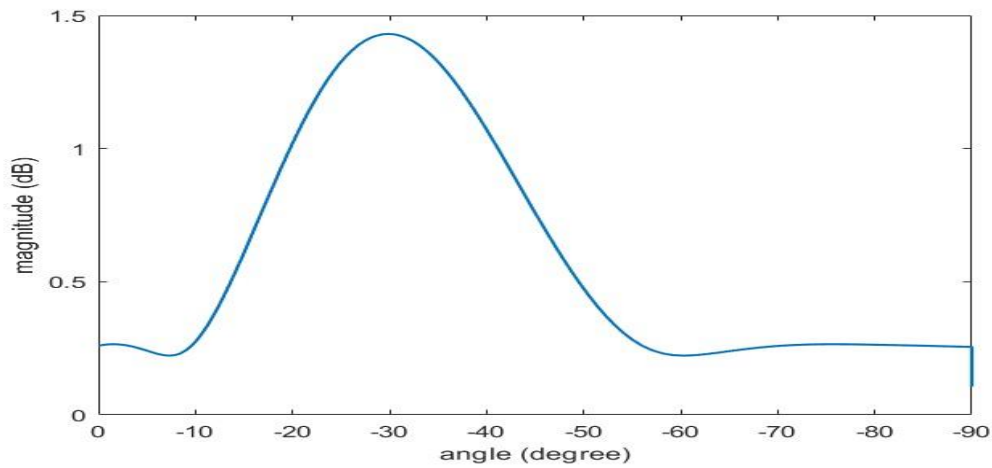
(a)
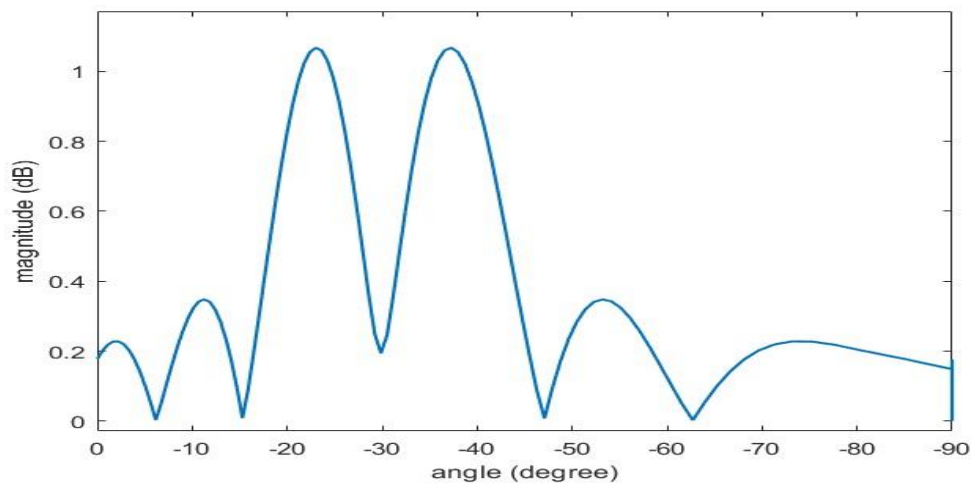
(b)

Figure 3.8 Double- sources simulation using FFT at Ɵ1 =-25 ° and Ɵ2=-35 without noise (a) M=8 (b) M=16

Figure 3.9 the difference between the two angles is increased to 15° one of them 20° and the other is 35°.When M is equal to 8, FFT distinguishes the two angles, however, the signals are almost overlapping, there is a need to either increase the number of elements or increase the difference between the two angles to recognize between them.

Figure 3.9-b when M is equal to 16 and the difference between the two angles is equal to 15° it can distinguish between the two angles easily but the sidelobe problem still appears. Also, the percentage error for the two angles (20° and 35°) that is equal to 2.9 % and 3.33% respectively. In figure 3.9-b when M is equal to 16 and the difference between the two-angles equal to 15° it can distinguish between the two angles easily but the sidelobe problem still happens also the percentage error for the two angles (20° and 35°) that equal to 2.9 % and 3.33% respectively.
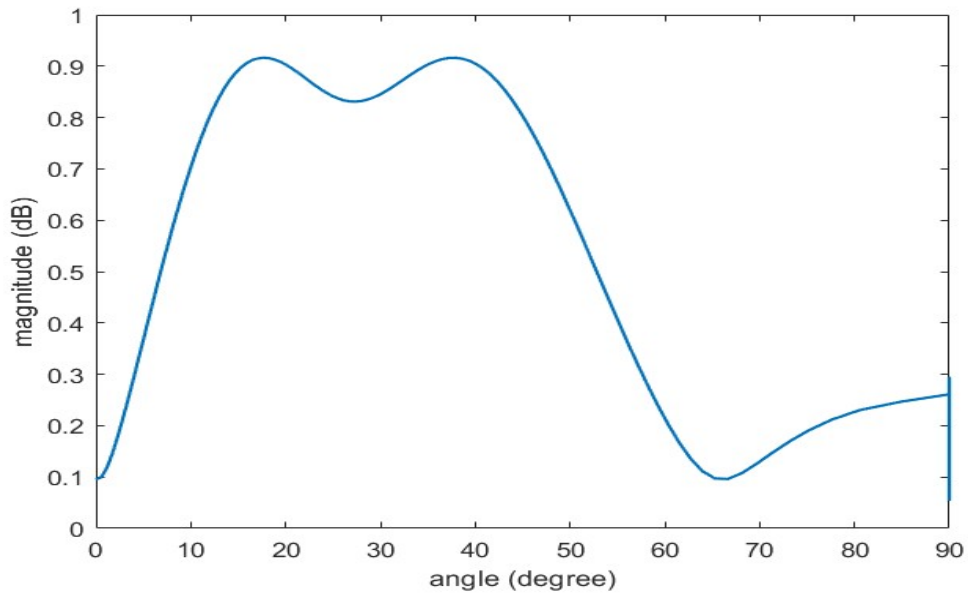
(a)
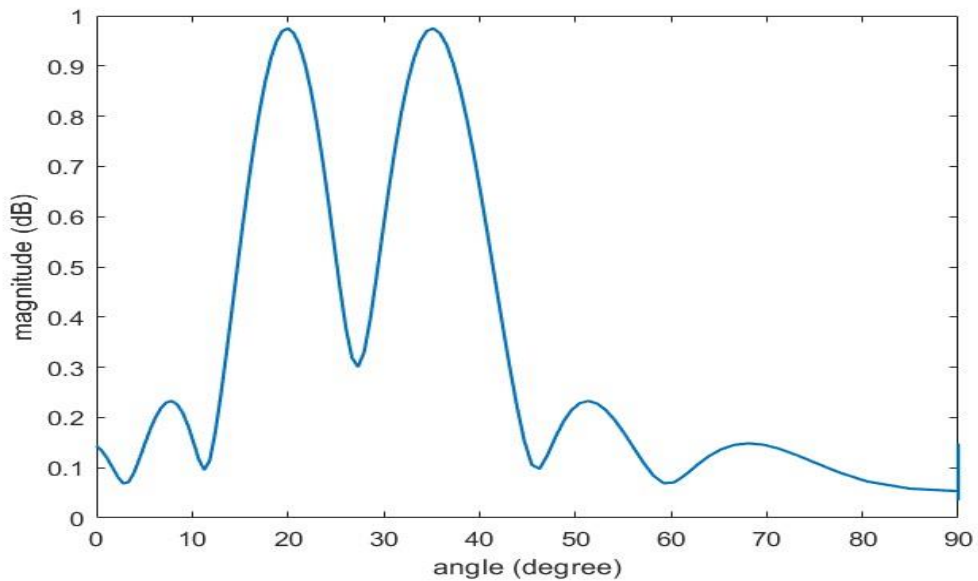
(b)

Figure 3.9 Double- sources simulation using FFT at Θ1 =20 ° and Θ2=35 without noise (a) M=8 (b) M=16

After FFT failed to distinguish the angles that the difference between them is five degrees, the same values are repeated, but using the high-resolution method of R-EV. This method achieved super results. Although the two angles are convergent, the difference between them is equal to $5°$ (Θ_1 =25 ° and Θ_2=30), and the numbers of elements do not exceed 10, it detects the two angles that run

into uniform linear array and estimate exact values of angles equal to $\theta_1 = 25°$ and $\theta_2 = 30$.

In figure 3. 10 using Eigen vector method by implement the spectrum at number of elements M equal 8, there are no side lobes, there are no need to increase number of elements.
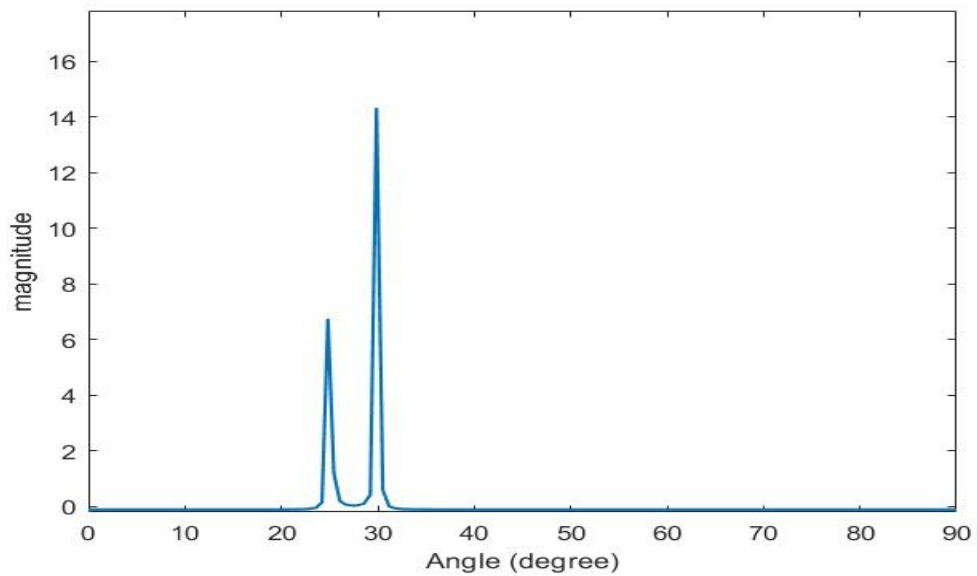
(a)
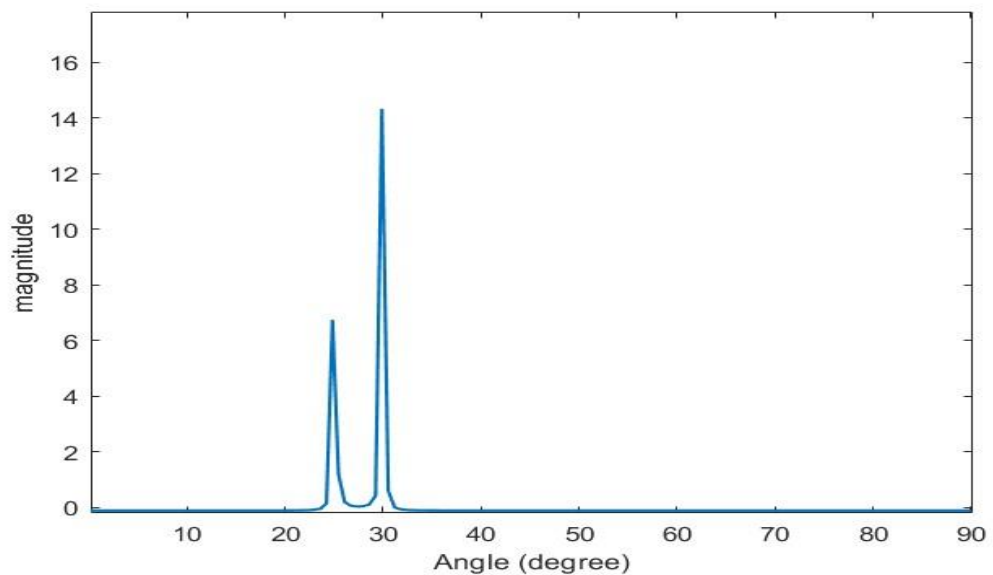
(b)

Figure 3.10 Double- sources simulation using EV $\theta_1 = 25°$ and $\theta_2 = 30$ without noise (a) M=8 (b) M=16

A comparison between the two figures 3.10 and 3.11 is presented, we observe that whether the difference between the angle is 5° or 10° this method

could distinguish between signals but in the next case when the difference between angles equal 10° the waveform has a better performance.
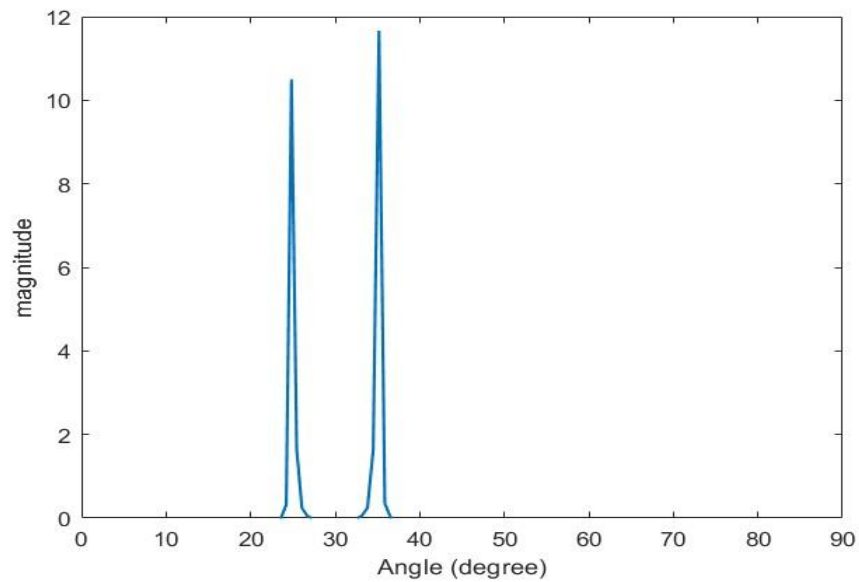
(a)
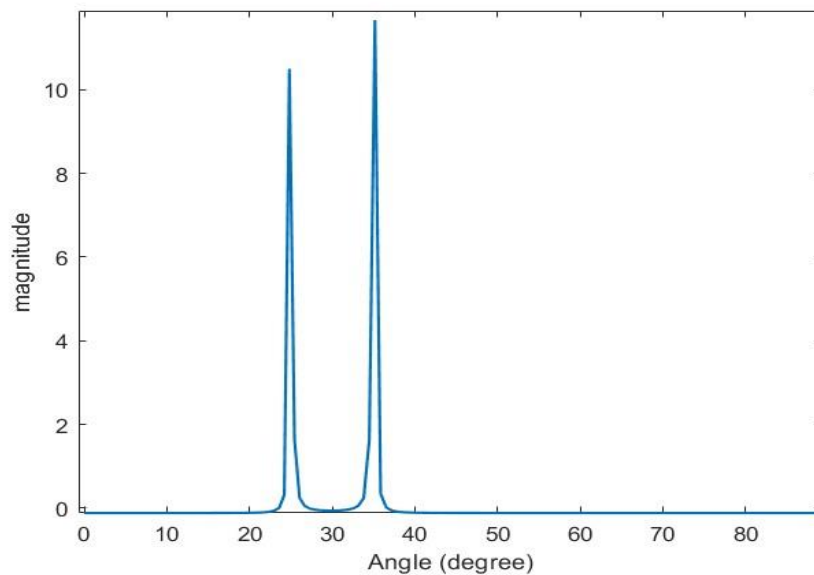
(b)

Figure 3.11 Double- sources simulation using EV Ɵ1 =25° and Ɵ2=35° without noise (a) M=8 (b) M=16

In contrast to the FTT, the EV succeeded in distinguishing the negative angle with an error rate of zero, as see in Fig. 3.12.
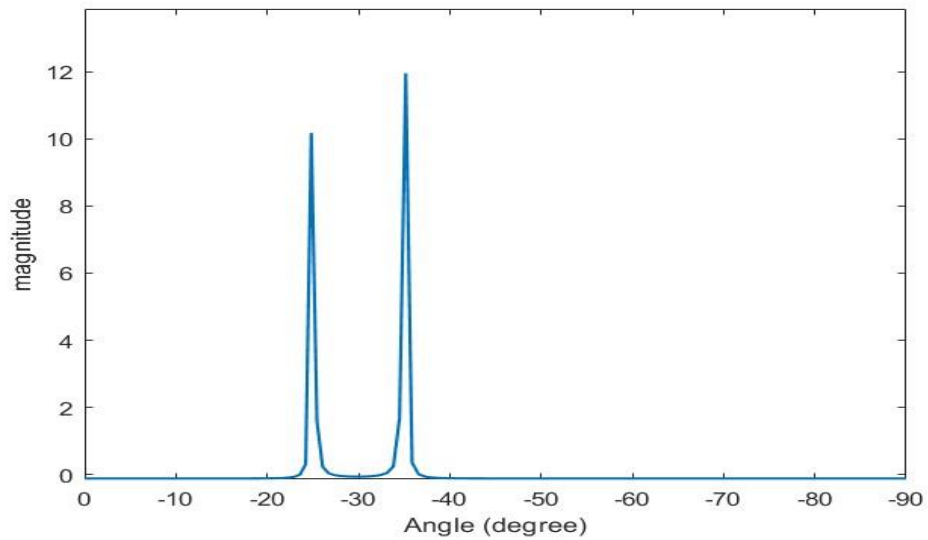
(a)
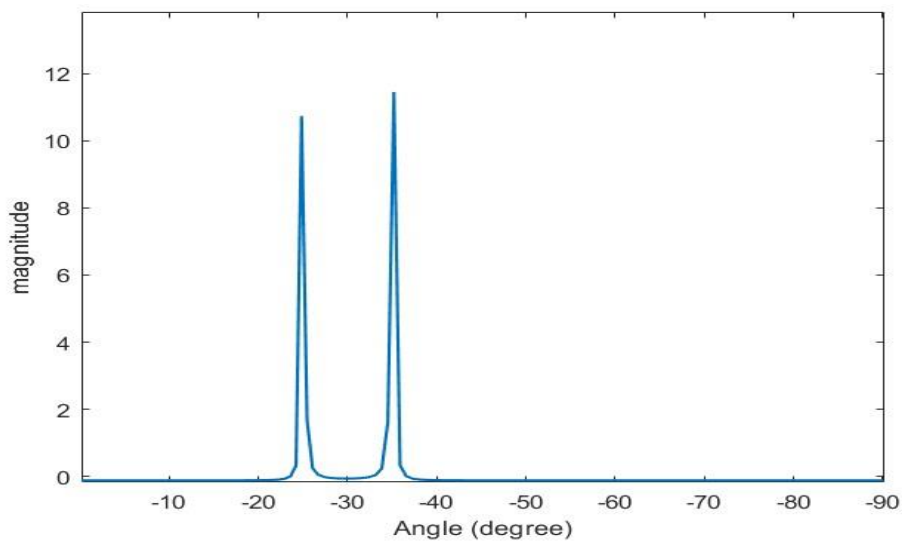
(b)

Figure 3.12 Double-sources simulation using EV at Ө1 =-25 ° and Ө2=-35 without noise (a) M=8 (b) M=16

The figures 3.13-a and 3.13-b represent a relation between the number of elements and the percentage of error for FFT and R-EV methods when the sources are double. The number of antennas (M) varies from 8 to 26 and the percentage error is computed also the two angles are set to 20° and 35°.

For FFT method , the error has different values and reaches a maximum 15% when M is equal to 9 elements while the percentage error is zero for all values of M. This means that the R-EV method estimates the exact angle for all

the impacting singles to ULA without any deviation from the real value as shown in the comparison table 3.1.

Table 3.1 comparison between the percentage error for FFT and R-EV without noise for different number of elements.

FFT method			R-EV method		
Θ_1	Number of elements	error	Θ_2	Number of elements	error
20°	8	8.5806%	35°	8	0%
20°	9	14.4768%	35°	9	0%
20°	10	11.5335%	35°	10	0%
20°	11	8.5806%	35°	11	0%
20°	12	5.6175%	35°	12	0%
20°	13	2.6439%	35°	13	0%
20°	14	0.3406%	35°	14	0%
20°	15	3.3366%	35°	15	0%
20°	16	3.3366%	35°	16	0%
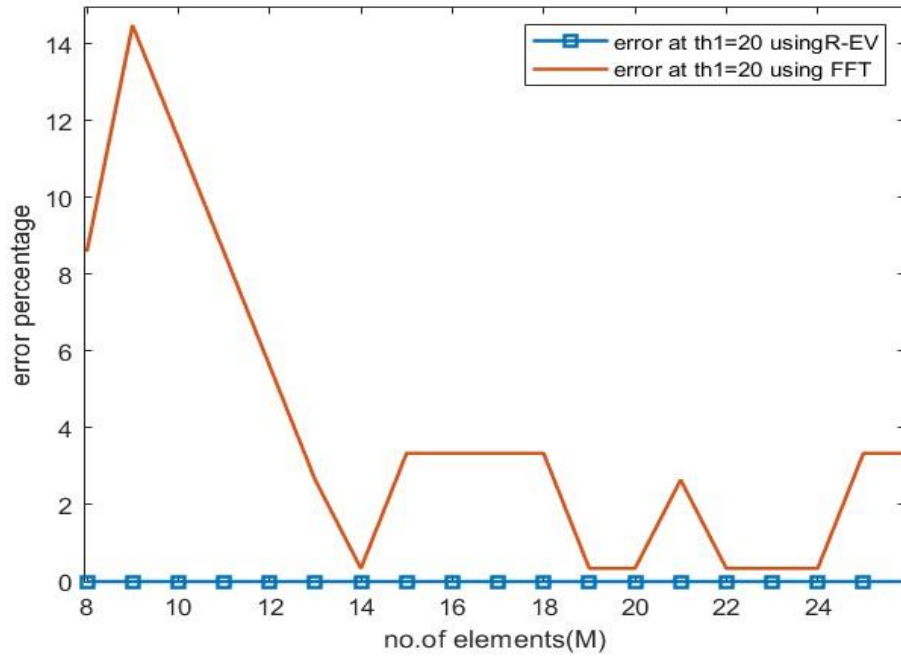
(a)
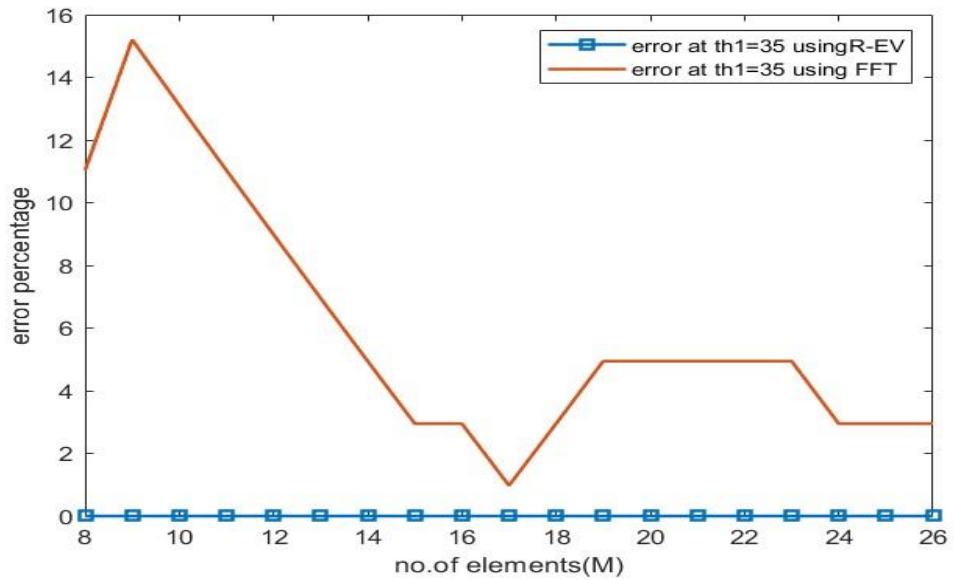
(b)

Figure 3.13 Relation between error and number of elements using FFT for double sources without noise (a) Θ₁=20 (b) Θ₂=35

CHAPTER FOUR

Simulation Results with Noise

4.1 Overview

In this part the noise is generated using MATLAB software for AoA Estimation. The MATLAB function AWGN additive white Gaussian) noise to a data array of inputs up to the appropriate final signal to noise ratio (S/N) power level, which by default is set in dB. The method used by the function AWGN to produce an array that represents the noise at a specified noise power level.

4.2 Simulation Results for Single Source AoA Estimation with Noise

Root eigenvector (R-EV) and FFT methods will be used to represent AoA initially under the assumption that there is a single source with noise, by setting the values of the variables for the spatial sampling interval to 0.8 cm, the number of elements M is variable, the angles have different values and as a start, the value of the signal to noise ratio (S/N) is set to 10 dB.

First, the noise is added to the signal, the angles are determined, and the resulting wave is observed. Therefore, by adjusted the angle (th1) in Figs. 4.1 and 4.2 to 20° and -20° respectively. The number of elements used in the uniform linear array receiving system is set between 8 and 16 in the two figures. As expected, adding noise causes an increase in the inaccuracy of AoA estimating.

For example, in the case of the number of elements equal to 8, the obtained value of the angle is equal to 21.66°. By calculating the error rate, it equaled 8.33%, and this is not a small percentage, considering this case is the simplest case, which is having only one source. Furthermore, when the number of elements increase to 16, we noticed that the value of the resulting angle did not change, and we obtained the same error value, also the width of the desired peak is less but the error is still high.
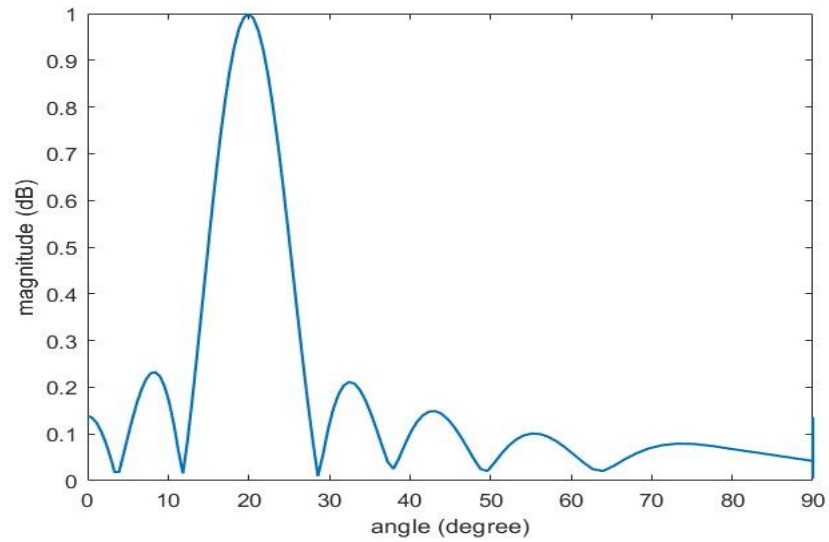
(a)
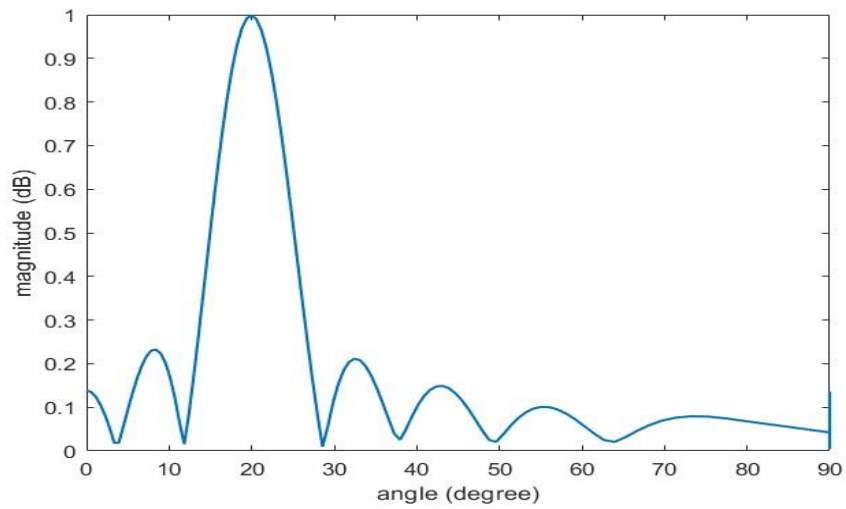
(b)

Figure 4.1 Single source simulation using FFT using Ө =20° with noise at

(a) M=8 (b)M=16

Likewise in the case of the negative angle, th1 equal to -20 as shown in Fig 4.2 the angle, it should be noted the resulted angle is equaled to -18, and the error percentage equaled to 11% and, as we increase the number of antennas to M equal to 16 the beam width is decrees.
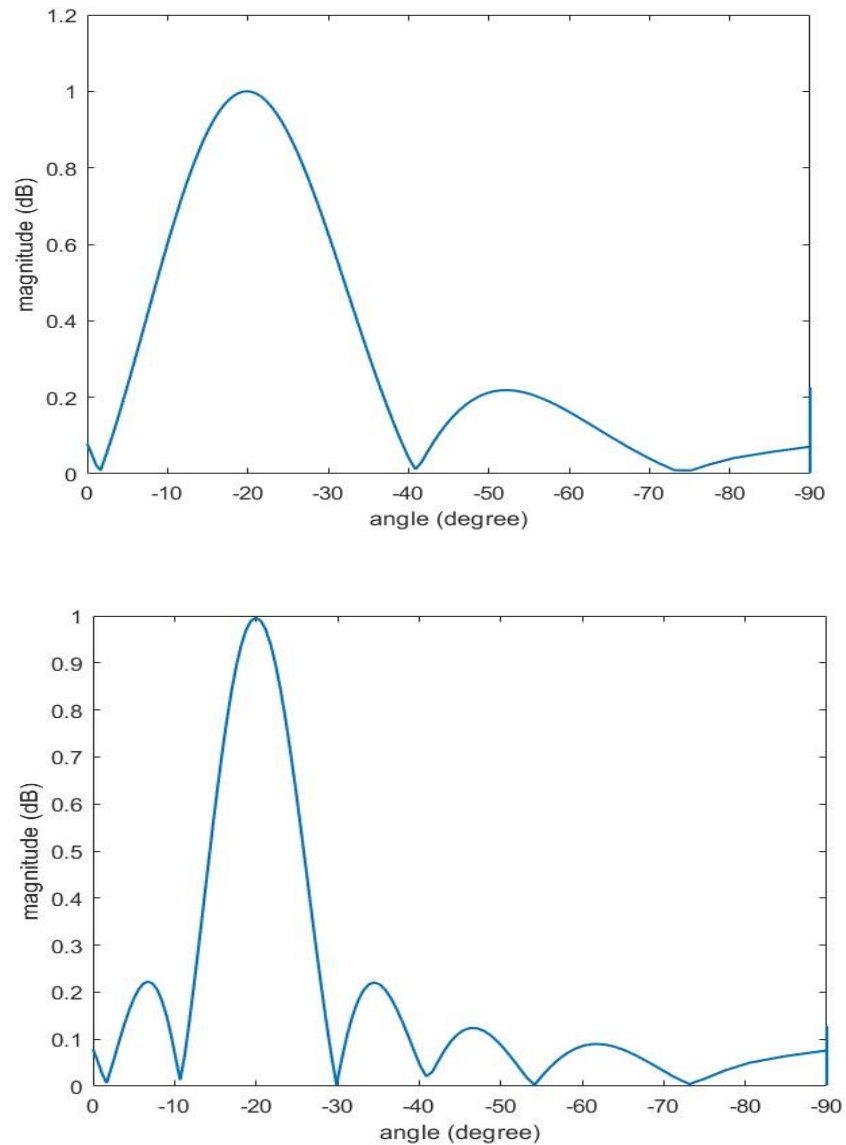
*Figure 4.2 Single source simulation using FFT using a negative angle of -20°
with noise at (a) M=8 (b) M=16*

On the other hand, to demonstrate the Root Eigenvector (R-EV) method, the noise is added and by setting the angle to 20 ° we get a value of 19.93°, so the error percentage is equal to 0.35 %. After increasing the value of M to 16 the resulting value is equal to 19.98° and the error rate decreased to 0.1%.

The spectrum is implemented using Eigen Vector (EV) as shown in Fig. 4.3 (a&b).
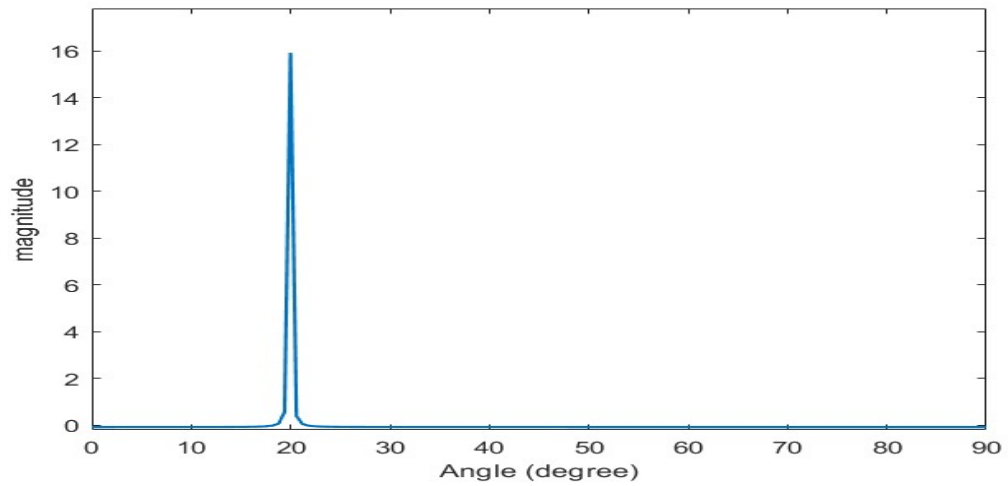
(a)
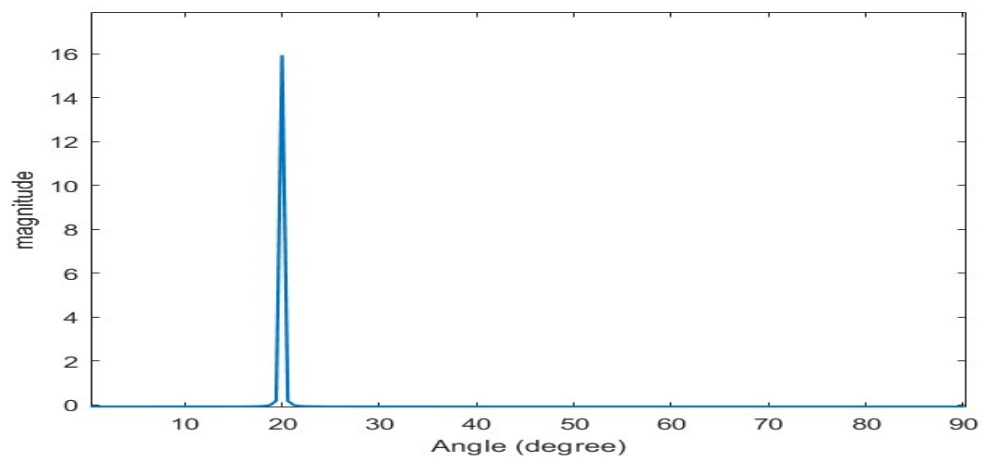
(b)

Figure 4.3 Single source simulation using EV using Ө=20° with noise at

(a) M=8 (b) M=16

Likewise, for the negative angle, the modern method R-EV also succeeded to distinguishing the angle with the lowest error rates, reaching a limit to 0.3% which is considered a very small percentage, compared to the previous percentages at the same angle when FFT was used.

The spectrum is implemented using Eigen Vector (EV) as shown in Fig. 4.4 (a&b).
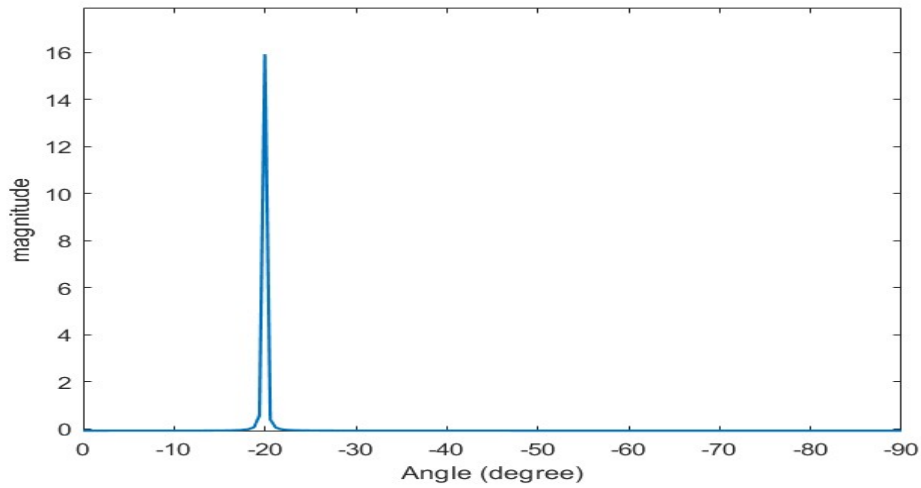
(a)
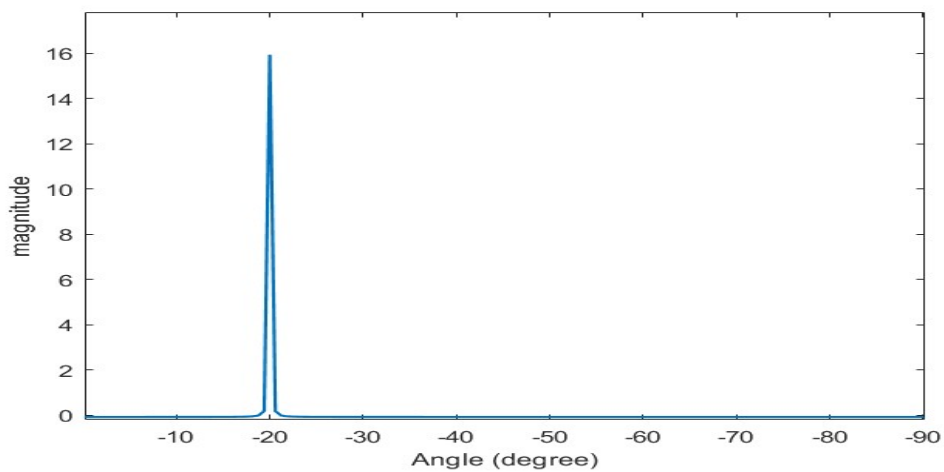
(b)

Figure 4.4 Single source simulation using EV using Ө= -20° with noise at (a) M=8 (b) M=16

4.3 Simulation Results for Double Sources AoA Estimation with Noise

An equally significant aspect is applied to both methods for double sources with additional noise and in the same conditions.

When the number of elements M is equal to eight, the FFT fails to distinguish between the two signals, and it's assumed that there is only one source, as shown in Fig. 4.5-a.

After increasing the number of elements, as it is clear in Fig 4.5-b, the appearance of two peaks one of them 23° representing the angle 25° and the

other is 38.1° representing the angle 35°, and the errors for them are 8.1365% and 8.7% respectively.
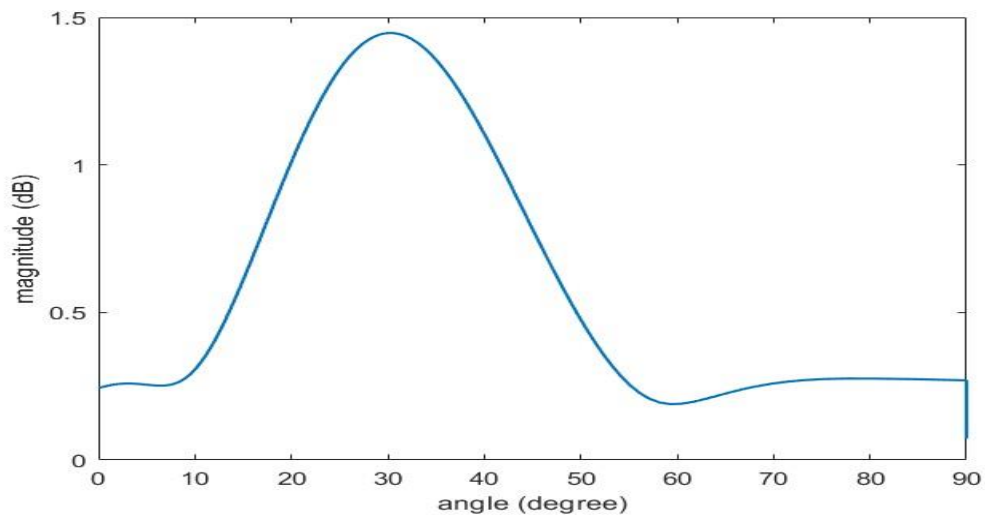
(a)
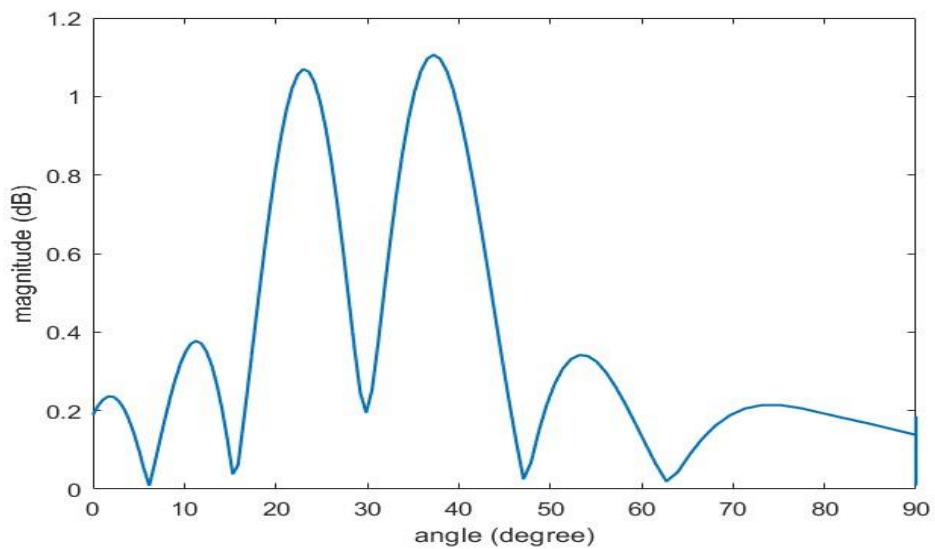
(b)

Figure 4.5 Double- sources simulation using FFT at Ө1 =25° and Ө2=35° with noise (a) M=8 (b) M=16

In the last case of dual-source FFT, using negative angles, we can see in Fig. 4.6 the detection of the negative angle is like the positive angle in terms of the

inability to detect when the number of elements is small, but when the number of elements increases, it is able to distinguish between the two signals and the percentage error equal to 9% and 6% when M equal to 16.

(a)

(b)
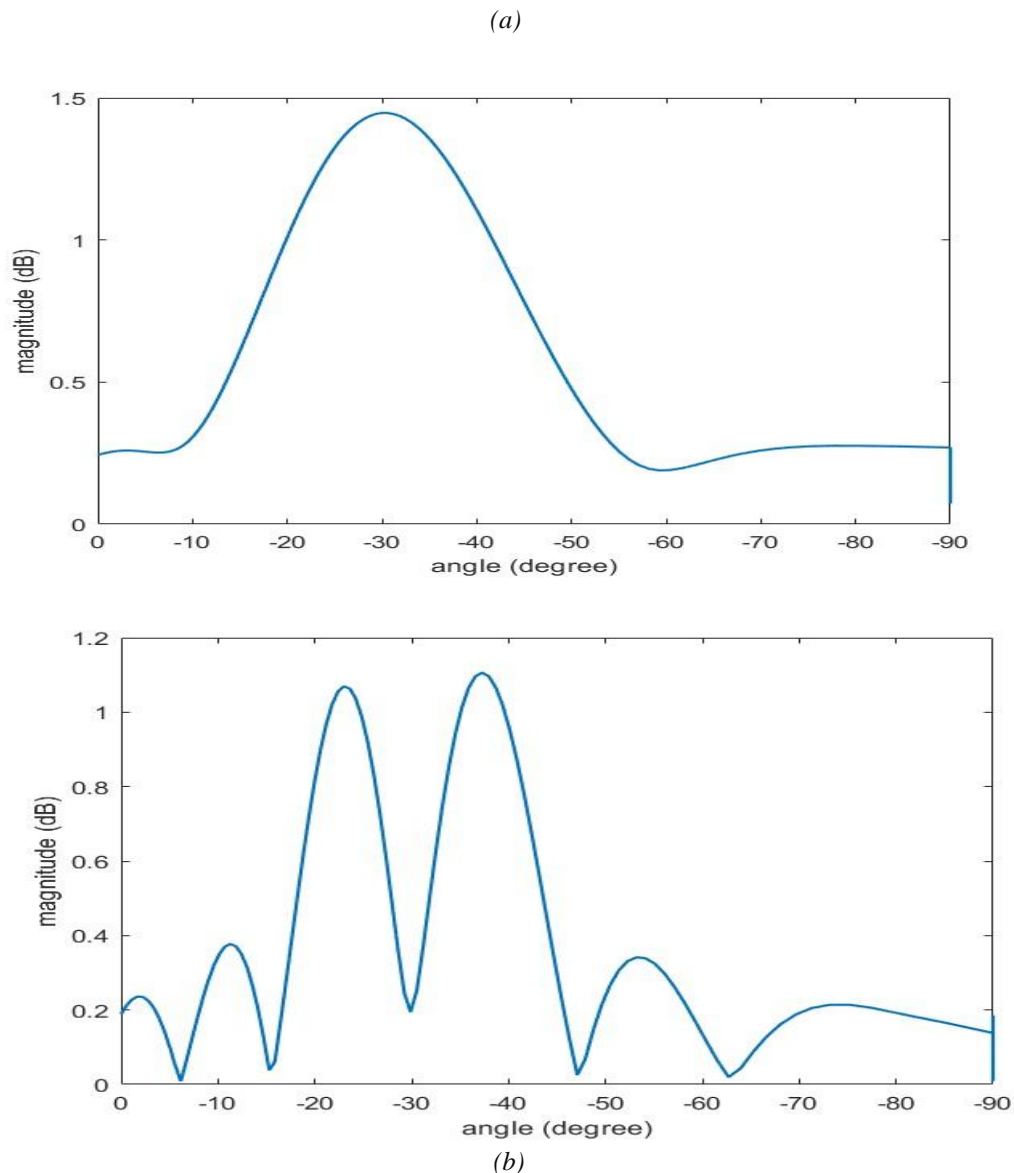
Figure 4.6 Double sources simulation using FFT at Ɵ1 =-25° and Ɵ2=-35°   with noise (a) M=8 (b) M=16

Moreover, after the dual sources with noise using FFT according to different values of M are studied, all the previous steps of FFT are applied to the Root eigenvector methods.

The R-EV method has a high ability to distinguish between two angles 20° and 30° even when the angle is less than 9. Therefore, the angles values are

simulated and found their values are closed to the true values (20° and 30°), and when calculating the error percentage, we get 1.6% and 0.5% for the two angles nonetheless M equal to 8, the same step for M is equal to 16 are maintained, errors reached to 1.1% and 0.02% for the same angle also the sidelobes insignificant values close to zero.
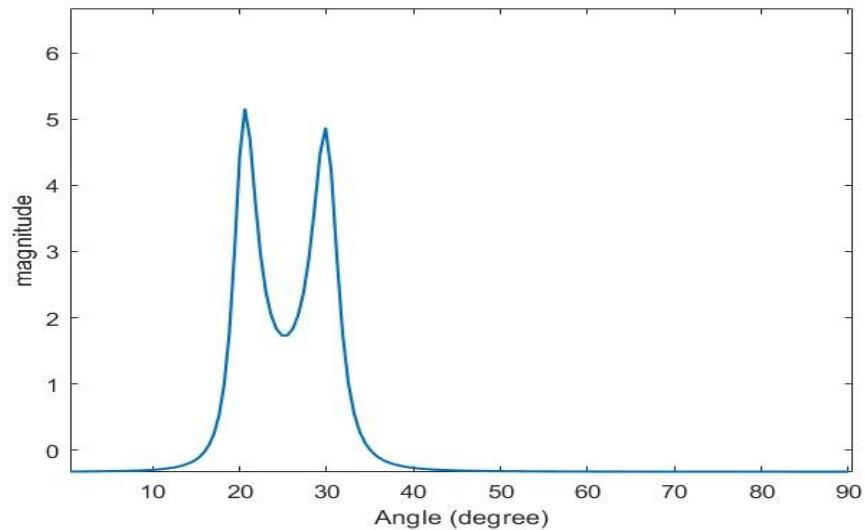
(a)
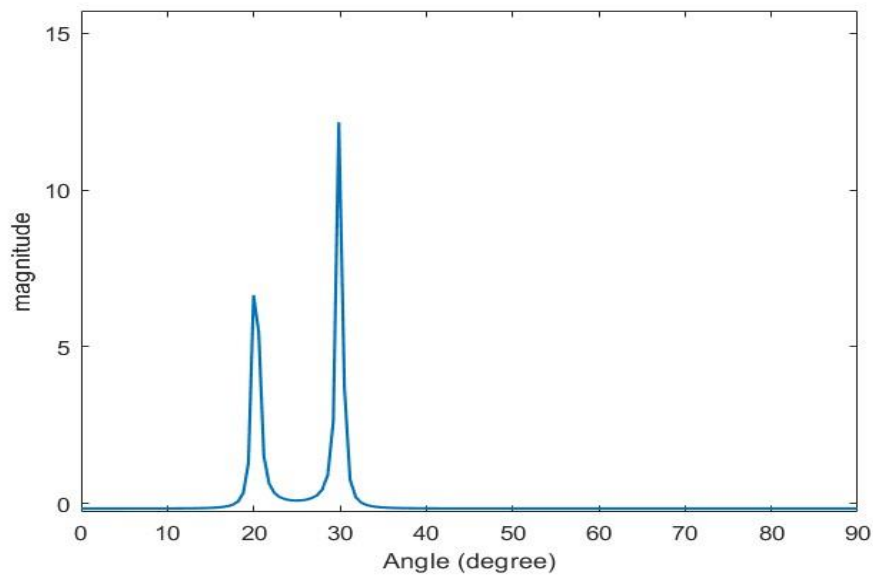
(b)

Figure 4.7 Double sources simulation using EV at Ɵ1=20 ° and Ɵ2=30° with noise(a) M=8 (b) M=16

The second case for R-EV is using negative angles for the two angles therefore this method succeeded in distinguishing between the two negative angles at M is equal to 8, and we also calculated the error rate for both angles.

The resulted angles values are equal to -20.0418°, -30.3413° for the two angles and the error is equal to 1.12% and 0.2% for M is equal to 16 and less than 3% for M is equal to 8.

As shown in Fig. 4.8 (a & b), the spectrum is implemented using the Eigen Vector method (EV), and the two angles are represented by the two peaks as it is clear in the figure.
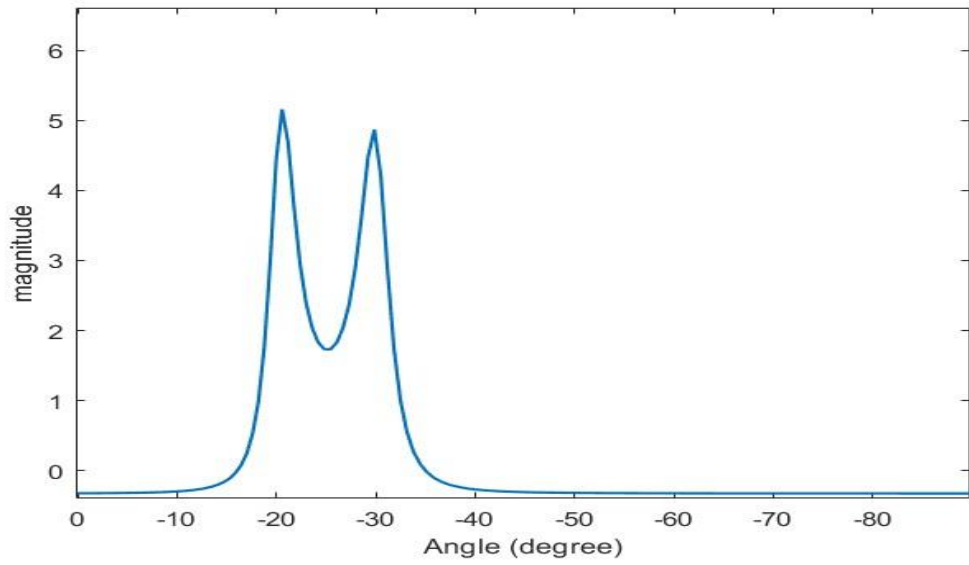
(a)
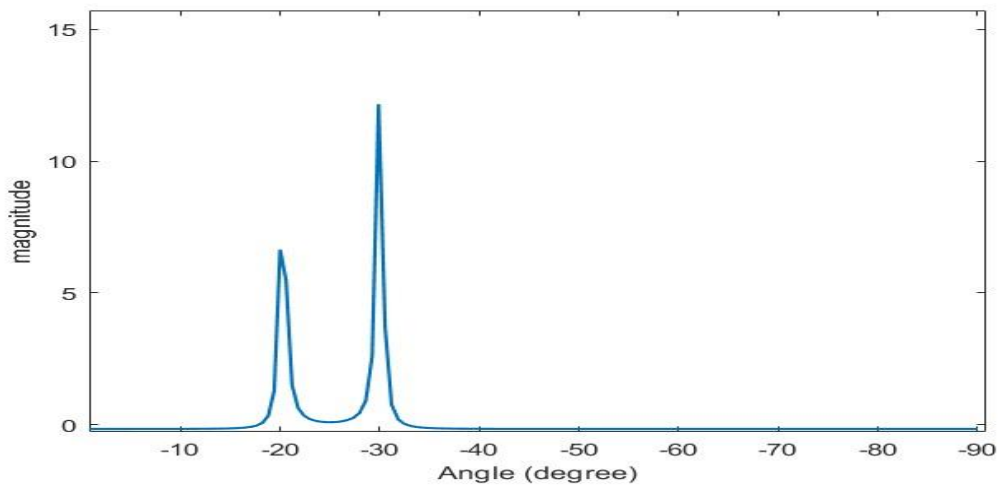
(b)

Figure 4.8 Double sources simulation using EV at Ɵ1=-20 ° and Ɵ2=-30°
with noise (a) M=8 (b) M=16
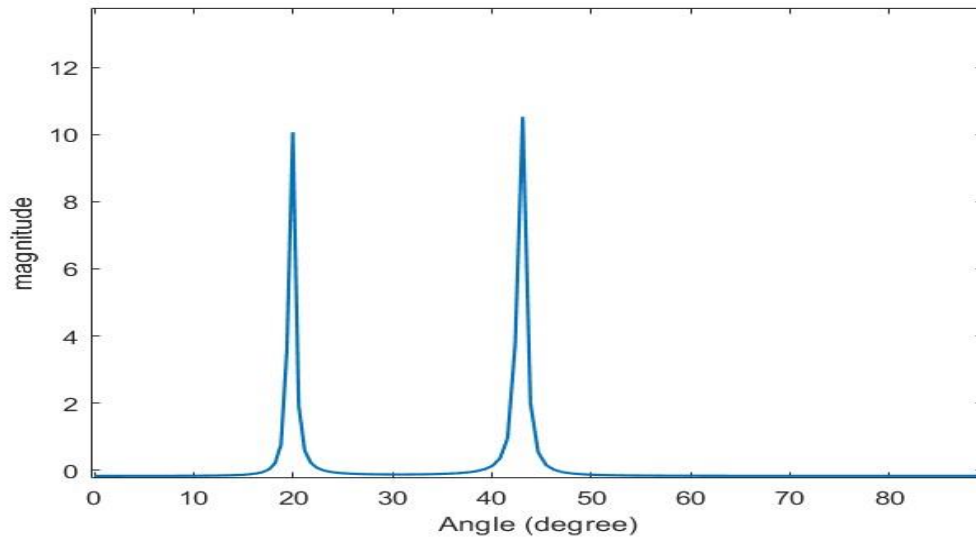
(a)
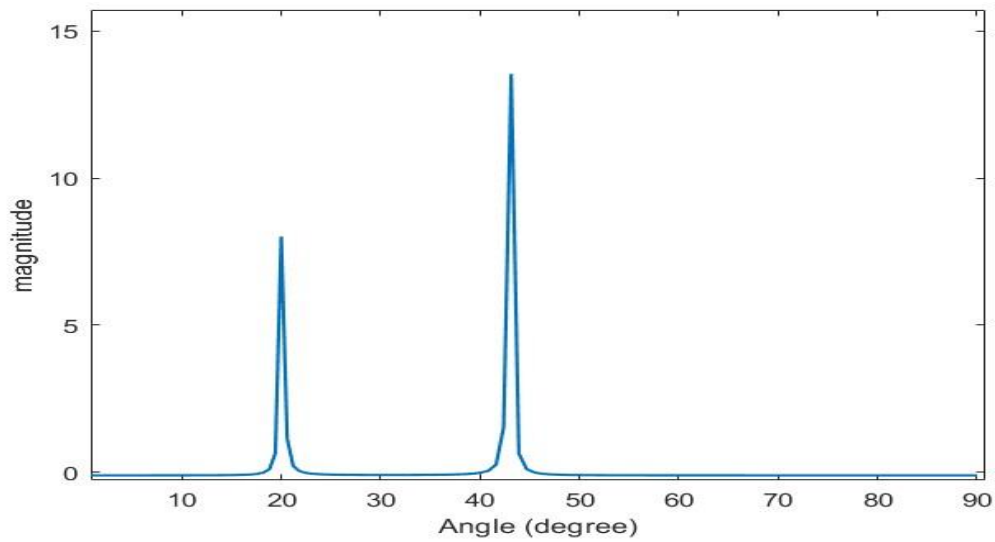
(b)

Figure 4.9 Double sources simulation using EV at Θ1=20° and Θ2=43° with noise (a) M=8 (b) M=16

After we studied the response for a range of angles using the two methods (R-EV and FFT), we studied the relation between the error rate of angles by changing the number of elements from 8 to 26.

In simulation of figure 4.10, the angles are set to 25° and 35°, the difference between angles fixed to 10°, the distance between element d is equal

to 0.8 cm and SNR equal to 10 dB, also the number of antennas was variable between 8 to 26 and the behavior of the methods are observed.

In figure 4.10-a when theta1 ($\Theta1$) is equal to 25°, the error rate of R-EV does not exceed 1% except at no. of samples M equal to 10 achieved 2% which is also considered a small percentage that means we obtained accurate angle values with high accuracy and a negligible error rate.

On the contrary, when the same mentioned values are set but for FFT method, we observed error values ranging between 8% to 2%.

An important point must be pointed out if we look closely at the FFT curve, it starts from M is equal to 10, that means when the number of antennas M equal to 8 FFT could not differentiate between the angles.

The same applies to figure 4.10-b. The error values for R-EV are less than one, except for M is equal to 10 the error value is 3%. As for the FFT, the error rates range between 12% to 3%.
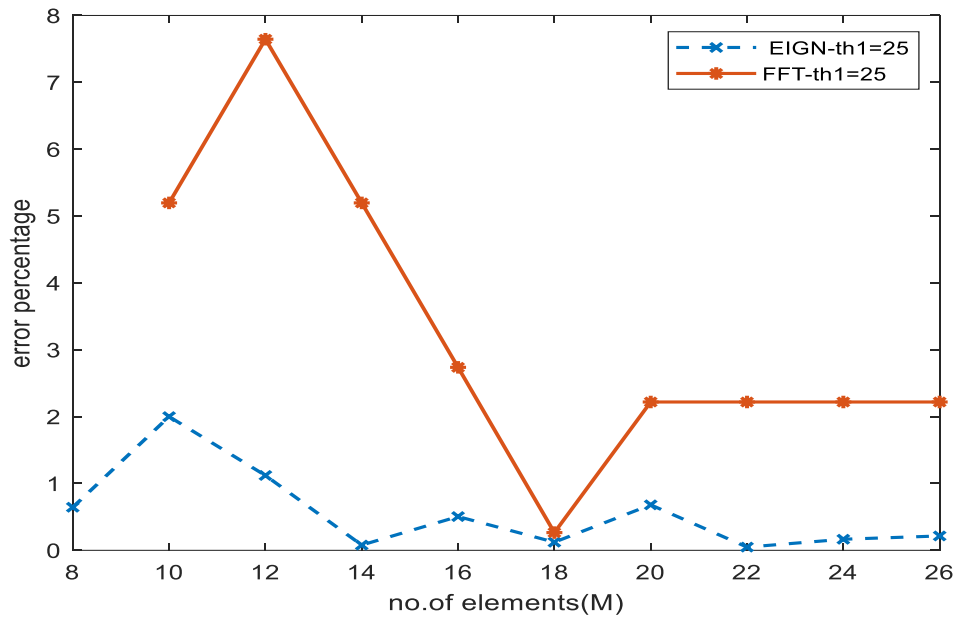
(a)
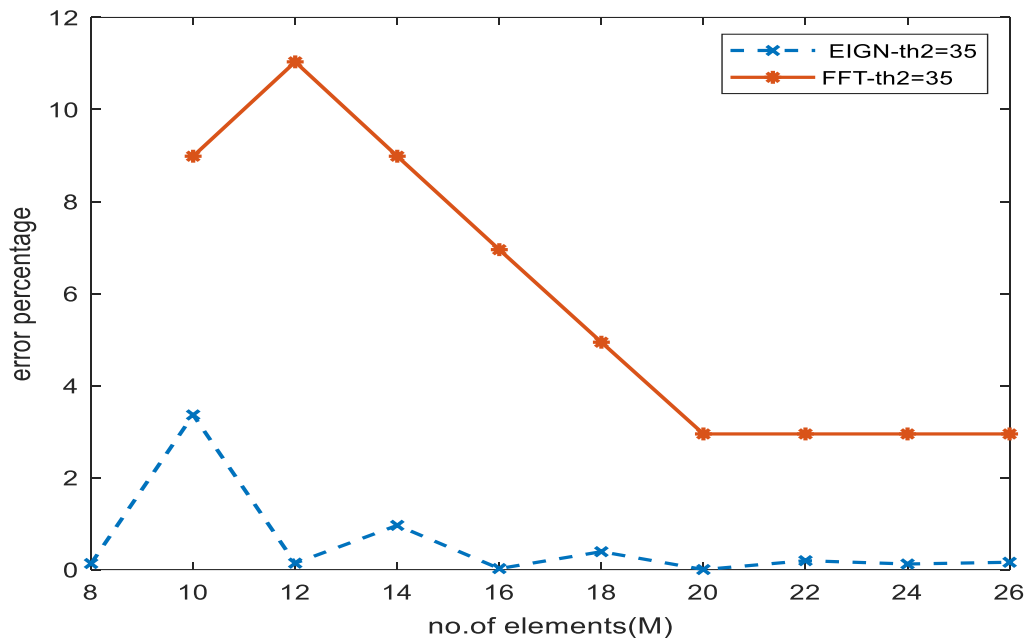
(b)

Figure 4.10 Relation between error and number of elements for double sources with noise (a)Ө1=25° (b) Ө2=35°

Table 4.1 comparison between the percentage error for FFT and R-EV for different number of elements with noise.

(a)θ1=25°

FFT method			R-EV method		
Theta 1	**Number of elements**	**error**	**Theta 2**	**Number of elements**	**error**
25°	8	un-define	25°	8	0.6446%
25°	10	5.1967	25°	10	2.0000%
25°	12	7.6449	25°	12	1.1199%
25°	14	5.1967	25°	14	0.0788%
25°	16	2.7370	25°	16	0.5051%
25°	18	0.2654	25°	18	0.1220%
25°	20	2.2188	25°	20	0.6802%
25°	22	2.2188	25°	22	0.0483%
25°	24	2.2188	25°	24	0.1657

(b)θ2=35°

FFT method			R-EV method		
Theta 1	**Number of elements**	**error**	**Theta 2**	**Number of elements**	**error**
35°	8	un-define	35°	8	0.1319%
35°	10	8.9843%	35°	10	3.3615%
35°	12	11.0352%	35°	12	0.1399%
35°	14	8.9843%	35°	14	0.9613%
35°	16	6.9535%	35°	16	0.0222%
35°	18	4.9417%	35°	18	0.3892%
35°	20	2.9482%	35°	20	0.0006%
35°	22	2.9482%	35°	22	0.1936%
35°	24	2.9482%	35°	24	0.1216%

We repeated the same operations, but for the negative angles -35° and -45°, at Fig. 4.11 a and b, FFT could not distinguish between the two angles except when the number of elements reached to 14 with error range between 11% to 3%, while using R-EV the curve starting with M is equal to 8 and low error less than 2%.

In figure 4.11 ,the curve of R-EV it is still limited to a small value of error not exceed 2% from M values between 8 to 26 , notes in the case of FFT there is an ups and down of the curve and there is no stable state , for example the errors when the number of elements equal to 14 is equal to the error when the numbers of elements equal to 26 and reached around 4%.
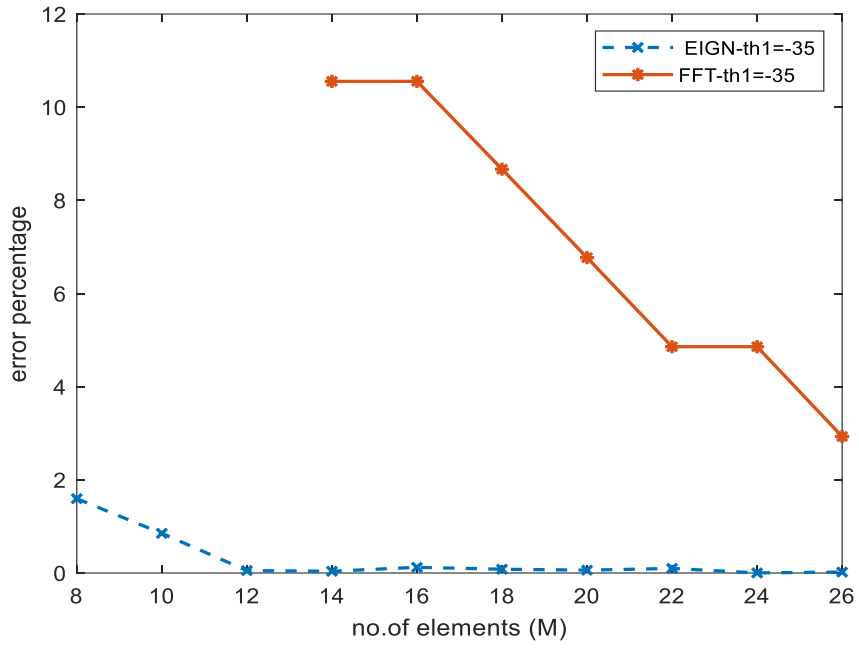
(a)
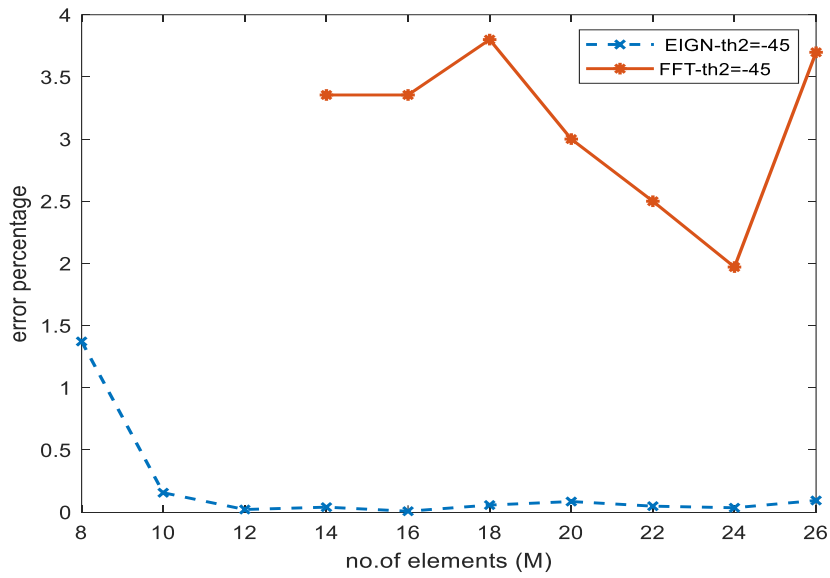
(b)

Figure 4.11 Relation between error and number of elements using FFT for double sources with noise (a)Ө1=-35° (b) Ө2=-45°

Table 4.2 comparison between the percentage error for FFT and R-EV for different number of elements with noise.

(a) Ө 1=-35

FFT method			R-EV method		
Theta 1	Number of elements	error	Theta 2	Number of elements	error
-35°	8	un-define	-35°	8	1.5957%
-35°	10	un-define	-35°	10	0.8513%
-35°	12	un-define	-35°	12	0.0523%
-35°	14	10.5544	-35°	14	0.0372%
-35°	16	10.5544	-35°	16	0.1219%
-35°	18	8.6694	-35°	18	0.0808%
-35°	20	6.7707	-35°	20	0.0609%
-35°	22	4.8578	-35°	22	0.0977%
-35°	24	4.8578	-35°	24	0.0024%

(b) Ө 2=-45

FFT method			R-EV method		
Theta 1	Number of elements	error	Theta 2	Number of elements	error
-45°	8	un-define	-45°	8	1.3723%
-45°	10	un-define	-45°	10	0.1556%
-45°	12	un-define	-45°	12	0.0207%
-45°	14	3.3548%	-45°	14	0.0395%
-45°	16	3.3548%	-45°	16	0.0069%
-45°	18	3.8000%	-45°	18	0.0565%
-45°	20	3.0000%	-45°	20	0.0848%
-45°	22	2.5000%	-45°	22	0.0476%
-45°	24	1.9706%	-45°	24	0.0347%

The last case for the relation between the error rate of angles and the variable number of elements (M) is using two angles, one of them is positive (20°), and the other is negative (-20°).

The error curve for FFT starting from M is equal to 8, by comparing this result with the previous case in Figures 4.10 and 4.11, we notice in Fig 4.10 (two positive angles) that FFT distinguishes between the two angles when M is equal to 10, also in Fig. 4.11 (two negative angles) until M is equal to 14 FFT distinguish between the two angles, so we consider this result in Fig. 4.12 is better than others.

In Figures 4.12-a R-EV reached less than 1% when the angle was equal to -20° and 2% when the angle was equal to 20°, also in Fig. 4.12-b R-EV reached 3% when the angle was equal to-20°.
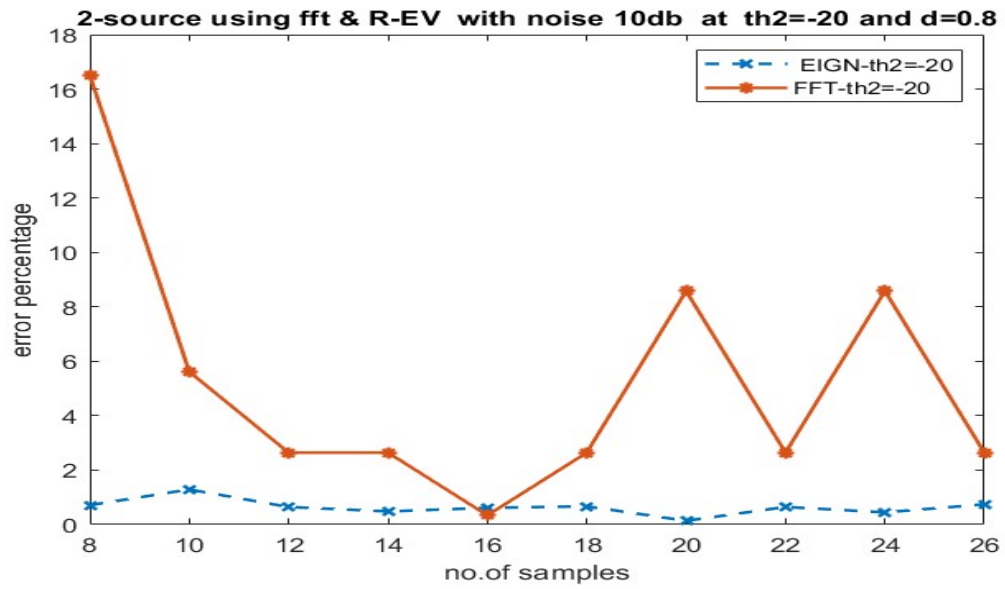
(a)
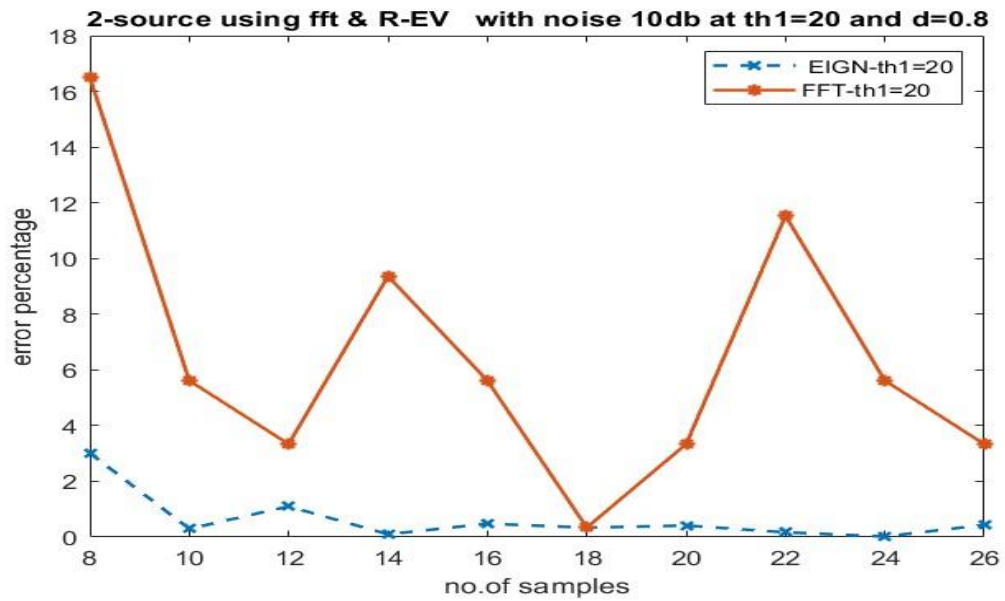
(b)

Figure 4.12 Relation between error and number of elements for double sources with noise (a)th1=-20° (b) th2=20°

4.4 Simulation for The Relation Between Error Rate and The Difference Between Angles with Noise.

This relation is based on fixing some elements and making others variable for double sources. In each case, we fixed the SNR to 10 dB, the number of elements M changed in different values, and fixed the first angle to 20° but set the second angle variable so that the difference between the two angles 5°, 10°, 15°....,30°.

Start analysis with a number of elements equal to 8 in Fig. 4.13, firstly, the R-EV was able to distinguish between the two angles despite the difference between the two angles being the smallest value, which is 5° and M is equal to 8 the resalted error rate reached 5%, we can consider it an acceptable percentage if we notice the small difference between the angles (5°), After that, as the difference between the two angles increases, we notice the error rate disappears, reaching a value close to 1%. As for FFT, if we observe the curve in the same figure, we will find that when the difference between the two angles began to increase to the point of 15°, this method was able to differentiate between the two angles with an error reached to 14%.
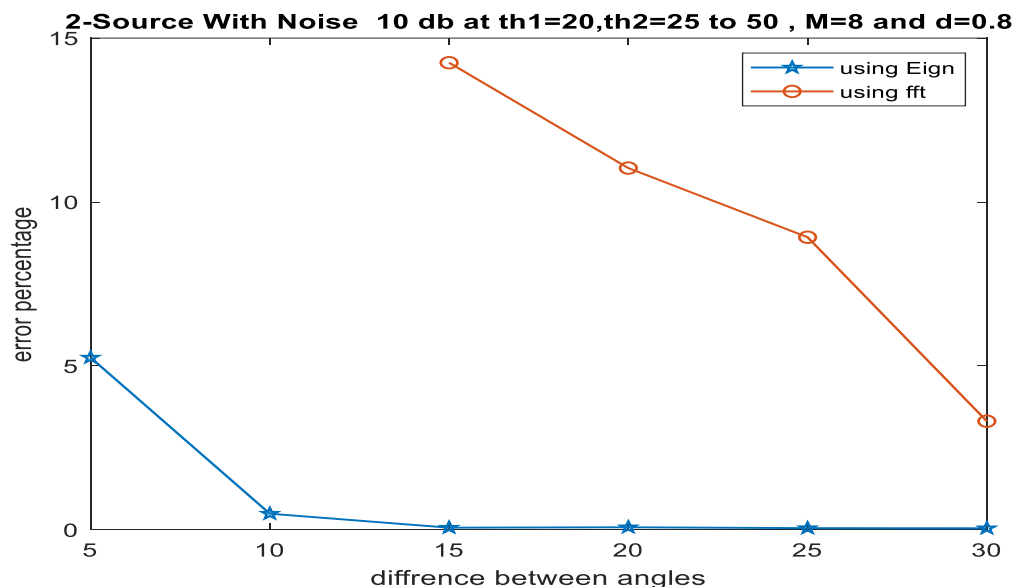
Figure 4.13 Relation between the error and the difference between angles at

M=8

In the same manner and with the same variables, except that we increased the number of elements to 12 and observed the behavior of both methods. In the case of the difference between the two angles was 5°, the error rate was equal to 4%, and compared to the previous case when M was 8, the error rate began to decrease gradually, so, the greater the difference between the angles, the lower the error rate.

The FFT shows a significant improvement, when the difference is equal to 10°, it begins to distinguish between the two angles with an error rate of 13 %.
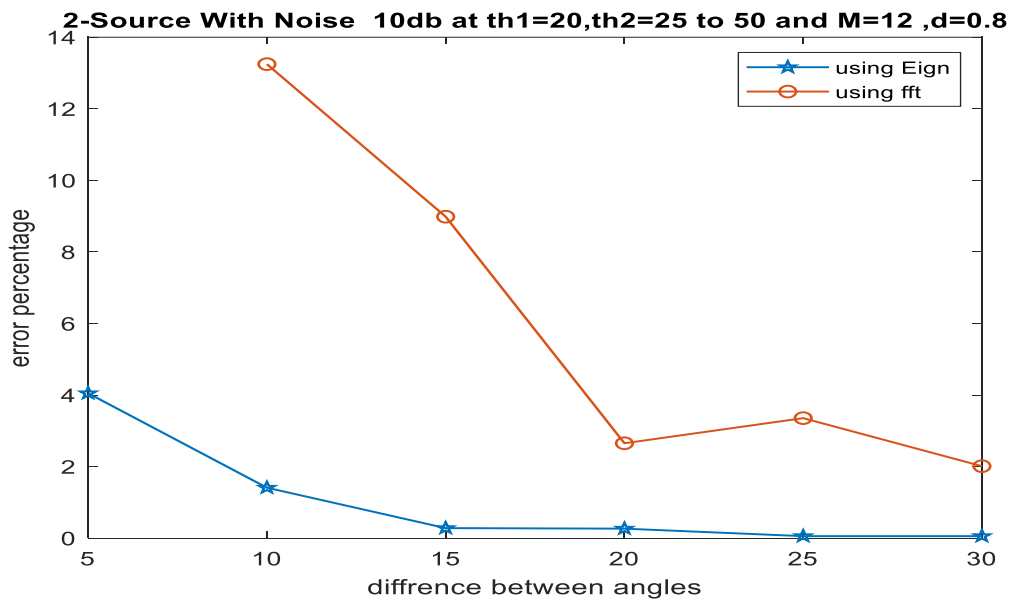
Figure 4.14 Relation between the error and the difference between angles at

M=12

Afterward, the number of elements are increased to 14, In R-EV there is a significant change compared to M is equal to 12, and the error rate is less than 2% at a difference equal to 5°, However, for FFT, it still couldn't differentiate between the two angles at a difference 5° but differentiate at a difference 10° with error rate higher than 10% as shown in Fig 4.15..
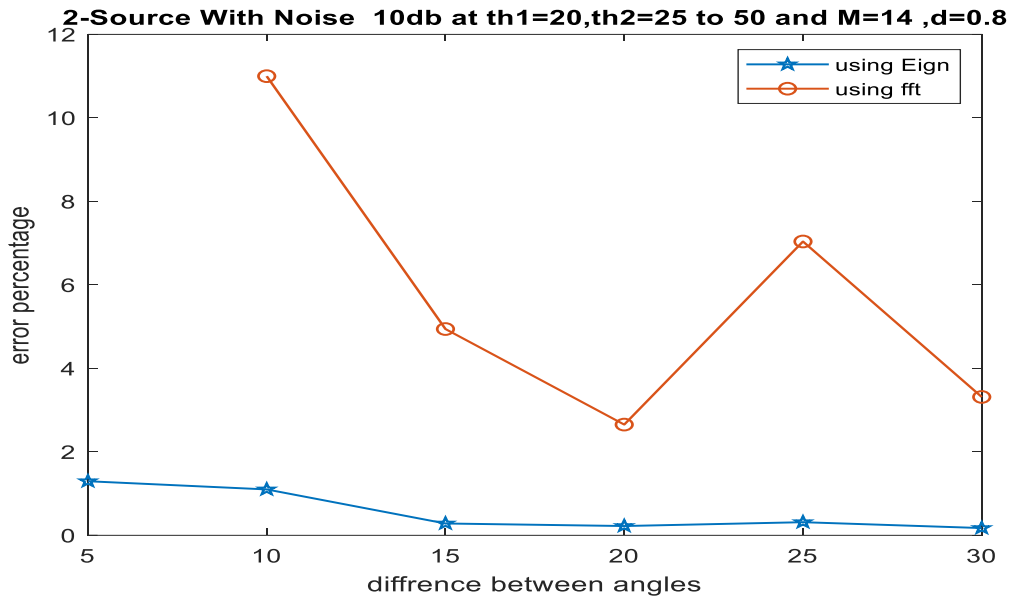
Figure 4.15 Relation between the error and the difference between angles at

M=14

Finally, we increased the number of elements to 16, the error reached around 1% and less for Root   Eigenvector   method,   also   FFT   couldn't recognized when difference equal 5° and the error at difference 10 starting with 9% as shown in Fig. 4.16.

This relation prove that it is possible to increase accuracy and reduce the error rate by increasing the number of antennas, but at the expense of cost and complexity, also it is possible to use a little number of antennas but instead of increasing the difference between angles at the expense of less ability to detect the angles of the close signals.

2-Source With Noise 10db at th1=20,th2=25 to 50 and M=16 ,d=0.8
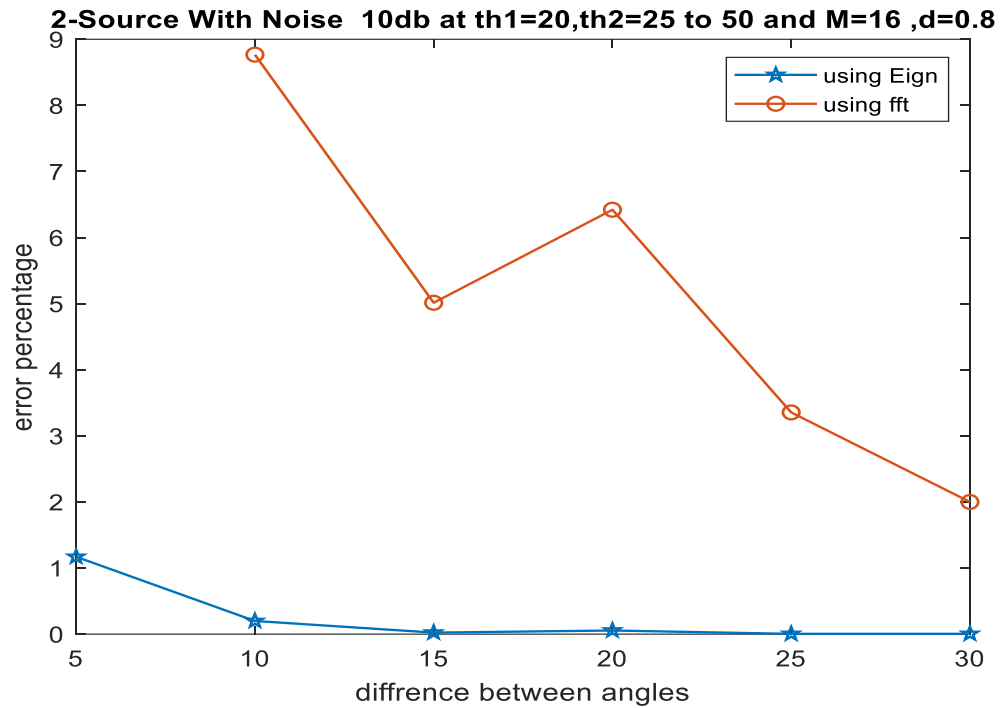
Figure 4. 16 Relation between the error and the difference between angles at

M=16

4.5 The effect of Inter-Elements Distance Between Elements on AoA

This section indicates the effect of changing the distance between elements d and the influence of increasing and decreasing this value on the relation between the error rate and the number of elements.

The study is conducted at a fixed angle difference equal to 10° and the number of elements M ranging between 8 to 24, in all previous cases, we fixed the value of d to 0.8 cm, in this case, the value of d changed between 0.8 cm and 0.6 cm. Figure 4.17 -a simulation for the relation between error rate and difference between angles at d is equal to 0.8 cm, If we start analyzing this curve, a low level of error is achieved when the number of elements (M) equals 8, and it continues to decrease until M is equal to 16. There is a slight increase when the number of elements equals 20, but the error rate is still less than 0.5%.

81
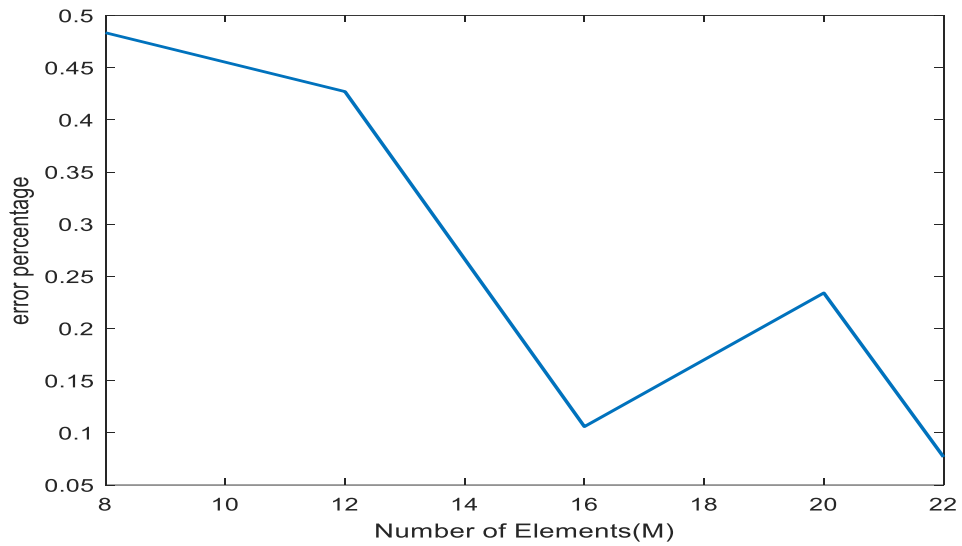
Figure 4. 17 Relation between the error and number of elements at a difference between angles equal to10 and d=0.8 cm

Also, the results are represented in a table 4.3 as shown:

Table 4.3 The results for the Relation between error and number of elements at a difference between angles equal to10 and d=0.8 cm.

Distance Between Elements	Number of elements	Percentage error
0.8 cm	8	0.49%
0.8 cm	12	0.41%
0.8 cm	16	0.13 %
0.8 cm	20	0.2 %
0.8 cm	22	0.09 %

The second case represented in Figure 4.18, in which d is equal to 0.6 cm if we start comparing this extent with the previous result (d equal to 0.8 cm), we notice the error rate starts from 3.5% when the number of elements are equal to 8, and then it begins to decrease gradually, and this is the effect of reducing the distance between the elements to this extent.
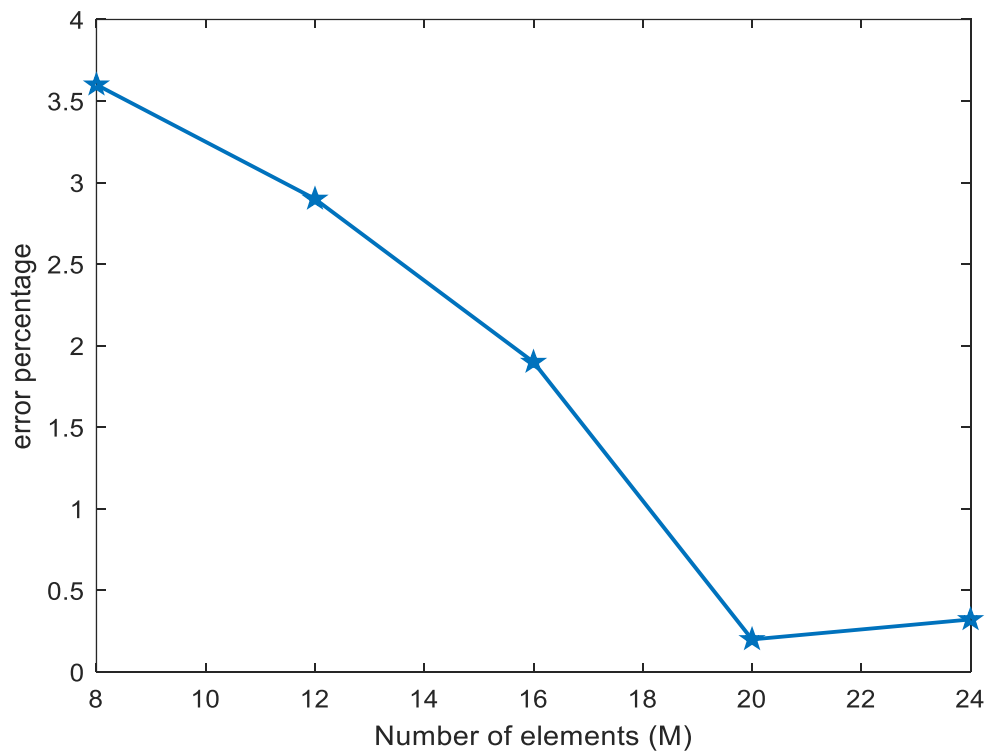
Figure 4. 18 Relation between the error and number of elements at a difference between angles equal to10 and d=0.6cm.

Also, the results are represented in a table 4.4 as shown:

Table 4.4 The results for the Relation between error and number of elements at a difference between angles equal to10 and d=0.6 cm.

Distance Between Elements	Number of elements	Percentage error
0.6 cm	8	3.6 %
0.6 cm	12	2.9 %
0.6 cm	16	1.9 %
0.6 cm	20	0.1 %
0.6 cm	22	0.4 %

4.6 The Relation Between the Error Percentage and the Distance Between Elements

These simulations are based on the relation of the distance between elements (d) and the error rate. In this section, the effect of changing the values of d from 0.5 cm to 0.9 cm are studied, also by fixing the number of elements to 16, and changing the values of the difference between the angles once when the difference is equal to 5°, another case when the difference is equal to 10°, and finally when the difference is equal to 15°.

In the first case in figure 4.19, the difference was equal to five degrees, and it is considered little value, we notice that when d is equal to 0.5 cm the error rate reaches 10 %. After that, as the value of d increases, the error rate decreases to a limit of 2%, and at 0.8 cm it stays in the same range.
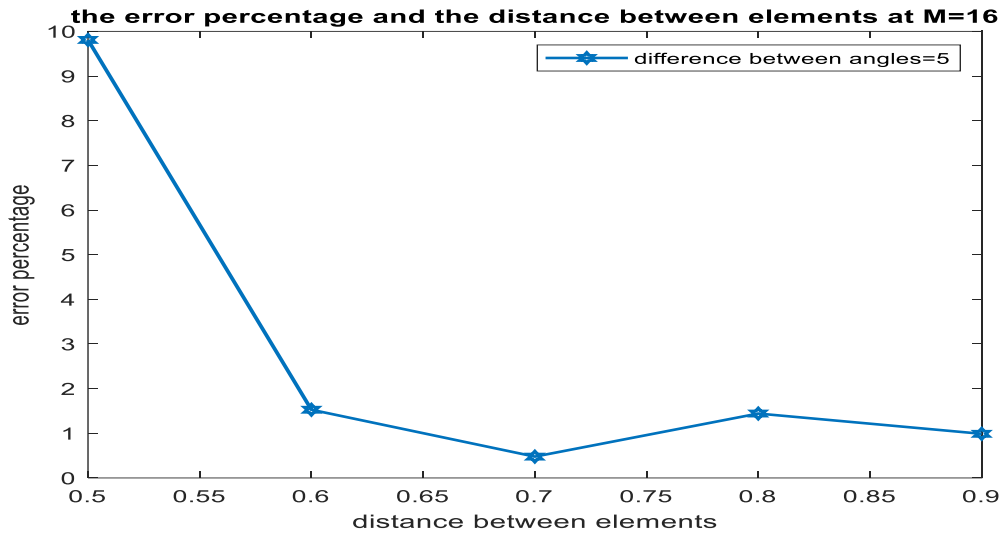
Figure 4.19 Relation between error and distance between elements at a difference between angles equal to 5° and M=16

The results of this relation are represented in table 4.5:

Table 4.5 The results for the Relation between error and distance between elements at a difference between angles equal to 5° and M=16

Difference between angles	Distance Between Elements	Percentage error
5 º	0.5 cm	10 %
5 º	0.6 cm	1.7 %
5 º	0.7 cm	0.5 %
5 º	0.8 cm	1.9%
5 º	0.9 cm	1 %

In the second case at figure 4.20 when the difference is equal to 10°, we have obtained better results with a small error rate, this is the case when the number of elements is equal to 16.

When d is equal to 0.5cm, the error rate is around 2%, as d increased to a value of 0.6cm, the error rate decreased to a limit of 0.2% and finally at a value of d equal to 0.8cm the error rate remains in the same region near 0.2%.
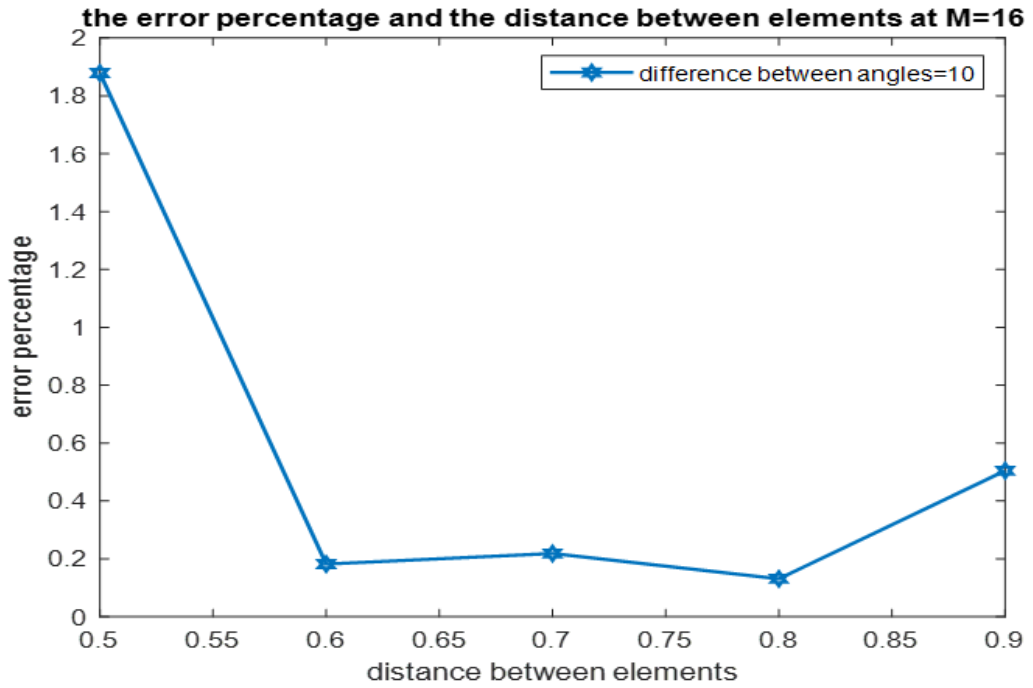
Figure 4.20 Relation between error and distance between elements at a difference between angles equal to 10° and M=16

Difference between angles	Distance Between Elements	Percentage error
10 ⁰	0.5 cm	1.9 %
10 ⁰	0.6 cm	0.2 %
10 ⁰	0.7 cm	0.21%
10 ⁰	0.8 cm	0.19%
10 ⁰	0.9 cm	0.4 %

Table 4.6 The results for the Relation between error and distance between elements at a difference between angles equal to 10° and M=16

In the third case in Figure 4.21, we have been increasing the difference between

the angles to 15° to observe the effects of this increase with changing values of *d*, we noticed that the value of the error rate is between 1.4% and 0.1%.

When the value of d is equal to 0.5 cm the error rate will become around 1.4% as the value of d increases the error value decreases to a value of 0.1%.

We obtained an error rate equal to 1.4%, which is a small error rate, however if we compare it with 0.1%, we realize that there will be a difference of 1.3%, wherefore we can rely on d equal to 0.5 cm, nevertheless our goal is to reduce the error rate to the lowest value. Therefore, in our research to determine the angle of arrival, we depend on the value equal to 0.8 cm which is why we obtained a small error rate.
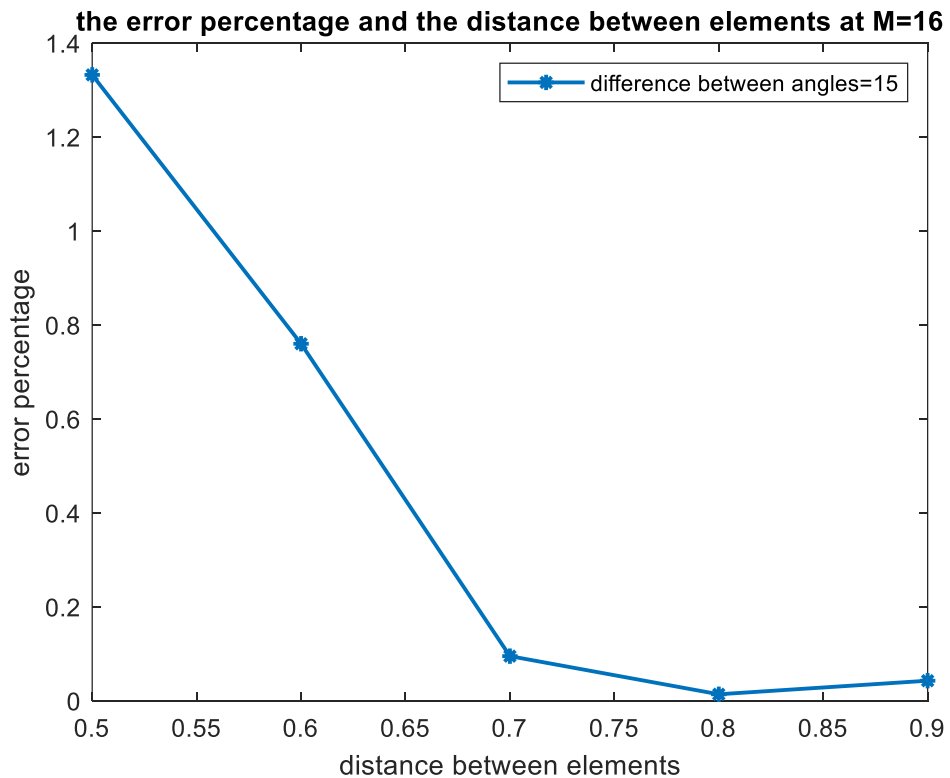
Figure 4.21 Relation between error and distance between elements at a difference between angles equal to 15° and M=16

In the previous cases, when the values of M were equal to 16, as we changed the values of d, the highest error value of 10% was obtained when the difference was equal to 5° and d was equal to 0.5 cm, therefore, we reduce the number of elements to 8 and increase the difference to 10° for observation the effect of these values on the error rate.

In Figure 4. 22, the value of error reached 19% when d is equal to 0.5 cm, in the rest of the cases, we notice that the error rate decreases to 4% and then to a value less than 1% when d is equal to 0.7cm and 0.8cm.
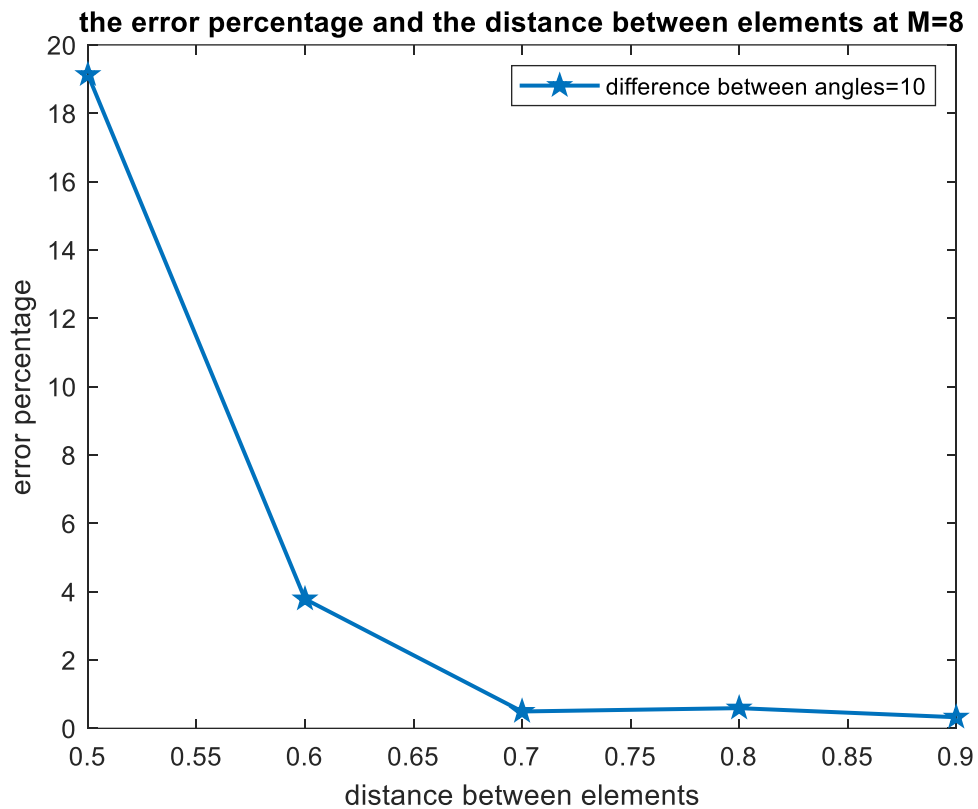
Figure 4.22 Relation between error and distance between elements at a difference between angles equal to 10° and M=8

CHAPTER FIVE

Conclusions and Future Works

5.1 Conclusion

This thesis presents a robust comparative analysis of the performances of the two methods: the classical fast Fourier transform (FFT) and,high-resolution Root_Eigenvector (R-EV) for the Angle-of-Arrival (AoA) electromagnetic waves, so the performance and resulted for the two methods are compared.

Conclusions for all circumstances of noise and noiseless are presented. The FFT method's percentage errors are significantly larger than those of the Root_Eigenvector, probably this error results from presence a group of sidelobes around the required peaks, sometimes, if we have two angles with two different signals, they can overlap each other and result as there is only one angle also to achieve reasonable error rates, we need more than 12 elements (sensors) in the uniform linear array as a result, increasing these elements leads to increased complexity and cost.

Consequently, the Root-Eigenvector's performance in the presence of noise has superior results, from the simulation figures in chapter 4, the maximum error reached 4 % when M, number of samples (sensors) equal to 8. For the rest of the cases, the error rate did not exceed 2%, that is a great example of the ability of this method to detect angle with low level errors.

As mentioned earlier in the disadvantage of FFT that the side lobes are obvious, but it is important to mention when using Root_Eigenvector there are no sidelobes except when using a small number of elements, they may appear (sidelobes), but it is very small proportions (negligible).

From the simulation of the difference between angles and the error rate in chapter 4, R-EV have the ability to distinguish between the angles even the difference between angles reached to 5 degrees (very low) and number of elements not exceeding 8 elements , while for FFT, the minimum acceptable difference between the angles must be exceeded 15 in order to be able to

distinguish between adjacent angles when the number of antennas are equal to 8 elements. Also exceed difference between angles to 10° when M is equal to 12, 14, and 16 elements. Despite the increase in the number of elements, it was not possible to differentiate between signals whose angle difference was equal to 5°.

Therefore, the proposed method R-EV could improve the poor angular resolution provided by a small number of antenna components. Through our study of the relation between the distance between elements d and the percentage error, concluded when d is equal to 0.5 and 0.6, and using number of elements equal to 16, the value of the error ratio does not exceed 2%, and whenever the values of d increase to 0.7, 0.8 and 0.9, the error values do not exceed 0.4%.

The suggested strategy (Root_Eigenvector) will be an effective and straight forward way to enhance AoA estimation. Moreover, the proposed method (Root_Eigenvector) would improve AoA estimation in a simple and effective manner.

5.2 Suggestion for future work

- Doing some experimental set to get experimental data and compare it with noisy data.
- Studying the problem for different wavelengths.

REFERENCES

[1] S. Haykin, J. P. Reilly, V. Kezys, and E. Vertatschitsch, "Some aspects of array signal processing," in *IEE Proceedings F (Radar and Signal Processing)*, IET, 1992, pp. 1–26.

[2] C. F. Dormann *et al.*, "Methods to account for spatial autocorrelation in the analysis of species distributional data: a review," *Ecography*, vol. 30, no. 5, pp. 609–628, 2007.

[3] S. U. Pillai and T. I. Shim, *Spectrum estimation and system identification*. Springer Science & Business Media, 2012.

[4] J. Yan, Q. Bao, and N. Zhong, "A DOA estimation method for array signals based on deep learning," in *Third International Conference on Advanced Algorithms and Signal Image Processing (AASIP 2023)*, SPIE, 2023, pp. 370–375.

[5] P. M. Djurić and S. M. Kay, "Spectrum estimation and modeling," in *Digital Signal Processing Fundamentals*, CRC Press, 2017, pp. 375–398.

[6] Z. Yang, J. Li, P. Stoica, and L. Xie, "Sparse methods for direction-of-arrival estimation," in *Academic Press Library in Signal Processing, Volume 7*, Elsevier, 2018, pp. 509–581.

[7] P. Gupta and S. P. Kar, "MUSIC and improved MUSIC algorithm to estimate direction of arrival," in *2015 International Conference on Communications and Signal Processing (ICCSP)*, IEEE, 2015, pp. 757–761.

[8] H. Wang, G. Liao, J. Xu, S. Zhu, and C. Zeng, "Direction-of-Arrival estimation for circulating space-time coding arrays: From beamspace MUSIC to spatial smoothing in the transform domain," *Sensors*, vol. 18, no. 11, p. 3689, 2018.

[9]   H. Krim and M. Viberg, "Two decades of array signal processing research: the parametric approach," *IEEE Signal Process Mag*, vol. 13, no. 4, pp. 67–94, 1996.

[10]   J. Winters, "Optimum combining for indoor radio systems with multiple users," *IEEE Transactions on communications*, vol. 35, no. 11, pp. 1222–1230, 1987.

[11]   G. Carter, "Time delay estimation," *IEEE Trans Acoust*, vol. 29, no. 3, pp. 461–462, 1981.

[12]   J. Capon, "High-resolution frequency-wavenumber spectrum analysis," *Proceedings of the IEEE*, vol. 57, no. 8, pp. 1408–1418, 1969.

[13]   S. K. S. Neelima, "A review of direction of arrival (DOA) estimation for smart antenna structure," *Journal of Information, Knowledge and Research in Electronics and Communication*, vol. 3, no. 2, pp. 1141–1146, 2014.

[14]   V. F. Pisarenko, "The retrieval of harmonics from a covariance function," *Geophys J Int*, vol. 33, no. 3, pp. 347–366, 1973.

[15]   R. Kumaresan and D. Tufts, "Estimating the parameters of exponentially damped sinusoids and pole-zero modeling in noise," *IEEE Trans Acoust*, vol. 30, no. 6, pp. 833–840, 1982.

[16]   Z. Ahmad and I. Ali, "Three decades of development in DoA estimation technology," *TELKOMNIKA Indonesian Journal of Electrical Engineering*, vol. 12, no. 8, pp. 6297–6312, 2014.

[17]   R. Schmidt, "Multiple emitter location and signal parameter estimation," *IEEE Trans Antennas Propag*, vol. 34, no. 3, pp. 276–280, 1986.

[18] G. Chaitanya, A. Jain, and N. Jain, "Performance analysis of direction of arrival estimation algorithms for smart antenna for mobile communication systems," *Int J Sci Eng Res*, vol. 3, no. 7, pp. 1–5, 2012.

[19] P. Stoica and K. C. Sharman, "Novel eigenanalysis method for direction estimation," in *IEE Proceedings F (Radar and Signal Processing)*, IET, 1990, pp. 19–26.

[20] B. Friedlander and A. J. Weiss, "Direction finding using spatial smoothing with interpolated arrays," *IEEE Trans Aerosp Electron Syst*, vol. 28, no. 2, pp. 574–587, 1992.

[21] G. V Serebryakov, "Direction-of-arrival estimation of correlated sources by adaptive beamforming," *IEEE transactions on signal processing*, vol. 43, no. 11, pp. 2782–2787, 1995.

[22] M. Haardt, "Efficient one-, two-, and multidimensional high-resolution array signal processing," *Ph. D. Thesis, Shaker Verlag, Aachen*, 1996.

[23] J. Luo and Z. Zhang, "Using eigenvalue grads method to estimate the number of signal source," in *WCC 2000-ICSP 2000. 2000 5th International Conference on Signal Processing Proceedings. 16th World Computer Congress 2000*, IEEE, 2000, pp. 223–225.

[24] Q. Chong-ying, Z. Yong-shun, H. A. N. Ying, and C. Xi-hong, "An algorithm on high resolution DOA estimation with unknown number of signal sources," in *ICMMT 4th International Conference on, Proceedings Microwave and Millimeter Wave Technology, 2004.*, IEEE, 2004, pp. 227–230.

[25] Z. Xiaofei, L. Wen, S. Ying, Z. Ruina, and X. Dazhuan, "A novel DOA estimation algorithm based on eigen space," in *2007 International*

Symposium on Microwave, Antenna, Propagation and EMC Technologies for Wireless Communications, IEEE, 2007, pp. 551–554.

[26] A. Liu, G. Liao, C. Zeng, Z. Yang, and Q. Xu, "An eigenstructure method for estimating DOA and sensor gain-phase errors," *IEEE Transactions on signal processing*, vol. 59, no. 12, pp. 5944–5956, 2011.

[27] P. Vallet, X. Mestre, and P. Loubaton, "Performance analysis of an improved MUSIC DoA estimator," *IEEE Transactions on Signal Processing*, vol. 63, no. 23, pp. 6407–6422, 2015.

[28] Q. Yan, J. Chen, G. Ottoy, and L. De Strycker, "Robust AOA based acoustic source localization method with unreliable measurements," *Signal Processing*, vol. 152, pp. 13–21, 2018.

[29] V. V Chudnikov, B. I. Shakhtarin, A. V Bychkov, and S. M. Kazaryan, "Doa estimation in radar sensors with colocated antennas," in *2020 Systems of Signal Synchronization, Generating and Processing in Telecommunications (SYNCHROINFO)*, IEEE, 2020, pp. 1–6.

[30] T. Margiani, S. Cortesi, M. Keller, C. Vogt, T. Polonelli, and M. Magno, "Angle of arrival and centimeter distance estimation on a smart UWB sensor node," *IEEE Trans Instrum Meas*, 2023.

[31] P. Stoica and R. L. Moses, *Spectral analysis of signals*, vol. 452. Pearson Prentice Hall Upper Saddle River, NJ, 2005.

[32] M. H. (Monson H.) Hayes, *Statistical digital signal processing and modeling*. John Wiley & Sons, 1996.

[33] W. T. Cochran *et al.*, "What is the fast Fourier transform?," *Proceedings of the IEEE*, vol. 55, no. 10, pp. 1664–1674, 1967.

[34] K. Hamid, "Two decades of array signal processing research," *IEEE Signal Process Mag*, pp. 67–94, 1994.

[35] H. R. Gupta, R. Mehra, and S. Batan, "Power spectrum estimation using Welch method for various window techniques," *International Journal of Scientific Research Engineering and Technology (IJSRET)*, vol. 2, no. 6, pp. 389–392, 2013.

[36] W. Alexander and C. M. Williams, *Digital Signal Processing: Principles, Algorithms and System Design*. Academic Press, 2016.

[37] A. Zaknich, *Principles of adaptive filters and self-learning systems*. Springer Science & Business Media, 2005.

[38] P.-J. Chung, M. Viberg, and J. Yu, "DOA estimation methods and algorithms," in *Academic Press Library in Signal Processing*, vol. 3, Elsevier, 2014, pp. 599–650.

[39] F. Castanié, *Spectral analysis: parametric and non-parametric digital methods*. John Wiley & Sons, 2013.

[40] Z. Chen, G. Gokeda, and Y. Yu, *Introduction to Direction-of-arrival Estimation*. Artech House, 2010.

[41] H. Huang, J. Yang, H. Huang, Y. Song, and G. Gui, "Deep learning for super-resolution channel estimation and DOA estimation based massive MIMO system," *IEEE Trans Veh Technol*, vol. 67, no. 9, pp. 8549–8560, 2018.

[42] Y. H. Hu and B. C. Phan, "Frequency estimation error in Pisarenko harmonic decomposition method," *Proceedings of the IEEE*, vol. 76, no. 1, pp. 82–84, 1988.

[43] X. Wei, Y. Xu, and X. Xiao, "Parameter estimation of voltage flicker based on Hilbert transform and Pisarenko harmonic decomposition," in *2009 International Conference on Energy and Environment Technology*, IEEE, 2009, pp. 189–192.

[44] F. Belloni, A. Richter, and V. Koivunen, "DoA estimation via manifold separation for arbitrary array structures," *IEEE Transactions on Signal Processing*, vol. 55, no. 10, pp. 4800–4810, 2007.

[45] A. Zahernia, M. J. Dehghani, and R. Javidan, "MUSIC algorithm for DOA estimation using MIMO arrays," in *2011 6th International Conference on Telecommunication Systems, Services, and Applications (TSSA)*, IEEE, 2011, pp. 149–153.

[46] L. Hecker, L. Tebartz van Elst, and J. Kornmeier, "Source Localization Using Recursively Applied and Projected MUSIC with Flexible Extent Estimation," *bioRxiv*, pp. 2021–2023, 2023.

[47] P. Vallet, X. Mestre, and P. Loubaton, "Performance analysis of an improved MUSIC DoA estimator," *IEEE Transactions on Signal Processing*, vol. 63, no. 23, pp. 6407–6422, 2015.

[48] H. Tang, "DOA estimation based on MUSIC algorithm." 2014.

[49] D. Johnson and S. DeGraaf, "Improving the resolution of bearing in passive sonar arrays by eigenvalue analysis," *IEEE Trans Acoust*, vol. 30, no. 4, pp. 638–647, 1982.

[50] L. Osman, I. Sfar, A. Gharsallah, and A. Gharsallah, "Comparative Study of High-Resolution Direction-of-Arrival Estimation Algorithms for Array Antenna System," *International Journal of Research and Reviews in Wireless Communications (IJRRWC)*, vol. 2, no. 1, 2012, [Online]. Available: www.sciacademypublisher.com

[51] H. K. Hwang, Z. Aliyazicioglu, M. Grice, and A. Yakovlev, "Direction of arrival estimation using a root-MUSIC algorithm," in *Proceedings of the International MultiConference of Engineers and Computer Scientists*, Citeseer, 2008, pp. 19–21.

[52] T. E. Tuncer and B. Friedlander, *Classical and modern direction-of-arrival estimation*. Academic Press, 2009.

[53] A. H. RAMLI, N. F. ABDULLAH, M. ISMAIL, and R. NORDIN, "Localization determination for radio communication using tdoa technique," *J Theor Appl Inf Technol*, vol. 99, no. 24, 2021.

[54] N. Dey and A. S. Ashour, *Direction of arrival estimation and localization of multi-speech sources*. Springer, 2018.

[55] R. Modonesi, M. Dalai, P. Migliorati, and R. Leonardi, "A note on probabilistic and geometric shaping for the AWGN channel," *IEEE Communications Letters*, vol. 24, no. 10, pp. 2119–2122, 2020.

[56] Z. Chen, G. Gokeda, and Y. Yu, *Introduction to Direction-of-arrival Estimation*. Artech House, 2010.

[57] P. Ioannides and C. A. Balanis, "Uniform circular arrays for smart antennas," *IEEE Antennas Propag Mag*, vol. 47, no. 4, pp. 192–206, 2005.

[58] A. Alexiou and M. Haardt, "Smart antenna technologies for future wireless systems: trends and challenges," *IEEE communications Magazine*, vol. 42, no. 9, pp. 90–97, 2004.

[59] J. Foutz, A. Spanias, and M. Banavar, *Narrowband direction of arrival estimation for antenna arrays*. Springer Nature, 2022.

[60] M. S. Amin, K. I. Ahmed, and Z. R. Chowdhury, "Estimation of direction of arrival (DOA) using real-time array signal processing," in *2008 International Conference on Electrical and Computer Engineering*, IEEE, 2008, pp. 422–427.

[61] J. Dmochowski, J. Benesty, and S. Affes, "Direction of arrival estimation using the parameterized spatial correlation matrix," *IEEE*

Trans Audio Speech Lang Process, vol. 15, no. 4, pp. 1327–1339, 2007.

[62] M. Esfandiari, "Advances and New Applications of Spectral Analysis," 2023.

Appendix

Matrices

A $(z * k)$ matrix is an array of numbers or mathematical functions containing z rows and k columns,

$$V = \{v_{zk}\} = \begin{bmatrix} v_{11} & b_{12} & \cdots & b_{1k} \\ v_{21} & b_{22} & \cdots & b_{2k} \\ \cdots & \cdots & \cdots & \cdots \\ v_{z1} & v_{z2} & \cdots & b_{zk} \end{bmatrix} \tag{1}$$

Is a $z * k$ matrix of v_{zk} ,if $z = k$ then the resulted matrix is a square matrix of z rows and k columns.

If V is a $z * k$ matrix, then the transpose represented by V^T, is the $k * z$ matrix that is contained by replacing rows by columns of V. Thus, the element $\{z, k\}$ becomes the element $\{k, z\}$ and vice versa.

If **V** is square, then the transpose V^T is easily by reflecting the element of **V** around the diagonal. For a square matrix if V is equal to its transpose, then **V** is a symmetric matrix.

$$V = V^T \tag{2}$$

For a matrix that is formed by a complex number, the Hermitian transpose is the complex conjugate transpose of **V** represented by V^H Thus.

$$V^H = (V^*)^T = (V^T)^* \tag{3}$$

When a square matrix (complex values) is equal to its Hermitian transpose, $V = V^H$ then the matrix is said to be Hermitian.

Eigenvectors and Eigenvalues

The eigenvalues and eigenvectors of a matrix can provide the most valuable and significant information about the matrix. It is feasible to tell whether the matrix is positive definite based on the eigenvalues. The matrix's

invertibility and the sensitivity of the calculation of the inverse to numerical error may both be determined using the eigenvalues [60].

Two subspaces, the signal subspace and the noise subspace can be formed from the signal. To achieve this decomposition, eigenvectors are used. They offer a crucial eigenvalue decomposition representation for matrices. Pisarenko Harmonic Decomposition (PHD), Multiple Signal Classification (MUSIC), Eigenvector spectrum estimation, and Root-Eigenvector will all be explained using this decomposition[28].

Let D be a n×n matrix and consider the following set of linear equations $\boldsymbol{Ds} = \lambda\,\boldsymbol{s}$ Where λ is a constant, it can also be stated as a set of homogeneous linear equations of the following form:

$$(\boldsymbol{D} - \lambda\,\boldsymbol{I})\boldsymbol{s} = \boldsymbol{0} \tag{4}$$

The matrix $D - \lambda\,I$ must be singular (a matrix is said to be unique if it does not have an inverse) for a nonzero vector to be a solution to this equation, therefore, the determinant of the singular matrix $(D - \lambda\,I)$ must be zero.

$$Det\,(D - \lambda\,I)\,s = 0 \tag{5}$$

Equation (5) is called the characteristic equation of the matrix D and its m roots, A, for $\lambda_i = 1, 2, \ldots, m$ are the eigenvalues of D.

For every eigenvalue λ_i the matrix $(D - \lambda\,I)$ will be singular and at least one nonzero vector will be present, s_i, that act as the solution of Equation 5, i.e.

$$Ds_i = \lambda_i\,s_i \tag{6}$$

The term "eigenvectors of D refers to these vectors, s_i. It is obvious that αs_i will also be an eigenvector for any constant for every eigenvector α. As a result, eigenvectors are frequently normalized to have a unit norm[32]

Eigen Decomposition of Autocorrelation Matrices

While it is theoretically feasible to calculate the frequencies of complex exponents from the peaks of the spectrum calculated using any method, this strategy would not fully use the process's presumed parametric shape. Utilizing

frequency estimate techniques while taking into consideration the process's characteristics is an alternative. These techniques are built on the autocorrelation matrix's eigen decomposition into a signal subspace and a noise subspace. Consider The first-order process as a method for frequency estimate [32], [61], [62]:

$$y(m) = A1\, e^{j\omega_1 M} +\, \eta\,(m) \tag{7}$$

$$y(m) = x(m) + \eta(m) \tag{8}$$

That consists of a single complex exponential in white noise, The amplitude of the complex exponential $A1 = |A1\, |e^{j\emptyset_1}\, \emptyset_1$ is a uniformly random distributed variable, the autocorrelation sequence of $y(m)$ is:

$$r_y(k) = P_1 e^{j\omega_1 k} + \sigma_\eta^2 \delta(k) \quad k = 0, \pm 1, \dots \dots, \pm(L-1) \tag{9}$$

where $P_1 = |A1|^2$ is the power in the complex exponential. The M * M autocorrelation matrix for $y(m)$ is, therefore, the sum of the autocorrelation matrices for the signal, R_x, and the noise, R_η as shown below:

$$R_y = R_x + R_\eta \tag{10}$$

where the signal autocorrelation matrix is:

$$R_x = \text{P1} \begin{bmatrix} 1 & e^{-j\omega_1} & e^{-j2\omega_1} & \cdots & e^{-j(M-1)\omega_1} \\ e^{j\omega_1} & 1 & e^{-j\omega_1} & \cdots & e^{-j(M-2)\omega_1} \\ e^{j2\omega_1} & e^{j\omega_1} & 1 & \cdots & e^{-j(M-3)\omega_1} \\ \cdots & \cdots & \cdots & \cdots & \cdots \\ e^{j(M-1)\omega_1} & e^{j(M-2)\omega_1} & e^{j(M-3)\omega_1} & \cdots & 1 \end{bmatrix} \tag{11}$$

and has a rank of one, and the autocorrelation matrix of the noise is diagonal,

$$R_\eta = \sigma_\eta^2 I\,, \tag{12}$$

and has full rank. Note that if we assume:

$$q_1 = \left[1, e^{j\omega_1}, e^{j2\omega_1}, \dots, e^{j(M-1)\omega_1}\right]^T, \tag{13}$$

then R_x can be written in terms of q_1 as follows:

$$R_x = P_1\, q_1 q_1{}^H, \tag{14}$$

Since the rank of R_x is equal to 1, then R_x has only one nonzero eigenvalue. With:

$$R_x q_1 = P_1(q_1 q_1{}^H)q_1 = P_1 q_1(q_1{}^H q_1) = M\, P_1 q_1 \tag{15}$$

it follows that the nonzero eigenvalue is equal to MP_1, and that q_1 is the corresponding eigenvector.

In addition, since R_x is Hermitian then the remaining eigenvectors, $u_2, u_3,$ ..., u_L, will be orthogonal to q_1

$$q_1{}^H u_i = 0 \text{ where i=2,3, 4,…, M} \tag{16}$$

Finally, note that if it allow to make λ_i^x be the eigenvalues of R_x, then:

$$R_y u_i = (R_x + \sigma_\eta^2 I)u_i = \lambda_i^x u_i + \sigma_\eta^2 u_i = (\lambda_i^x + \sigma_\eta^2)u_i \tag{17}$$

Therefore, there is a similar between the eigenvectors of R_y and R_x ,but the eigenvalues of R_y are:

$$\lambda_i = \lambda_i^x + \sigma_\eta^2 \tag{18}$$

As a result, eigenvalue of R_y are represent by:

$$\lambda_{max} = MP_1 + \sigma_\eta^2 \tag{19}$$

and the remaining M-1 eigenvalues are equal to σ_η^2 so, all information about y (m) from the eigenvalues and eigenvectors of R_y are got as shown:

1. Achieving an eigen-decomposition of the autocorrelation matrix, R_y the largest eigenvalue is equal to $MP_1 + \sigma_\eta^2$ and the eigenvalues that remain will be equal to σ_η^2.

2. Using the eigenvalues of R_y to find a solution for the power P_1 and the noise variance as follows:

$$\lambda_{min} = \sigma_\eta^2 \tag{20}$$

$$P_1 = \frac{1}{M}(\lambda_{max} - \lambda_{min}) \tag{21}$$

3. Determining the frequency ω from the eigenvector u_{max} that is deal with the largest eigenvalue.

$$\omega = arg\{u_{max}\} \tag{22}$$

الخلاصة

يعد تحسين دقة تخمين زاوية الوصول (AoA) مفيدا للموجات الراديوية الواردة التي تستقبلها مصفوفة من الهوائيات الخطية(ULA) . واحدة من التقنيات الحديثة لتحديد زاوية أي هدف يقترب أو يستقبل هي جذور المتجهات الذاتية Root Eigenvector (R-EV).

تعد خوارزمية Root Eigenvector (R-EV) ، والتي تتم مقارنتها في هذه الأطروحة بالطريقة التقليدية لتحويلات فورييه السريعة (FFT) ، إحدى الطرق عالية الدقة لتحديد الزوايا والعثور عليها.وقيم الزاوية لأي موجة مشعة لجسم يقترب أو يستقبل تكون بمعدل خطأ صغير مقارنة بالطرق الأخرى ل AoA.

تركز الخوارزميات عالية الدقة على الخصائص المميزة لمصفوفة التغاير المشترك للإشارة بالإضافة إلى تقسيم الاشارة إلى فضاءين فرعيين ، أحدهما للإشارة والآخر للضوضاء.

قبل البدء في دراسة طريقة R-EV ، توجد بعض التحديدات للطرق البارامترية لتحديد زاوية الوصول (AoA). سبقت هذه التحديدات R-EV من حيث النتائج المحققة والتمثيل الرياضي مثل التحلل التوافقي Pisarenko (PHD) وتصنيف الإشارات المتعددة (MUSIC).

تم تنفيذ طرق R-EV و FFT في بيئة MATLAB. تمت محاكاة مجموعة من الدراسات بأعداد مختلفة من الهوائيات, قيم مختلفة للزاوية وقيم مختلفة للمسافة بين العناصر سواء كانت مصادر مفردة أو متعددة. أيضا ، تم تحليل نتائج المحاكاة لمعرفة تأثير تغيير هذه العناصر على تحديد زاوية الوصول باستخدام R-EV و FFT عن طريق حساب النسبة المئوية للخطأ في كل حالة.

أثبتت النتائج الدقة الفائقة ل R-EV وحققت معدلات خطأ منخفضة بشكل استثنائي حتى مع إضافة الضوضاء ، وصل الحد الأقصى للخطأ الذي حصلنا عليه إلى 4٪ عندما M ، عدد العناصر (المستشعرات) يساوي 8. بالنسبة لبقية الحالات ، لم يتجاوز معدل الخطأ 2٪ ،. في المقابل ، لم يحقق FFT نفس كفاءة R-EV بسبب وجود معدلات خطأ أعلى ويتطلب عددا أكبر من العناصر .

إقرار لجنة المناقشة

نشهد بأننا أعضاء لجنة التقويم والمناقشة قد اطلعنا على الرسالة الموسومة (**تحسين الدقة في تخمين زاوية الوصول للموجات باستخدام طريقة جذور المتجهات الذاتية**) وناقشنا الطالبة (**اية سعود عبود الشاكر**) في محتوياتها وفيما له علاقة بها بتاريخ   /   /2024   وقد وجدنا ها جديرة بنيل شهادة الماجستير / علوم في اختصاص هندسة الالكترونيك .

التوقيع:

رئيس اللجنة: أ.م.د. عبدالستار محمد خضر

التاريخ: /   / ٢٠٢٤

التوقيع:

عضو اللجنة: أ.م.د اوس زهير يونس الأشقر

التاريخ: /   / ٢٠٢٤

التوقيع:

عضو اللجنة: م.د. زينب رامي صالح العمري

التاريخ: /   / ٢٠٢٤

التوقيع:

عضو اللجنة (المشرف): أ.م.د. مجاهد فهمي ابراهيم العزو

التاريخ: /   / ٢٠٢٤

قرار مجلس الكلية

اجتمع مجلس كلية هندسة الالكترونيات بجلسته .... المنعقدة بتاريخ :   /   / ٢٠٢٤ وقرر المجلس منح الطالبة شهادة الماجستير علوم في اختصاص هندسة الألكترونيك

مقرر المجلس :أ.م.د. بلال علاء الدين جبر

التاريخ :   /   / ٢٠٢٤

رئيس مجلس الكلية : أ.د. خالد خليل محمد

التاريخ: /   / ٢٠٢٤

إقرار المشرف

اشهد بأن الرسالة الموسومة ب (**تحسين الدقة في تخمين زاوية الوصول للموجات باستخدام طريقة جذور المتجهات الذاتية**) تم اعدادها من قبل الطالبة (**اية سعود عبود الشاكر**) تحت اشرافنا في قسم هندسة الالكترونيك /كلية هندسة الالكترونيات /جامعة نينوى , وهي جزء من متطلبات نيل شهادة الماجستير/علوم في اختصاص هندسة الالكترونيك.

التوقيع:

المشرف : أ.م.د. مجاهد فهمي ابراهيم العزو

التاريخ: /   / ٢٠٢٤

إقرار المقيم اللغوي

اشهد باني قمت بمراجعة الرسالة هذه الرسالة من الناحية اللغوية وتصحيح ما ورد فيها من أخطاء لغوية وتعبيرية وبذلك أصبحت الرسالة مؤهلة للمناقشة بقدر تعلق الامر بسلامة الأسلوب أوصحة التعبير.

التوقيع:

المقوم اللغوي: أ.م.د. صالح عبدالله عبدالرحمن

التاريخ: /   / ٢٠٢٤

إقرار رئيس لجنة الدراسات العليا

بناء على التوصيات المقدمة من قبل المشرف والمقوم اللغوي أرشح هذه الرسالة للمناقشة.

التوقيع:

الاسم: أ.د. قيس ذنون نجم

التاريخ: /   / ٢٠٢٤

إقرار رئيس القسم

بناء على التوصيات المقدمة من قبل المشرف والمقوم اللغوي ورئيس لجنة الدراسات العليا أرشح هذه الرسالة للمناقشة.

التوقيع:

الاسم: أ.م.د.حارث احمد محمد

التاريخ: /   / ٢٠٢٤

تحسين الدقة في تخمين زاوية الوصول
للموجات باستخدام طريقة جذور المتجهات الذاتية

الأطروحة بإعداد

اية سعود عبود الشاكر

الى

مجلس كلية هندسة الالكترونيات

جامعة نينوى

كجزء من متطلبات نيل شهادة الماجسير

في

هندسة الألكترونيك

بإشراف

أ.م.د مجاهد فهمي ابراهيم العزو

جامعة نينوى
كلية هندسة الالكترونيات
قسم الألكترونيك

تحسين الدقة في تخمين زاوية الوصول للموجات باستخدام طريقة جذور المتجهات الذاتية

الأطروحة بإعداد

اية سعود عبود الشاكر

ماجسير

في

هندسة الألكترونيك

بإشراف

أ.م.د مجاهد فهمي ابراهيم العزو